

A 1-mm spectral line survey toward GLIMPSE Extended Green Objects (EGOs).¹

J.H. He¹, S. Takahashi², and X. Chen³

jinhuahe@ynao.ac.cn, satoko_t@asiaa.sinica.edu.tw, chenxi@shao.ac.cn

ABSTRACT

A northern subsample of 89 *Spitzer* GLIMPSE extended green objects (EGOs), the candidate massive young stellar objects, are surveyed for molecular lines in two 1-GHz ranges: 251.5-252.5 and 260.188-261.188 GHz. A comprehensive catalog of observed molecular line data and spectral plots are presented. Eight molecular species are undoubtedly detected: H¹³CO⁺, SiO, SO, CH₃OH, CH₃OCH₃, CH₃CH₂CN, HCOOCH₃, and HN¹³C. H¹³CO⁺ 3-2 line is detected in 70 EGOs among which 37 ones also show SiO 6-5 line, demonstrating their association to dense gas and supporting the outflow interpretation of the extended 4.5 μm excess emission. Our major dense gas and outflow tracers (H¹³CO⁺, SiO, SO and CH₃OH) are combined with our previous survey of ¹³CO, ¹²CO and C¹⁸O 1-0 toward the same sample of EGOs for a multi-line multi-cloud analysis of line width and luminosity correlations. Good log-linear correlations are found among all considered line luminosities, which requires a universal similarity of density and thermal structures and probably of shock properties among all EGO clouds to explain. It also requires that the shocks should be produced within the natal clouds of the EGOs. Diverse degrees of correlation are found among the line widths. However, both the line width and luminosity correlations tend to progressively worsen across larger cloud subcomponent size-scales, depicting the increase of randomness across cloud subcomponent sizes. Moreover, the line width correlations among the three isotopic CO 1-0 lines show data scatter as linear functions of the line width itself, indicating that the velocity randomness also increases with whole-cloud sizes and has some regularity behind.

Subject headings: Turbulence — Stars: formation — ISM: clouds — ISM: jets and outflows — ISM: kinematics and dynamics — Radio lines: ISM

1. Introduction

Formation and evolution of massive young stars is still a matter of debate. As reviewed

by Zinnecker & Yorke (2007), the high luminosity, high protostar temperature, and much shorter formation time scales make the formation of massive stars distinct from that of low mass stars. Particularly, many observed massive protostars reside in proto-clusters, which further complicates their formation processes by introducing possible interplay between neighboring forming massive stars and their lower mass siblings.

The paucity of known massive star forming regions is one of the major obstacles in observational studies. Thus, the recently uncovered new sample of over 300 massive young stellar object (MYSO) candidates – Extended Green Objects (EGOs) – that are identified from the *Spitzer* Galactic Legacy Infrared Mid-Plane Survey Ex-

¹Key Laboratory for the Structure and Evolution of Celestial Objects, Yunnan Astronomical Observatory/National Astronomical Observatory, Chinese Academy of Sciences, P.O. Box 110, Kunming, 650011, Yunnan Province, PR China

²Academia Sinica, Institute of Astronomy and Astrophysics, P.O. Box 23-141, Taipei 10617

³Key Laboratory for Research in Galaxies and Cosmology, Key Laboratory for Research in Galaxies and Cosmology, Shanghai Astronomical Observatory, Chinese Academy of Sciences, 80 Nandan Road, Shanghai 200030, PR China

¹The observation project was funded by Academia Sinica, Institute of Astronomy and Astrophysics, Taipei

traordinaire (*GLIMPSE*) at 3.6, 4.5, 5.8, 8.0, and *MIPSGAL* at $24\ \mu\text{m}$, have significantly extended the working sample for massive star formation studies (Cyganowski et al. 2008). The EGOs are so named because they show excess emission in extended structures in the Infrared Array Camera (*IRAC*) $4.5\ \mu\text{m}$ band images that are conventionally coded as green in the *IRAC* false color images.

EGOs are candidate birth places of MYSOs because, as shown by Cyganowski et al. (2008), many of them are associated with Class II CH_3OH masers and/or infrared dark clouds (IRDCs). Both the Class II CH_3OH masers (Cragg et al. 2005; Ellingsen 2006) and the IRDCs (Simon et al. 2006a,b; Rathborne et al. 2006, 2007) are signposts of massive star formation sites. A more detailed interferometric thermal millimeter line mapping of two EGOs by Cyganowski et al. (2011b) has lent further support to EGOs being MYSOs or massive protoclusters.

EGOs very possibly possess prominent outflows, because the characteristic extended green structures in them are possibly shock originated (Noriega-Crespo et al. 2004; Smith & Rosen 2005; De Buizer & Vacca 2010). Studies have confirmed that it is the $4.5\ \mu\text{m}$ excess instead of the $4.5\ \mu\text{m}$ total flux that traces the outflow shocks (e.g., Simpson et al. 2012; Lee et al. 2012). The outflow nature of the EGO samples is further confirmed by the high detection rate of SiO 5-4 line in a selected subsample of 10 EGOs (Cyganowski et al. 2009). Furthermore, the interferometric mapping of two EGOs by Cyganowski et al. (2011b) has also revealed their outflow nature.

These EGOs are possibly still in early cloud collapse stage, because their *Spitzer* [3.6]-[5.8] and [8.0]-[24] colors mimic that of the youngest massive star formation models that are still in early cloud collapse phase (Cyganowski et al. 2008). Furthermore, infall tracers such as $\text{HCO}^+ 1-0$ have been surveyed by Chen et al. (2010) toward a subsample of 88 EGOs with a single dish telescope in the northern hemisphere. They found more blue skewed $\text{HCO}^+ 1-0$ line profiles than red skewed ones, which statistically supports the existence of infall motions in these EGOs. The early stage of star formation in EGOs is also confirmed by the non-detection of continuum emission at 3.6 or 1.3 cm (before the onset of UCHII region) by Cyganowski et al. (2011a).

The existing methanol (CH_3OH) maser data have provided rich information to diagnose the physical conditions in EGOs. Many EGOs associate with both Class I and II methanol masers. On the basis of methanol maser surveys in literature, Chen et al. (2009) found that about two third of the observed EGOs are spatially coincident with known Class I methanol masers at 44 and/or 95 GHz. The high detection rate of Class I methanol masers has been confirmed by the 55 per cent detection rates of the 95 GHz methanol maser in a recent Mopra survey of almost all EGOs in the Cyganowski et al. (2008) catalog by the same group (Chen et al. 2011). Thus, more than half of the EGOs should be undoubtedly associated with active outflow shocks.

The VLA mapping of both classes of methanol masers by Cyganowski et al. (2009) illustrated that the two classes of masers actually occur in different spatial components of the objects: Class II 6.7 GHz maser spots concentrate on the peak of the $24\ \mu\text{m}$ emission sources, tracing the warm star forming cores, whilst the Class I 44 GHz masers usually scatter around the extended $4.5\ \mu\text{m}$ emission structures, tracing the interface between the proposed outflows and interstellar medium. The coexistence of both classes of methanol masers in some EGOs may complicate the interpretation of methanol thermal lines observed by single dishes, because part of the detected emission could be mainly excited by strong IR radiation in the hot star-forming cores while the rest part could be contributed by collisional excitation in the hot and dense shock regions around the outflows.

Up to now, these new objects are still lack of large scale survey of thermal molecular lines beside our previous survey of the three isotopic CO 1-0 and $\text{HCO}^+ 1-0$ lines (Chen et al. 2010). To further explore the nature of the clouds around EGOs (EGO clouds hereafter), we have performed a survey of outflow tracers, SiO 6-5 and $\text{CH}_3\text{OH J}_3\text{-J}_2\text{ A}$ line series, toward a sample of 89 EGOs mainly in the northern sky, nearly the same sample as in Chen et al. (2010). Our observations also simultaneously cover some rotational transitions of H^{13}CO^+ , SO, and other interesting complex species such as CH_3OCH_3 , $\text{CH}_3\text{CH}_2\text{CN}$ and HCOOCH_3 .

In this paper, we mainly present the spectral plots, line parameters and discuss the observed

line width and luminosity correlations among the considered molecules, while more detailed analysis of the results will be presented in future papers. Sects. 2 and 3 of this paper present target selection and observations. Some notes on line identification are given in Sect. 4. We present the results in Sect. 5 and also discuss the dense gas, outflows, distance and line width and luminosity correlations in Sect. 6. In the end, the main points are summarized in Sect. 7.

2. Sample selection

We have selected 89 EGOs with $\text{DEC} > -38$ deg from the over 300 EGOs in Cyganowski et al. (2008) as our working sample. The infrared positions from the same paper are used. It is nearly identical to the sample of the isotopic CO 1-0 observations by Chen et al. (2010). During the object selection, we found five pairs of EGOs that are so close to each other that our telescope beam ($29''$) can hardly get them resolved. Thus, only one source in each pair was selected and the observed lines should be deemed as contributed by both EGOs. The five dropped sources were G24.11-0.18, G43.04-0.45(b), G54.45+1.02, G54.11-0.05² and G58.78+0.65. In addition, two EGOs, G19.01-0.03 O-N and G19.01-0.03 O-S, were also excluded from our sample, because they were covered by the beam toward their associated point source, G19.01-0.03.

3. Observations and data reduction

The observations were done with the Arizona Radio Observatory 10-m Submillimeter Telescope (AROSMT) in several nights during two epochs: 2009 April 24 to May 11 and 2010 March 29 to April 27. The ALMA band-6 sideband-separating receiver was used with two Filter Banks to record the upper and lower sidebands (USB and LSB) separately. The observed frequency ranges were 251.5-252.5 GHz (USB) and 260.188-261.188 GHz (LSB). The LRS velocities of most of our EGOs from the C^{18}O 1-0 observations of Chen et al. (2010) had been used for tuning. The spectral resolution was 1 MHz in the 1 GHz bandwidth

²Later we recognized that this EGO is actually far enough away from G54.11-0.04 so that it should be included in our sample. We realized this only after the observations were done.

in both sidebands. We tested several off positions that were selected on the basis of the CO 1-0 survey result of Dame et al. (2001) at locations several arc minutes to degrees away from some targets but found no line emission. However, our test runs in position-switch mode were found to suffer from strong ripples in baseline. Thus, we adopted beam switch mode with a 2-arcmin throw at 1 Hz for all our targets to improve the spectral baseline. This was viable perhaps because our observed lines are mostly high density tracers. This strategy was justified by the fact that no obvious absorption like features were seen in the final data. Although the existence of weak emission at the off-positions can not be excluded, their effects to our data should be hopefully small.

The telescope pointing and focus was checked roughly every two hours with a planet. The representative beam width is $29''$ (at 260 GHz), which is corresponding to a linear resolution of roughly 0.56 pc at a representative distance of 4 kpc. Main beam efficiencies of 0.65 and 0.55 were applied to the LSB and USB, respectively, to obtain the main beam temperature T_{mb} from the antenna temperature T_{A}^* . Line flux can be computed from T_{mb} with the nominal conversion factor of 46.5 Jy/K (at 260 GHz) for the ARO SMT. The typical T_{sys} during most of the observations were ~ 280 K in the LSB and ~ 311 K in the USB.

Sideband leakage can produce false line features to make trouble to line identification. Fortunately, it can be checked in our data by comparing the USB and LSB data which are obtained simultaneously and separately. We did not find leakage in most of our data, except for the cases of G14.33-0.64 and G24.33+0.14 of which the strong SO line in the LSB leaked into the USB as a small artificial line feature. The rareness of the leakage is due to the image rejection ratio of about 10 to 20 dB during most of our observations.

Gildas/CLASS software³ was used to reduce the data and analyze the line profiles. A linear baseline was removed from almost all spectra, except the LSB spectrum of G11.92-0.61 for which a cubic baseline was subtracted to correct for the gently curvy baseline. With an on+off exposure time of 10 minutes, the average baseline RMS (in mainbeam temperature) are ~ 25 mK in the

³<http://www.iram.fr/IRAMFR/GILDAS>

LSB and ~ 33 mK in the USB at a resolution of 1 km s^{-1} . The rms of individual objects are listed in Table 1 (together with their LRS velocity and distance that will be discussed in later sections).

4. Line identification

Systemic velocity (V_{LSR}) is needed for line identification. Although some EGOs already have their velocity known from the C^{18}O observations of Chen et al. (2010), we still use the strongest lines in our results, H^{13}CO^+ 3-2 in the USB, $\text{SO}^3\Sigma 5_6 - 4_5$ and the $\text{CH}_3\text{OH J}_3\text{-J}_2 \text{ A}$ line series (with blended lines excluded) in the LSB, to determine the systemic velocity for each target independently. A single Gaussian profile is fit to each line to determine observed line frequencies and uncertainties. (Note that some lines with broad line wings will be fit with double Gauss profiles to determine their line parameters in later sections.) The velocities determined from all lines are averaged together with the weight T_{mb}/σ_V , where σ_V is the statistic error of the velocity and T_{mb} is the line peak temperature. With this weighting scheme, the strongest line, H^{13}CO^+ 3-2, actually always plays the major role in determining V_{LSR} . The uncertainty of the systemic velocity is also computed during the weighted average.

Line identification turns out to be a hard task because of the limited frequency coverage. In the first step, we recognize all line-like features that are stronger than 3σ level in terms of integrated line intensity in the spectra data. Then, the obtained line frequencies (corrected for the object velocity) are compared with the line frequency lists, SPLATALOGUE ⁴, CDMS ⁵(Müller et al. 2001, 2005) and JPL ⁶(Pickett et al. 1998), to identify the carriers of the lines. For simple molecules of which only one transition is observed in our observed frequency ranges, their identification is usually tentative (e.g., H_2CCO and OC^{34}S), unless they are well known abundant species (e.g., H^{13}CO^+ , SiO, CH_3OH and SO). On the opposite side, line-rich spectra of some complex molecules (some are the so called ‘weeds’ lines) are covered by our observations and used as fingerprints for these species. We plot the expected relative line

strengths at various representative LTE temperatures in optically thin cases to help the line identification by eyes.

5. Results

5.1. Detected lines

All the detected lines are listed in Table 2 which includes 46 entries. We confidently identified eight molecular species in our EGOs: H^{13}CO^+ (70 objects), SiO (37 objects), SO (43 objects), CH_3OH (38 objects), CH_3OCH_3 (8 objects), $\text{CH}_3\text{CH}_2\text{CN}$ (5 objects), HCOOCH_3 (6 objects), and HN^{13}C (1 objects), and possibly three additional species: H_2CCO (9 objects), c-HCCCH (7 objects) and OC^{34}S (1 objects). There are also five weak unidentified lines (U-lines). All the lines in Table 2 are grouped for the two sidebands and sorted in increasing frequency order, for the ease of comparison with the spectral plots presented in Fig. 10.

5.2. Line parameters and spectral plots

The detailed line parameters of each detected lines are presented in Table A4. The columns are (1) object name, (2) transition, (3-4) observed frequency ν and uncertainty σ_ν (MHz), (5-6) full width at half maximum (FWHM) of the line and uncertainty σ_{FWHM} (km s^{-1}), (7-8) main-beam temperature T_{MB} and uncertainty (mK), (9-10) line area I_{int} and uncertainty σ_I (K km/s), and (11) signal to noise ratio ($\text{SNR} = I_{\text{int}}/\sigma_I$). Most of the line parameters determined by fitting a single Gaussian profile using GILDAS/CLASS software, while the integrated line area (I_{int}) is usually obtained by directly integrating the observed line profiles. However, there are several special cases: 1) Some lines that show obvious broad line wings are fit with two-Gaussian profiles forced to the same line center position. The two overlapped components are listed as separate records in Table A4; 2) Blended lines, such as the methanol lines in the LSB, are fit with multiple Gaussian profiles at fixed catalog frequencies. The integrated line areas (I_{int}) of these lines are computed from the fitting; 3) Some blended lines that are not differentiable ($\Delta\nu < 1 \text{ MHz}$) are fit with a single Gaussian profile and the same line parameters are assigned to both blended lines. Baseline RMS is used to estimate upper limit for undetected lines.

⁴splatalogue at <http://www.splatalogue.net/>

⁵CDMS at <http://www.astro.uni-koeln.de/cdms/catalog>

⁶JPL line list at <http://spec.jpl.nasa.gov/ftp/pub/catalog/catform.html>

Table 1: Parameters of the EGOs: baseline RMS level at a resolution of 1 km s^{-1} , V_{sys} (Sect. 4), and kinematic distances (Sect. 6.3).

Object	RA(2000)	DEC(2000)	RMS-LSB (mK)	RMS-USB (mK)	$V_{\text{sys}}(\sigma)$ (km s^{-1})	NoteV ^a	D_{kin} (kpc)	NoteD ^b
G10.29−0.13	18 ^h 08 ^m 49.3 ^s	−20 ^d 05 ^m 57 ^s	24	30	13.32(17)		2.11 ^{+0.72} _{−0.92}	IRDC
G10.34−0.14	18 ^h 09 ^m 00.0 ^s	−20 ^d 03 ^m 35 ^s	23	34	12.32(08)		1.99 ^{+0.74} _{−0.95}	IRDC
G11.11−0.11	18 ^h 10 ^m 28.3 ^s	−19 ^d 22 ^m 31 ^s	38	50	29.79(10)		3.45 ^{+0.45} _{−0.53}	IRDC
G11.92−0.61	18 ^h 13 ^m 58.1 ^s	−18 ^d 54 ^m 17 ^s	23	33	35.88(06)		3.72 ^{+0.39} _{−0.46}	IRDC
G12.02−0.21	18 ^h 12 ^m 40.4 ^s	−18 ^d 37 ^m 11 ^s	26	34	−3.43(30)	weak	16.92 ^{+1.57} _{−1.17}	Outer
G12.20−0.03	18 ^h 12 ^m 23.6 ^s	−18 ^d 22 ^m 54 ^s	39	51	51.15(14)		4.47 ^{+0.30} _{−0.33}	11.95 ^{+0.33} _{−0.30} N/F
G12.42+0.50	18 ^h 10 ^m 51.1 ^s	−17 ^d 55 ^m 50 ^s	18	28	17.76(01)		2.30 ^{+0.59} _{−0.73}	Z1/2
G12.68−0.18	18 ^h 13 ^m 54.7 ^s	−18 ^d 01 ^m 47 ^s	40	52	55.54(10)	new	4.59 ^{+0.23} _{−0.31}	11.80 ^{+0.31} _{−0.28} N/F
G12.91−0.03	18 ^h 13 ^m 48.2 ^s	−17 ^d 45 ^m 39 ^s	27	33	56.46(08)		4.60 ^{+0.27} _{−0.31}	IRDC
G12.91−0.26	18 ^h 14 ^m 39.5 ^s	−17 ^d 52 ^m 00 ^s	24	33	37.40(03)		3.67 ^{+0.38} _{−0.44}	12.71 ^{+0.44} _{−0.38} N/F
G14.33−0.64	18 ^h 18 ^m 54.4 ^s	−16 ^d 47 ^m 46 ^s	26	35	22.16(02)		2.47 ^{+0.51} _{−0.59}	IRDC
G14.63−0.58	18 ^h 19 ^m 15.4 ^s	−16 ^d 30 ^m 07 ^s	25	30	18.32(04)		2.13 ^{+0.55} _{−0.63}	IRDC
G16.58−0.08	18 ^h 21 ^m 15.0 ^s	−14 ^d 33 ^m 02 ^s	21	29	39.74(72)	weak	3.38 ^{+0.36} _{−0.40}	IRDC
G16.59−0.05	18 ^h 21 ^m 09.1 ^s	−14 ^d 31 ^m 48 ^s	24	33	59.54(05)		4.31 ^{+0.27} _{−0.30}	IRDC
G16.61−0.24	18 ^h 21 ^m 52.7 ^s	−14 ^d 35 ^m 51 ^s	26	32	42.87(22)	new	3.54 ^{+0.34} _{−0.38}	IRDC
G17.96+0.08	18 ^h 23 ^m 21.0 ^s	−13 ^d 15 ^m 11 ^s	24	32	22.30(26)	weak	2.18 ^{+0.47} _{−0.54}	HISA
G18.67+0.03	18 ^h 24 ^m 53.7 ^s	−12 ^d 39 ^m 20 ^s	22	29	80.04(28)		11.01 ^{+0.25} _{−0.28}	HISA
G18.89−0.47	18 ^h 27 ^m 07.9 ^s	−12 ^d 41 ^m 36 ^s	23	28	66.21(07)		4.38 ^{+0.26} _{−0.28}	IRDC
G19.01−0.03	18 ^h 25 ^m 44.8 ^s	−12 ^d 22 ^m 46 ^s	15	22	59.78(04)		4.11 ^{+0.28} _{−0.30}	IRDC
G19.36−0.03	18 ^h 26 ^m 25.8 ^s	−12 ^d 03 ^m 57 ^s	22	28	26.69(05)		2.38 ^{+0.43} _{−0.48}	IRDC
G19.61−0.12	18 ^h 27 ^m 13.6 ^s	−11 ^d 53 ^m 20 ^s	26	34	57.03(20)		3.95 ^{+0.29} _{−0.31}	11.87 ^{+0.31} _{−0.29} N/F
G19.61−0.14	18 ^h 27 ^m 16.8 ^s	−11 ^d 53 ^m 51 ^s	19	23	56.98(19)	new	3.95 ^{+0.29} _{−0.31}	11.87 ^{+0.31} _{−0.29} N/F
G19.88−0.53	18 ^h 29 ^m 14.7 ^s	−11 ^d 50 ^m 23 ^s	21	29	43.67(02)		3.31 ^{+0.34} _{−0.37}	HISA
G20.24+0.07	18 ^h 27 ^m 44.6 ^s	−11 ^d 14 ^m 54 ^s	22	29	70.03(32)	weak	4.44 ^{+0.26} _{−0.28}	11.32 ^{+0.28} _{−0.26} N/F
G21.24+0.19	18 ^h 29 ^m 10.2 ^s	−10 ^d 18 ^m 11 ^s	22	28	25.40(09)		2.19 ^{+0.43} _{−0.47}	HISA
G22.04+0.22	18 ^h 30 ^m 34.7 ^s	−09 ^d 34 ^m 47 ^s	21	30	51.16(05)		3.54 ^{+0.31} _{−0.34}	HISA
G23.01−0.41	18 ^h 34 ^m 40.2 ^s	−09 ^d 00 ^m 38 ^s	18	28	77.45(05)		4.58 ^{+0.26} _{−0.27}	HISA
G23.82+0.38	18 ^h 33 ^m 19.5 ^s	−07 ^d 55 ^m 37 ^s	21	28	76.41(24)		4.52 ^{+0.27} _{−0.28}	10.85 ^{+0.28} _{−0.27} N/F
G23.96−0.11	18 ^h 35 ^m 22.3 ^s	−08 ^d 01 ^m 28 ^s	21	30	72.10(10)	new	4.34 ^{+0.27} _{−0.29}	21cm
G24.00−0.10	18 ^h 35 ^m 23.5 ^s	−07 ^d 59 ^m 32 ^s	21	30	70.61(16)		4.28 ^{+0.28} _{−0.29}	21cm
G24.11−0.17	18 ^h 35 ^m 52.6 ^s	−07 ^d 55 ^m 17 ^s	22	32	80.48(20)		4.66 ^{+0.27} _{−0.27}	IRDC
G24.17−0.02	18 ^h 35 ^m 25.0 ^s	−07 ^d 48 ^m 15 ^s	21	30				
G24.33+0.14	18 ^h 35 ^m 08.1 ^s	−07 ^d 35 ^m 04 ^s	22	30	113.79(07)	new	5.93 ^{+0.30} _{−0.28}	9.37 ^{+0.28} _{−0.30} N/F
G24.63+0.15	18 ^h 35 ^m 40.1 ^s	−07 ^d 18 ^m 35 ^s	23	30	53.16(16)		3.51 ^{+0.31} _{−0.33}	HISA
G24.94+0.07	18 ^h 36 ^m 31.5 ^s	−07 ^d 04 ^m 16 ^s	24	32	41.25(16)		2.92 ^{+0.35} _{−0.37}	12.32 ^{+0.37} _{−0.35} N/F
G25.27−0.43	18 ^h 38 ^m 57.0 ^s	−07 ^d 00 ^m 48 ^s	26	35	59.14(03)	chen10	3.75 ^{+0.30} _{−0.32}	HISA
G25.38−0.15	18 ^h 38 ^m 08.1 ^s	−06 ^d 46 ^m 53 ^s	20	28	95.12(07)		5.21 ^{+0.28} _{−0.27}	IRDC
G27.97−0.47	18 ^h 44 ^m 03.6 ^s	−04 ^d 38 ^m 02 ^s	25	34				
G28.28−0.36	18 ^h 44 ^m 13.2 ^s	−04 ^d 18 ^m 04 ^s	32	45	49.07(24)		3.20 ^{+0.33} _{−0.35}	11.60 ^{+0.35} _{−0.33} N/F
G28.83−0.25	18 ^h 44 ^m 51.3 ^s	−03 ^d 45 ^m 48 ^s	32	44	87.31(12)		4.92 ^{+0.32} _{−0.31}	HISA
G28.85−0.23	18 ^h 44 ^m 47.5 ^s	−03 ^d 44 ^m 15 ^s	24	31	96.68(23)	weak,new	5.35 ^{+0.35} _{−0.32}	9.37 ^{+0.32} _{−0.35} N/F
G29.84−0.47	18 ^h 47 ^m 28.8 ^s	−02 ^d 58 ^m 03 ^s	32	42				
G29.89−0.77	18 ^h 48 ^m 37.7 ^s	−03 ^d 03 ^m 44 ^s	33	45	83.85(02)	chen10	4.78 ^{+0.33} _{−0.32}	IRDC
G29.91−0.81	18 ^h 48 ^m 47.6 ^s	−03 ^d 03 ^m 31 ^s	33	44	83.90(02)	chen10	4.78 ^{+0.33} _{−0.32}	Z1/2
G29.96−0.79	18 ^h 48 ^m 50.0 ^s	−03 ^d 00 ^m 21 ^s	33	40	85.12(03)	chen10	4.84 ^{+0.33} _{−0.32}	IRDC
G34.26+0.15	18 ^h 53 ^m 16.4 ^s	+01 ^d 15 ^m 07 ^s	23	30	58.88(03)		3.64 ^{+0.36} _{−0.36}	21cm
G34.28+0.18	18 ^h 53 ^m 15.0 ^s	+01 ^d 17 ^m 11 ^s	27	36	55.99(09)		3.49 ^{+0.36} _{−0.36}	IRDC
G34.39+0.22	18 ^h 53 ^m 19.0 ^s	+01 ^d 24 ^m 08 ^s	24	31	57.46(05)		3.57 ^{+0.36} _{−0.36}	IRDC
G34.41+0.24	18 ^h 53 ^m 17.9 ^s	+01 ^d 25 ^m 25 ^s	25	36	57.86(04)		3.59 ^{+0.36} _{−0.36}	IRDC
G35.03+0.35	18 ^h 54 ^m 00.5 ^s	+02 ^d 01 ^m 18 ^s	27	36	53.11(05)		3.35 ^{+0.37} _{−0.37}	10.41 ^{+0.37} _{−0.37} N/F
G35.04−0.47	18 ^h 56 ^m 58.1 ^s	+01 ^d 39 ^m 37 ^s	28	38	50.73(12)		3.23 ^{+0.37} _{−0.37}	IRDC

Table 1: (continued)

Object	RA(2000)	DEC(2000)	RMS-LSB (mK)	RMS-USB (mK)	$V_{\text{sys}}(\sigma)$ (km s^{-1})	NoteV ^a	D_{kin} (kpc)	NoteD ^b
G35.13-0.74	18 ^h 58 ^m 06.4 ^s	+01 ^d 37 ^m 01 ^s	28	38	34.20(04)		2.34 ^{+0.38} _{-0.40}	HISA
G35.15+0.80	18 ^h 52 ^m 36.6 ^s	+02 ^d 20 ^m 26 ^s	28	40	74.89(18)		4.53 ^{+0.42} _{-0.39}	Z1/2
G35.20-0.74	18 ^h 58 ^m 12.9 ^s	+01 ^d 40 ^m 33 ^s	28	39	33.49(03)		2.30 ^{+0.38} _{-0.40}	Z1/2
G35.68-0.18	18 ^h 57 ^m 05.0 ^s	+02 ^d 22 ^m 00 ^s	28	37	27.76(10)		1.97 ^{+0.40} _{-0.41}	IRDC
G35.79-0.17	18 ^h 57 ^m 16.7 ^s	+02 ^d 27 ^m 56 ^s	28	35	61.54(13)	new	3.81 ^{+0.39} _{-0.38}	IRDC
G35.83-0.20	18 ^h 57 ^m 26.9 ^s	+02 ^d 29 ^m 00 ^s	23	30	28.38(04)	chen10	2.01 ^{+0.40} _{-0.41}	HISA
G36.01-0.20	18 ^h 57 ^m 45.9 ^s	+02 ^d 39 ^m 05 ^s	27	34	87.25(04)	chen10	5.44 ^{+0.51} _{-0.52}	8.15 ^{+0.52} _{-0.52} N/F
G37.48-0.10	19 ^h 00 ^m 07.0 ^s	+03 ^d 59 ^m 53 ^s	29	39	58.93(20)		3.72 ^{+0.41} _{-0.39}	9.61 ^{+0.39} _{-0.41} N/F
G37.55+0.20	18 ^h 59 ^m 07.5 ^s	+04 ^d 12 ^m 31 ^s	28	38				
G39.10+0.49	19 ^h 00 ^m 58.1 ^s	+05 ^d 42 ^m 44 ^s	28	40	23.10(23)		11.34 ^{+0.43} _{-0.42}	HISA
G39.39-0.14	19 ^h 03 ^m 45.3 ^s	+05 ^d 40 ^m 43 ^s	31	42	65.64(15)		4.24 ^{+0.51} _{-0.45}	8.74 ^{+0.45} _{-0.51} N/F
G40.28-0.22	19 ^h 05 ^m 41.3 ^s	+06 ^d 26 ^m 13 ^s	24	32	73.52(04)		4.97 ^{+0.58} _{-0.58}	7.85 ^{+0.58} _{-0.58} N/F
G40.28-0.27	19 ^h 05 ^m 51.5 ^s	+06 ^d 24 ^m 39 ^s	26	36	71.26(42)	weak	4.76 ^{+0.54} _{-0.54}	Z1/2
G40.60-0.72	19 ^h 08 ^m 03.3 ^s	+06 ^d 29 ^m 15 ^s	20	27	64.43(88)	weak	4.27 ^{+0.56} _{-0.48}	8.49 ^{+0.48} _{-0.56} N/F
G43.04-0.45	19 ^h 11 ^m 38.9 ^s	+08 ^d 46 ^m 39 ^s	27	34	57.50(12)		3.99 ^{+0.61} _{-0.51}	8.29 ^{+0.51} _{-0.61} N/F
G44.01-0.03	19 ^h 11 ^m 57.2 ^s	+09 ^d 50 ^m 05 ^s	27	35	64.48(05)	chen10	4.80 ^{+0.70} _{-0.70}	7.28 ^{+0.70} _{-0.70} N/F
G45.47+0.05	19 ^h 14 ^m 25.6 ^s	+11 ^d 09 ^m 28 ^s	27	35	62.81(05)		5.89 ^{+1.74} _{-1.74}	Ave
G45.47+0.13	19 ^h 14 ^m 07.3 ^s	+11 ^d 12 ^m 16 ^s	27	34	61.61(08)		6.95 ^{+0.79} _{-0.79}	HII
G45.50+0.12	19 ^h 14 ^m 13.0 ^s	+11 ^d 13 ^m 30 ^s	18	25	61.19(05)	chen10	7.00 ^{+0.77} _{-0.77}	HII
G45.80-0.36	19 ^h 16 ^m 31.1 ^s	+11 ^d 16 ^m 11 ^s	19	26	59.18(14)	new	4.59 ^{+0.73} _{-0.73}	7.12 ^{+0.73} _{-0.73} N/F
G48.66-0.30	19 ^h 21 ^m 48.0 ^s	+13 ^d 49 ^m 21 ^s	26	36	33.60(03)	chen10	8.48 ^{+0.56} _{-0.51}	HISA
G49.07-0.33	19 ^h 22 ^m 41.9 ^s	+14 ^d 10 ^m 12 ^s	19	26	60.85(13)	new	5.50 ^{+1.57} _{-1.57}	Tan
G49.27-0.32	19 ^h 23 ^m 02.2 ^s	+14 ^d 20 ^m 52 ^s	20	26	66.04(07)	chen10	5.48 ^{+1.58} _{-1.58}	Tan
G49.27-0.34	19 ^h 23 ^m 06.7 ^s	+14 ^d 20 ^m 13 ^s	28	36	67.76(05)		5.48 ^{+1.58} _{-1.58}	Tan
G49.42+0.33	19 ^h 20 ^m 59.1 ^s	+14 ^d 46 ^m 53 ^s	19	26	-20.76(30)	weak	12.20 ^{+0.56} _{-0.53}	Outer
G49.91+0.37	19 ^h 21 ^m 47.5 ^s	+15 ^d 14 ^m 26 ^s	20	27	8.33(26)	new	0.84 ^{+0.49} _{-0.49}	9.98 ^{+0.49} _{-0.49} N/F
G50.36-0.42	19 ^h 25 ^m 32.8 ^s	+15 ^d 15 ^m 38 ^s	20	25	38.87(23)	weak,new	3.18 ^{+0.61} _{-0.61}	HISA
G53.92-0.07	19 ^h 31 ^m 23.0 ^s	+18 ^d 33 ^m 00 ^s	20	25	42.90(09)		4.95 ^{+1.68} _{-1.68}	Tan
G54.11-0.04	19 ^h 31 ^m 40.0 ^s	+18 ^d 43 ^m 53 ^s	20	27				
G54.11-0.08	19 ^h 31 ^m 48.8 ^s	+18 ^d 42 ^m 57 ^s	20	26	38.41(13)		3.81 ^{+0.93} _{-0.93}	6.04 ^{+0.93} _{-0.93} N/F
G54.45+1.01	19 ^h 28 ^m 25.7 ^s	+19 ^d 32 ^m 20 ^s	26	35	34.72(35)	weak	3.32 ^{+0.79} _{-0.79}	Z1/2
G56.13+0.22	19 ^h 34 ^m 51.5 ^s	+20 ^d 37 ^m 28 ^s	29	36				
G57.61+0.02	19 ^h 38 ^m 40.8 ^s	+21 ^d 49 ^m 35 ^s	27	35	37.01(14)	new	4.50 ^{+1.76} _{-1.76}	Tan
G58.09-0.34	19 ^h 41 ^m 03.9 ^s	+22 ^d 03 ^m 39 ^s	28	39				
G58.78+0.64	19 ^h 38 ^m 49.6 ^s	+23 ^d 08 ^m 40 ^s	25	35	32.55(13)		4.35 ^{+1.78} _{-1.78}	Tan
G58.79+0.63	19 ^h 38 ^m 55.3 ^s	+23 ^d 09 ^m 04 ^s	26	37				
G59.79+0.63	19 ^h 41 ^m 03.1 ^s	+24 ^d 01 ^m 15 ^s	26	36	33.97(12)		4.23 ^{+1.80} _{-1.80}	Tan
G62.70-0.51	19 ^h 51 ^m 51.1 ^s	+25 ^d 57 ^m 40 ^s	26	34				

A machine-readable format of this table is also available through ADS.

^a**new** – new velocity not presented in Chen et al. (2010);

chen10 – velocity from Chen et al. (2010), non-detection of H¹³CO⁺ 3-2 in this work;

weak – the detection level of H¹³CO⁺ 3-2 is lower than 5 σ in terms of integrated line area in our observations. Thus the velocity should be used with caution.

^b**Tan** – No near/far kinematic distance ambiguity at the tangential point;

Outer – No near/far kinematic distance ambiguity outside of the solar circle;

IRDC – Near kinematic distance determined by the association to IRDCs;

Z1/2 – Near distance is preferred if the perpendicular distance is smaller than the scale height of 60 pc of the Galaxy but larger than or nearly equal to two times of the scale height;

HISA – HI self absorption method (Roman-Duval et al. 2009);

21cm – The 21cm continuum absorption line method (Roman-Duval et al. 2009);

HII – HI absorption line method for H II regions (Kolpak et al. 2003);

Ave – Average of near and far kinematic distances, with the near/far difference included in uncertainty;

N/F – Both the near and far kinematic distances are given.

Table 2: Detected lines toward the EGOs. Note that the string ‘(E+A)’ after the transition $\text{CH}_3\text{OCH}_3, 10_{2,9} - 9_{1,8}$ means it is a blending of four transitions: EA, AE, EE, and AA.

ν_{Catalog} (MHz)	Transition (Lower Sideband)	Note ^a	ν_{Catalog} (MHz)	Transition (Lower Sideband)	Note ^a
251501.40980	$\text{CH}_3\text{CH}_2\text{CN } 28_{5,24} - 27_{5,23}$		260191.98200	$\text{H}_2\text{CCO } 13_{1,13} - 12_{1,12}$	
251517.26200	$\text{CH}_3\text{OH } 8_{3,5} - 8_{2,6} - +$		260221.65800	$\text{CH}_3\text{CH}_2\text{CN } 29_{6,24} - 28_{6,23}$	
251527.30230	$c\text{-HCCCH } 6_{2,5} - 5_{1,4}$		260229.15800	$\text{CH}_3\text{CH}_2\text{CN } 29_{6,23} - 28_{6,22}$	
251583.62730	$\text{CH}_3\text{OCH}_3 10_{2,9} - 9_{1,8}(\text{E+A})$		260244.49800	$\text{HCOOCH}_3 21_{3,18} - 20_{3,17}\text{E}$	
251607.12090	$\text{CH}_3\text{CH}_2\text{CN } 28_{5,23} - 27_{5,22}$		260255.08000	$\text{HCOOCH}_3 21_{3,18} - 20_{3,17}\text{A}$	b
251641.66700	$\text{CH}_3\text{OH } 7_{3,4} - 7_{2,5} - +$		260255.33900	$\text{H}^{13}\text{CO}^+ 3-2$	b
251668.84660	$\text{CH}_3\text{CH}_2\text{CN } 28_{4,25} - 27_{4,24}$		260329.31200	$\text{CH}_3\text{OCH}_3 19_{5,15} - 19_{4,16}\text{EE}$	
251738.52000	$\text{CH}_3\text{OH } 6_{3,3} - 6_{2,4} - +$		260365.00000	U260365	
251811.88200	$\text{CH}_3\text{OH } 5_{3,2} - 5_{2,3} - +$		260384.26800	$\text{HCOOCH}_3 21_{8,13} - 20_{8,12}\text{E}$	
251825.77000	$\text{SO}^3\Sigma 6_5 - 5_4$		260403.39210	$\text{CH}_3\text{OCH}_3 16_{5,11} - 16_{4,12}\text{EE}$	b
251866.57900	$\text{CH}_3\text{OH } 4_{3,1} - 4_{2,2} - +$		260404.02600	$\text{HCOOCH}_3 21_{8,14} - 20_{8,13}\text{E}$	b
251890.90100	$\text{CH}_3\text{OH } 5_{3,3} - 5_{2,4} + -$		260518.12200	$\text{SiO}, 6-5$	
251895.72800	$\text{CH}_3\text{OH } 6_{3,4} - 6_{2,5} + -$	p	260664.76700	$\text{CH}_3\text{CH}_2\text{CN } 29_{5,26} - 28_{5,25}$	b
251900.49500	$\text{CH}_3\text{OH } 4_{3,2} - 4_{2,3} + -$	p	260664.77000	$\text{CH}_3\text{CH}_2\text{CN } 29_{4,26} - 28_{4,25}$	b
251905.81200	$\text{CH}_3\text{OH } 3_{3,0} - 3_{2,1} - +$	p	260727.86540	$\text{CH}_3\text{OCH}_3 18_{5,14} - 18_{4,15}\text{EE}$	
251917.04200	$\text{CH}_3\text{OH } 3_{3,1} - 3_{2,2} + -$	p	260758.38210	$\text{CH}_3\text{OCH}_3 6_{3,3} - 5_{2,4}\text{EE}$	
251923.63100	$\text{CH}_3\text{OH } 7_{3,5} - 7_{2,6} + -$	p	260796.74435	U260797	
251984.70200	$\text{CH}_3\text{OH } 8_{3,6} - 8_{2,7} + -$	p	260864.87361	U260865	
252090.38000	$\text{CH}_3\text{OH } 9_{3,7} - 9_{2,8} + -$		260991.80790	$\text{OC}^{34}\text{S } 22-21$	
252252.85000	$\text{CH}_3\text{OH } 10_{3,8} - 10_{2,9} + -$		261147.89810	$\text{CH}_3\text{OCH}_3 17_{5,13} - 17_{4,14}\text{EE}$	b
252477.92270	U252478		261148.90400	$\text{HCOOCH}_3 21_{5,17} - 20_{5,16}\text{E}$	b
252485.64900	$\text{CH}_3\text{OH } 11_{3,9} - 11_{2,10} + -$		261165.45600	$\text{HCOOCH}_3 21_{5,17} - 20_{5,16}\text{A}$	
252557.33758	U252557		261263.31010	$\text{HN}^{13}\text{C } 3-2$	

^a**p** = usually partially blended with neighbouring lines, depending on the line width in each object; **b** = totally blended (undistinguishable).

The spectral plots of both sidebands are presented in Fig. A10 source by source. The molecular species is marked for each detected line. The identity of each transition in the plots can be recognized by referring to the line list in Table 2 in which lines are sorted in increasing frequency order for the LSB and USB separately.

5.3. Individual species

The detected species can be divided into two groups: surely detected species – those well known abundant species or those with characteristic multiple lines in our frequency ranges; tentatively detected species – those with only one transitions detectable in our frequency ranges and unidentified lines.

5.3.1. Surely detected species

H¹³CO⁺ 3-2 (260255 MHz) is detected in 79 per cent (70 out of 89) of the EGOs. The main beam temperature ranges from 67 mK (3.12 Jy) to 3.084 K (143.4 Jy). Five EGOs show broad H¹³CO⁺ 3-2 line wings that could be caused by high velocity outflows. We fit these broad lines with double Gaussian profiles that are forced to the same line center and the second component (usually the broader one) is marked by ‘s’ in the last column of Table A4. The widths of the broad component range from 5.5–31.6 km s⁻¹. The widths of the narrow component of these EGOs and that of the other narrow-line EGOs, range from 1.5–5.7 km s⁻¹, with equal mean and median width of 3.4 km s⁻¹.

SiO 6-5 (260518 MHz) is detected in about 42 per cent (37 out of 89) of our observed EGO samples. Excluding those H¹³CO⁺ 3-2 non-detections (due to limited sensitivity), a higher detection rate of ~ 53 per cent among the 70 H¹³CO⁺ 3-2 detected EGOs is found and it may be closer to the true occurrence frequency of outflows among EGOs. The line strength ranges from 40–448 mK. Most of them have broad line widths (FWHM > 5 km s⁻¹), supporting that the SiO line might be emitted from outflow regions. For 11 EGOs that show obvious line wings, we fit the SiO line profiles with a double Gaussian profile. The obtained line width (FWHM) of the broad components has a median value of ~ 37 km s⁻¹, indicating the existence of fast outflows. The FWHM of

the narrow component ranges from 2.1–9.2 km s⁻¹. The diversity of the SiO line profiles will be discussed in detail in a separate paper.

CH₃OH line series (251517–252486 MHz) are detected in 43 per cent (38 out of 89) of our EGOs. They appear only in the lower sideband, all belonging to the A-type J₃–J₂ inter-K ladder transitions. They are composed of two series corresponding to the + and – parities of the upper levels, respectively. Several lines are partially blended in the center of our LSB. The fitted line strength ranges from 25–489 mK. The fitted FWHM ranges from 1.8–25.2 km s⁻¹, with a mean of 5.7 km s⁻¹. Three EGOs, G10.34–0.14, G12.91–0.26 and G23.01–0.41, show clear evidence of broad line wings. With a double Gaussian profile fitting, the FWHM of the broad components are found to range from 13.6–23.52 km s⁻¹, possibly indicating fast outflows.

SO³Σ_g 6₅–5₄ (251826 MHz) is detected in 43 EGOs, with a detection rate of ~ 48 per cent among all 89 EGOs or ~ 61 per cent among the 70 H¹³CO⁺ emitters. The line strength ranges from 43–2097 mK. Eight EGOs show broad SO line wings. Double Gaussian profiles are fit to them. The width of the broad SO line component of the eight EGOs ranges from 11.0–21.1 km s⁻¹ which possibly originate from fast outflows. The central narrow component of the eight EGOs and the other 35 detected objects have their FWHM line width in the 2.2–14.2 km s⁻¹ range, with a mean of 5.8 km s⁻¹.

CH₃OCH₃ line series (251583–251971, 261329–261148 MHz) All strong transitions of the EE symmetry species of dimethyl ether with its lower energy level up to 300 cm⁻¹ are definitely detected at least in three EGOs (all associated with well known HII regions): G12.91–0.26, G14.33–0.64, and G34.41+0.24. We do not detect the lines of the other three symmetry species: AA, AE, and EA, except the case of the line at 251583.62730 MHz that could be a mixture of the AA, AE, EA, and EE transitions. However, because no other lines of the AA, AE, and EA states are seen, we assign this line for the EE species only (see in Table 2). Weaker CH₃OCH₃ EE lines are possibly also detected in another six objects. The line strength ranges from 48–203 mK. Their FWHM ranges from 1.9–10.6 km s⁻¹, with a mean width of 6.9 km s⁻¹.

HCOOCH₃ line series (260244-261166 MHz) Similarly, many lines of methyl formate fall in the USB of our observations. Several strongest lines whose lower energy levels are lower than ~ 120 K are clearly detected in the USB at least in two EGOs (both associated with well known objects): G12.91-0.26, and G34.41+0.24, and possibly in another three EGOs: G35.20-0.74, G12.68-0.18, and G23.01-0.41. For the case of another object, G24.33+0.14, we take it as non-detection, due to the blending of the lines with that of CH₃OCH₃. The detection of a single line, HCOOCH₃ 30_{3,28} – 30_{2,29}, in G14.33–0.64 is also doubtful, unless it is a maser line, because the other transitions that are expected to be equally strong are not detected. The line strength ranges from 55-186 mK, the FWHM from 1.9-12.3 km s⁻¹, with a mean width of 6.9 km s⁻¹.

CH₃CH₂CN line series (251503-251669, 260221-260665 MHz) Many lines of ethyl cyanide are covered by our observed frequency ranges. Several strongest transitions are clearly detected at least in two EGOs, G12.91-0.26 and G34.41+0.24, and possibly in another three EGOs, G12.68-0.18, G23.01-0.41, and G24.33+0.14. The line strengths are in the 44-243 mK range. Their FWHM ranges from 1.5-9.3 km s⁻¹, with a mean width of 6.1 km s⁻¹.

HN¹³C 3-2 (261263 MHz) is surely detected by chance in only one source, G24.33+0.14. This object has a very large $V_{\text{sys}} \approx 114$ km s⁻¹, so that the HN¹³C 3-2 line comes into our frequency coverage by large Doppler shift when the object was initially observed by assuming zero source velocity. The frequency of this line is not covered by any other of our observations. The strength of this line is stronger than one half of the H¹³CO⁺ 6-5 line and thus is in agreement with an abundant species like HN¹³C.

5.3.2. Tentatively detected species

H₂CCO (260192 MHz) Only a group of the 13_{Ka,Kc}–12_{Ka,Kc} transitions of ethenone fall in our frequency range, among which only the 13_{1,13} – 12_{1,12} transition is strong enough to be detectable by our observations. This line is clearly detected in 9 of our observed EGOs. Further observations of more transitions will hopefully confirm the detection of this molecule in these star forming regions.

c-HCCCH (251527 MHz) Cyclopropenyliene is an asymmetric top with ring structure. Some transitions fall in our covered frequency ranges. However, only the ortho c-HCCCH transition 6_{2,5}-5_{1,4} is possibly seen in our data. This line is clearly detected in seven EGOs: G12.42+0.50, G12.91-0.26, G16.59-0.05, G19.88-0.53, G34.41+0.24, G35.20-0.74, and G49.27-0.34. We note that the line looks relative very strong in G49.27-0.34, say, it reaches about one half of the strength of the SO ³Σ 5₆ – 4₅ line and is stronger than all CH₃OH lines which are almost not detected in this object. We caution that, because only one line is detected for this species, other transitions need to be observed to get its identity confirmed.

OC³⁴S 22-21 (260992 MHz) The only transition of this species covered in our frequency ranges is possibly detected in one target, G23.01-0.41. But we note that the line is weak and shifted by ~ 5 MHz to lower frequency. The identification of this line is quite tentative.

U-lines There are five line-like features for which we can not find reasonable carriers in either of the line list databases. They are all weak lines with 3σ-4σ detection levels in terms of integrated line intensity. *U260865* is clearly detected as a weak narrow line in four objects. Its average observed frequency is 260864.89 ± 0.99 MHz. The other U-lines are only detected in a single object and thus their detection is even less certain. *U260797* has a frequency close to that of OS¹⁷O 4_{4,1}-5_{3,2}, but the non-detection of an expected equally strong line OS¹⁷O 4_{4,0}-5_{3,3} (260808.384 MHz) in our data casts doubt on OS¹⁷O as its carrier.

6. Discussions

In this section, we will discuss the detectability of dense gas and outflow tracers and demonstrate that most of the observed EGOs are associated with outflows and dense gas. We also compare the velocity-integrated spectral line luminosities and the line widths between or among our high density tracer lines and lower density tracer lines (isotopic CO 1-0 lines) and continuum fluxes from literature to discuss the multiple subcomponent size-scale properties of the EGO clouds. Further analysis of the complex organic species and out-

flows will be retained for future papers.

Supplemented literature data used in this work include

- ^{12}CO , ^{13}CO , and C^{18}O 1-0 lines. They are from Chen et al. (2010) for nearly the same sample of EGOs. Several EGOs have multiple C^{18}O 1-0 line peaks in which case only the peak closest to our H^{13}CO^+ 3-2 line is used.
- *Spitzer MIPS* $24\ \mu\text{m}$ continuum fluxes. They are taken from Cyganowski et al. (2008) as tracers of warm dusty cloud cores. Note that some EGOs do have $24\ \mu\text{m}$ counterparts on their *Spitzer MIPS* images but their fluxes were not measured by Cyganowski et al. (2008) due to spatial confusion issues. Thus the available $24\ \mu\text{m}$ fluxes are not complete and are available only for 53 of our 89 EGO samples (including $24\ \mu\text{m}$ upper limits).
- BGPS 1.1 mm continuum fluxes. They are taken from the CSO Bolocam Galactic Plane Survey by Rosolowsky et al. (2010) as tracers of dense molecular clumps. We adopt the flux measurements made with an aperture diameter of $40''$, because it is the closest to our beam size ($29''$). The cross identification is done by cone search in Vizier⁷ database within a radius of $40''$ around the EGO positions. The 1.1 mm counterpart are found for 67 of our 89 EGOs and the resulting position discrepancies are $\sim 18''$ on average.

6.1. Dense molecular cloud cores in EGOs

Two dense gas tracers, H^{13}CO^+ 3-2 and $\text{SO } ^3\Sigma_{6_5-5_4}$, have been observed in our survey. Their critical densities are $\sim 2.11 \times 10^6\ \text{cm}^{-3}$ and $\sim 1.34 \times 10^6\ \text{cm}^{-3}$, respectively, which are computed using the molecular transition data from the LAMDA database⁸ (Schöier et al. 2005). The H^{13}CO^+ 1-0 and $\text{SO } ^3\Sigma_{6_5-5_4}$ are always the first and second strongest lines in our observed frequency range for the EGOs. Although the SO line is detected only in 43 of the 70 H^{13}CO^+ detected EGOs, all the remaining 27 SO non-detections have the weakest H^{13}CO^+ 3-2 line strengths and

also the lowest line luminosities (see Sect. 6.4), which indicates that the SO non-detections are probably due to our limited sensitivity. Thus, we conclude that all the 70 EGOs with H^{13}CO^+ detection have dense cloud cores (with density over $10^6\ \text{cm}^{-3}$) detected in our $29''$ beam.

Integrated H^{13}CO^+ 3-2 line intensities (or $3\text{-}\sigma$ upper limits) are compared with available $24\ \mu\text{m}$ and 1.1 mm continuum flux densities in Fig. 1. Clear linear correlations are found in logarithmic scales in both panels, confirming that the H^{13}CO^+ 3-2 line is a good tracer of both cool and warm dense molecular gas (similar correlations will be discussed in detail in later sections). Eighteen of the 19 H^{13}CO^+ 3-2 non-detection EGOs have counterparts in the $24\ \mu\text{m}$ or 1.1 mm or both data, but their fluxes are all among the smallest, which indicates that these H^{13}CO^+ 3-2 non-detection EGOs are also associated with dense and/or warm molecular cloud cores while the non-detection of the line could be due to our limited sensitivity.

Thus, we conclude that most of the 89 observed EGOs are associated with dense and/or warm molecular cloud cores.

6.2. Outflows in the EGOs

Our major outflow tracer SiO is a refractory species and its J=6-5 line has a high critical density of $6.22 \times 10^6\ \text{cm}^{-3}$. It should be produced through disruption of dust grains in active shock regions and excited in the post-shock region of fast outflows (Hartquist et al. 1980; Neufeld & Dalgarno 1989a; Schilke et al. 1997; Gusdorf et al. 2008). Thus, its high detection rate of 53 per cent among our H^{13}CO^+ 3-2 detected EGOs supports the idea of Cyganowski et al. (2008) that the extended green ($4.5\ \mu\text{m}$ excess) emission structures are produced by active outflow shocks. This is also in agreement to the broad line wings found in many of our SiO 6-5 lines, as exemplified in Fig. 2.

6.3. Kinematic distance

Kinematic distances are computed from the source velocity for 80 EGOs (70 H^{13}CO^+ 3-2 detections and another 10 C^{18}O 1-0 detections from Chen et al. 2010) with the updated Galactic rotation model of Reid et al. (2009). The error in the

⁷Vizier: <http://vizier.u-strasbg.fr/viz-bin/VizieR>

⁸LAMDA database: <http://www.strw.leidenuniv.nl/~moldata/>

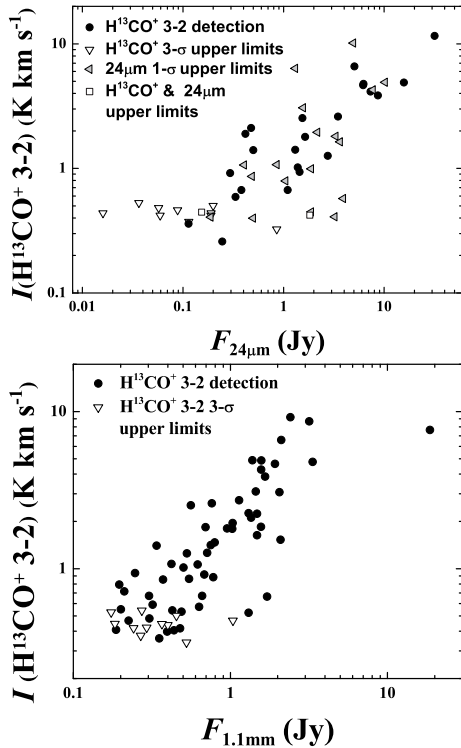


Fig. 1.— The comparison of the H^{13}CO^+ 3-2 line strength with literature 1.1 mm and $24\ \mu\text{m}$ continuum flux densities. See the analysis in Sect. 6.1.

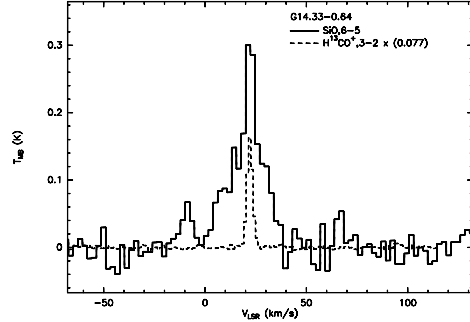


Fig. 2.— Example of the broad line wings in the SiO 6-5 profile (solid line) of G 14.33-0.64. The systemic velocity of the object is indicated by the peak of the narrower H^{13}CO^+ 3-2 line (dashed line).

distance only reflects the uncertainty of the model itself. The velocities of 12 EGOs are new compared to Chen’s results, either because of multi-peak C^{18}O 1-0 profile confusion or non-detection of HCO^+ 1-0 line in their data (they did not observe C^{18}O if this line was not detected). They are marked as ‘new’ in the ‘NoteV’ column of Table 1. Another 10 EGOs with their H^{13}CO^+ 3-2 lines not detected by us but with their C^{18}O 1-0 lines detected by Chen et al. (2010) are marked as ‘chen10’ in Table 1. Ten of our EGOs whose H^{13}CO^+ 3-2 line is weaker than 5σ in terms of velocity integrated line strength are marked as ‘weak’ in the table, because their V_{LSR} values are not as reliable as the others.

Nine EGOs do not have near/far kinematic distance ambiguity: two located outside of the solar circle (marked as ‘Outer’ in the ‘NoteD’ column in Table 1) and seven located at the tangential points of the Galactic rotation orbit (marked as ‘Tan’ in the table). For the remaining objects, we apply following criteria to differentiate the near/far kinematic distances:

- If an EGO is in front of an IRDC in the Spitzer maps (Cyganowski et al. 2008) and its near and far kinematic distances are different by more than 4 kpc, we adopt the near kinematic distance, because the chance to see IRDCs far beyond the tangential point is low, due to the lack of infrared background (marked as ‘IRDC’ in Table 1);
- If the perpendicular distance of an object

above the Galactic plane is smaller than the scale height (60 pc) of the Galaxy at near kinematic distance but larger than or roughly equal to two times of the scale height at the far distance, according to Solomon et al. (1987), the near kinematic distance is preferred (marked as ‘Z1/2’ in Table 1);

- If an EGO is associated with a ^{13}CO 1-0 molecular cloud (within $2'$ radius) whose kinematic distance ambiguity has been resolved with the HI self absorption method or 21 cm continuum absorption line method by Roman-Duval et al. (2009), their choice of near/far distance is adopted (marked as ‘HISA’ and ‘21cm’, respectively, in Table 1);
- If an EGO is associated with an HII region whose kinematic distance ambiguity has been resolved with the HI absorption line method for HII regions by Kolpak et al. (2003), their choice of near/far distance is adopted (they are marked as ‘HII’ in Table 1);
- If the near/far kinematic distances differ by less than 2 kpc, we adopt the average distance and treat the difference between the near/far distances as a part of uncertainty (marked as ‘Ave’ in Table 1).

Thus, in the last criterion, the distance uncertainty is added with $(D_{\text{far}} - D_{\text{near}})/2$. As a result, unique kinematic distance is determined for 58 EGOs in Table 1, while both near and far distances are given for the rest 22 EGOs for which the kinematic distance ambiguity can not be lifted.

6.4. The line luminosity correlations

EGOs should have a centrally enhanced gas density and temperature gradient as typical star forming clouds, because the extended green structures ($4.5 \mu\text{m}$ excess) and $24 \mu\text{m}$ point sources in the Spitzer infrared images of some or all of them already indicate the existence of active star formation activities. Thus, we can expect that our four dense gas tracers (H^{13}CO^+ 3-2, $\text{SO}^3\Sigma$ 5₆-4₅, SiO 6-5 and the CH_3OH J₃-J₂ A line series) trace relatively smaller cloud substructure size-scales, while the lower density tracer lines, ^{12}CO , ^{13}CO

and C^{18}O 1-0, trace relatively larger substructure size-scales of the EGO clouds. The three isotopic CO 1-0 lines themselves also trace slightly different cloud densities and substructure size-scales due to their different abundances. Thus, comparison of their line luminosities among different objects would shed light on how the various cloud size scales are physically related.

Line or continuum luminosity is defined as

$$L = 4\pi D^2 F,$$

where D is the distance from Sect. 6.3 and F is the velocity (kms^{-1}) integrated line flux or continuum flux density. Nominal telescope efficiency of 46.5 Jy/K is used for the ARO SMT (our survey) and 42.3 Jy/K for the PMO 13.7-m (observation of Chen et al. 2010) telescopes. For CH_3OH J₃-J₂ line series, the average line strength of all the detected transitions is used. Note that the continuum luminosities are not bolometric but monochromatic luminosities.

6.4.1. The correlations

We first check the correlations of the three possibly optically thin lines, H^{13}CO^+ 3-2, C^{18}O and ^{13}CO 1-0, with the *Spitzer MIPS* $24 \mu\text{m}$ and BGPS 1.1 mm continuum luminosities, as shown in Fig. 3. The very good correlations in the top panels demonstrates that all three lines are good tracers of dense and dusty molecular clumps. A straight line with fixed slope of unity is fit to each plot in log-log scale as (the solid lines in the figure, far distance quantities shown in open circles and upper limits shown in triangles are not used and hence forth)

$$\begin{aligned} \lg L_{\text{H}^{13}\text{CO}^+} &= \lg L_{1.1\text{mm}} + 1.78(0.03), \\ R &= 0.79, \sigma = 0.24; \end{aligned} \quad (1)$$

$$\begin{aligned} \lg L_{\text{C}^{18}\text{O}} &= \lg L_{1.1\text{mm}} + 2.42(0.03), \\ R &= 0.68, \sigma = 0.26; \end{aligned} \quad (2)$$

$$\begin{aligned} \lg L_{^{13}\text{CO}} &= \lg L_{1.1\text{mm}} + 3.11(0.03), \\ R &= 0.66, \sigma = 0.26, \end{aligned} \quad (3)$$

where R is the correlation efficient and σ is the sample standard deviation in all fitted formulas in logarithmic space hereafter.

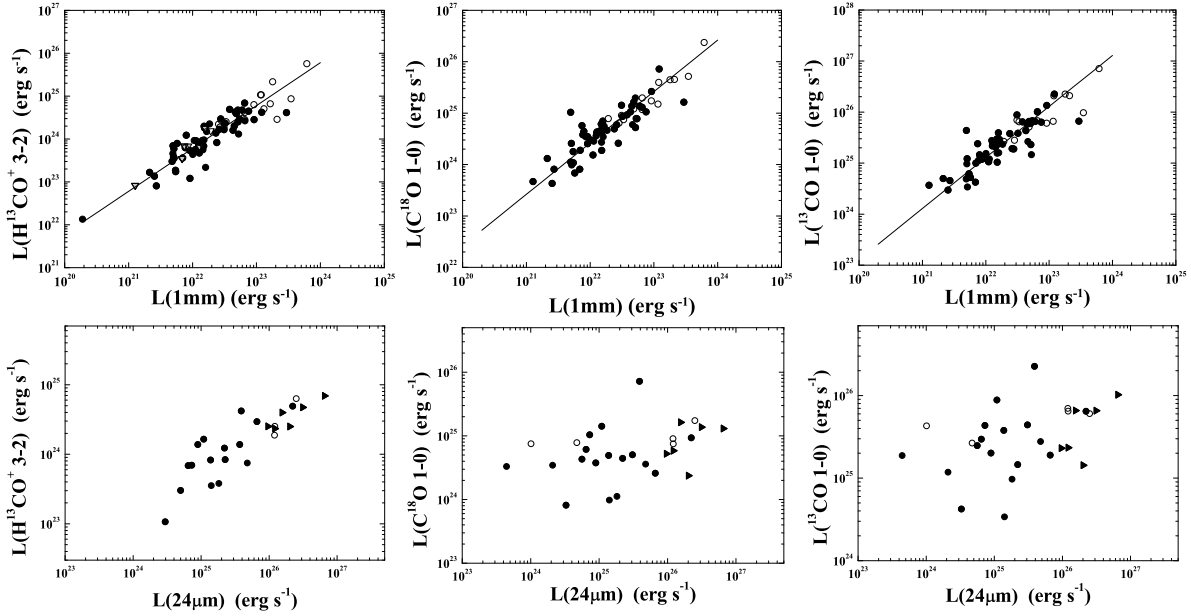


Fig. 3.— The comparison of the luminosities of the three optically thin lines, H^{13}CO^+ 3-2, C^{18}O 1-0 and ^{13}CO 1-0 of EGOs with their corresponding BGPS 1.1 mm and *Spitzer IRAC* $24\ \mu\text{m}$ continuum monochromatic luminosities. Upper limits of H^{13}CO^+ 3-2 and lower limits of $24\ \mu\text{m}$ luminosities are shown as triangles. For several EGOs whose near and far kinematic distance ambiguity is not resolved, their far kinematic distance quantities are shown in open symbols, while their near distance quantities are shown in filled symbols (the same as those with unique distance). Only near distance quantities with certain detection of the lines are used in regression.

Distinctively, only the H^{13}CO^+ 3-2 shows a clear correlation with the $24\ \mu\text{m}$ luminosities (but worse than with the 1.1 mm) in the bottom panels of the figure, which indicates that only the H^{13}CO^+ 3-2 line is a tracer of warm molecular cloud cores. This is not unexpected because H^{13}CO^+ 3-2 has three orders of magnitude higher critical density than the other two lines. However, we stress that the $24\ \mu\text{m}$ data are incomplete due to spatial confusion issues on the *Spitzer MIPS* maps (see in Cyganowski et al. 2008). Furthermore, diverse masses and evolution status of the hidden central forming stars that dictate the $24\ \mu\text{m}$ emission could also contribute to the badness of the correlations.

Then, the correlations among our four dense gas (small size-scale) and shock tracers and the three isotopic CO 1-0 lines (large size-scale tracers) are shown in Fig. 4. Good log-linear correlations are found among all lines. A straight line with fixed slope of unity is fit to each plot in log-log scale as (the solid lines in the figure)

$$\begin{aligned} \lg L_{\text{SO}} &= \lg L_{\text{H}^{13}\text{CO}^+} - 0.22(0.03), \\ R &= 0.78, \sigma = 0.18; \end{aligned} \quad (4)$$

$$\begin{aligned} \lg L_{\text{SiO}} &= \lg L_{\text{H}^{13}\text{CO}^+} - 0.16(0.04), \\ R &= 0.61, \sigma = 0.23; \end{aligned} \quad (5)$$

$$\begin{aligned} \lg L_{\text{CH}_3\text{OH}} &= \lg L_{\text{H}^{13}\text{CO}^+} - 0.61(0.04), \\ R &= 0.57, \sigma = 0.23; \end{aligned} \quad (6)$$

$$\begin{aligned} \lg L_{\text{C}^{18}\text{O}} &= \lg L_{\text{H}^{13}\text{CO}^+} + 0.60(0.04), \\ R &= 0.38, \sigma = 0.33; \end{aligned} \quad (7)$$

$$\begin{aligned} \lg L_{^{13}\text{CO}} &= \lg L_{\text{H}^{13}\text{CO}^+} + 1.31(0.04), \\ R &= 0.39, \sigma = 0.31; \end{aligned} \quad (8)$$

$$\begin{aligned} \lg L_{^{12}\text{CO}} &= \lg L_{\text{H}^{13}\text{CO}^+} + 1.70(0.05), \\ R &= 0.16, \sigma = 0.36; \end{aligned} \quad (9)$$

$$\begin{aligned} \lg L_{^{13}\text{CO}} &= \lg L_{\text{C}^{18}\text{O}} + 0.71(0.02), \\ R &= 0.87, \sigma = 0.14; \end{aligned} \quad (10)$$

$$\begin{aligned} \lg L_{^{12}\text{CO}} &= \lg L_{^{13}\text{CO}} + 0.37(0.02), \\ R &= 0.75, \sigma = 0.21; \end{aligned} \quad (11)$$

$$\begin{aligned} \lg L_{^{12}\text{CO}} &= \lg L_{\text{C}^{18}\text{O}} + 1.08(0.03), \\ R &= 0.61, \sigma = 0.26. \end{aligned} \quad (12)$$

The ubiquitous correlations (Eqs. 4-12) are unexpected, because the various lines trace different physical subcomponents of the EGO clouds due to different critical densities and/or chemistry: H^{13}CO^+ 3-2 traces dense and warm cloud cores, SiO 6-5 traces active outflow shocks, $\text{SO}^3\Sigma 6_5 - 5_4$ (Wakelam et al. 2004; Charnley 1997; van der Tak et al. 2003) and the CH_3OH line series (van der Tak et al. 2003; Cyganowski et al. 2011b) may trace both components to some extent, while the three isotopic CO 1-0 lines trace large scale cloud structures. As discussed by (Goodman et al. 1998), a molecular line probes a density range of usually no more than 2 orders of magnitude above its critical density, due to opacity and chemistry (and perhaps beam dilution). Thus, our dense gas tracers very possibly probe completely different density regimes and size-scales than the three isotopic CO 1-0 lines due to their very different critical densities. Therefore, the good correlations we found have a strong indication that not only the emission from the very different cloud sub-component size-scales are closely related, but the strength of the shock-region line emission is also tightly linked to that of the cloud emission in most of the observed EGO clouds.

Particularly, SiO molecules are usually highly depleted in quiescent cold clouds (Herbst et al. 1989; Ziurys et al. 1989) and also deficient in photon dominated regions (Walmsley et al. 1999), but can be enriched in shocked regions where the silicon element is eroded or sputtered off dust grains by non-dissociative shocks (Hartquist et al. 1980; Schilke et al. 1997; Gusdorf et al. 2008) or fast dissociative shocks (Neufeld & Dalgarno 1989a,b). Moreover, dense ambient clouds are needed to obstruct the stellar outflows to produce observable enhancement in SiO abundance. Otherwise, the outflows would simply escape away, leaving little SiO molecules behind, as illustrated by the one-sided SiO outflow in the low mass star forming region L1157 (Mikami et al. 1992).

Therefore, we argue that the good correlations between the shock emission and all cloud emission, as found in our data, can be explained if *most of the EGOs are embedded in molecular clouds that have very similar density and thermal*

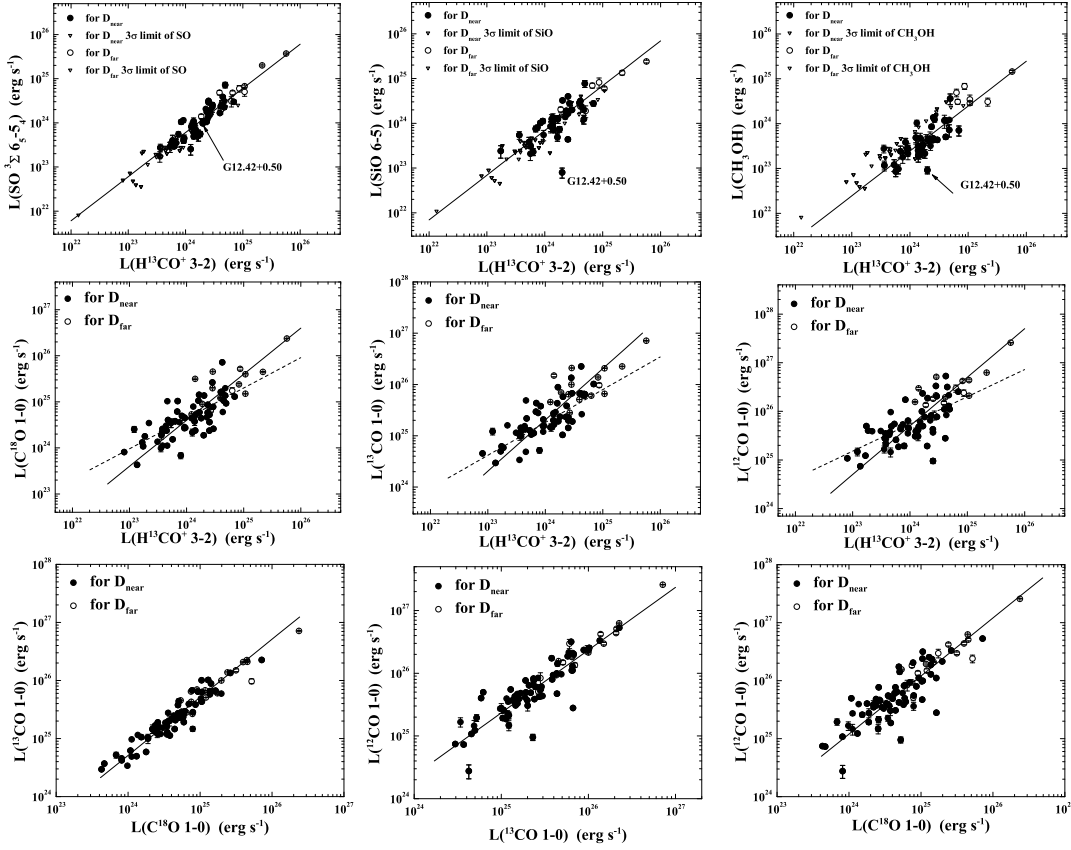


Fig. 4.— The comparison of observed and literature line luminosities. Upper limits are shown in triangles in the top row, and far distance quantities are shown in open symbols in all panels. The marked object, G12.42+0.50, has exceptionally weak SiO and CH₃OH lines and thus is excluded from the log-linear fitting.

structures and the stellar outflows are mainly obstructed by the peripheral parts of their own natal clouds ('cloud shocks' by Hollenbach 1997).

In another word, although the SiO 6-5 and the H^{13}CO^+ 3-2 line emission comes from different regions of the EGO clouds, their strengths are linked through the very similar density and thermal structures of the clouds and similar properties of shocks, such as shock velocity and density jump across the shock front.

The worst correlations between H^{13}CO^+ 3-2 and isotopic CO 1-0 line luminosities can be improved a little by loosening the slope of the log-linear fit and thus obtain (the dashed lines in the plots)

$$\begin{aligned} \lg L_{\text{C}^{18}\text{O}} &= 0.66(0.08) \lg L_{\text{H}^{13}\text{CO}^+} + 8.8(2.0), \\ R &= 0.52, \sigma = 0.29; \end{aligned} \quad (13)$$

$$\begin{aligned} \lg L_{^{13}\text{CO}} &= 0.64(0.07) \lg L_{\text{H}^{13}\text{CO}^+} + 9.9(1.8), \\ R &= 0.56, \sigma = 0.26; \end{aligned} \quad (14)$$

$$\begin{aligned} \lg L_{^{12}\text{CO}} &= 0.56(0.08) \lg L_{\text{H}^{13}\text{CO}^+} + 12.3(2.0), \\ R &= 0.42, \sigma = 0.30. \end{aligned} \quad (15)$$

Here the slopes are all smaller than unity, indicating that the H^{13}CO^+ 3-2 emission from the warm cores tends to overshine the isotopic CO 1-0 line emission from larger size-scales in more luminous (and thus more massive) EGO clouds. Note however that the smaller slopes can be increased if far kinematic distance (open circles in the middle row of Fig. 4) are adopted for several objects.

We confirm that the above luminosity correlations are not artifact due to variation of distances, because most of our EGOs have similar kinematic distances of about 2-6 kpc.

6.4.2. The progressive de-correlations

The quality of the luminosity correlations are diverse. Compared to error bars (statistic error) in Fig. 4, the data scatter in the luminosity correlation plots can not be explained by observational errors. Even if taking into account the nominal 20 per cent of flux calibration error when comparing H^{13}CO^+ 3-2 luminosity with that of the isotopic CO 1-0 lines (obtained with different telescopes at different time), it is still far from enough to explain the large scatter. Thus, the data scatter should

reflect some intrinsic randomness in the thermal and/or density structures of the EGO clouds.

The sample standard deviations (σ) of the log-linear fits are gathered and compared in Table 3. The correlations are the best (with the smallest σ) between $^{13}\text{CO} - \text{C}^{18}\text{O}$ and $\text{SO} - \text{H}^{13}\text{CO}^+$, progressively worse between $^{12}\text{CO} - ^{13}\text{CO}$ and $^{12}\text{CO} - \text{C}^{18}\text{O}$, and the worst between H^{13}CO^+ and the three isotopic CO 1-0 lines. This is an evidence of a progressive de-correlation of line luminosities across larger and larger size-scales of the EGO clouds, given that the tracers are progressively tracing larger cloud subcomponent sizes along the $\text{H}^{13}\text{CO}^+ - \text{SO} - \text{C}^{18}\text{O} - ^{13}\text{CO} - ^{12}\text{CO}$ sequence. It suggests that the randomness increases with cloud substructure size-scale.

Table 3: Compare the sample standard deviation (σ) of the log-linear fits to the luminosity correlations.

X	Y	σ	Equation
1.1 mm	H^{13}CO^+	0.24	(1)
1.1 mm	C^{18}O	0.26	(2)
1.1 mm	^{13}CO	0.26	(3)
H^{13}CO^+	SO	0.18	(4)
H^{13}CO^+	SiO	0.23	(5)
H^{13}CO^+	CH_3OH	0.23	(6)
H^{13}CO^+	C^{18}O	0.29	(13)
H^{13}CO^+	^{13}CO	0.26	(14)
H^{13}CO^+	^{12}CO	0.30	(15)
C^{18}O	^{13}CO	0.14	(10)
^{13}CO	^{12}CO	0.21	(11)
C^{18}O	^{12}CO	0.26	(12)

In a summary for this subsection, good correlations are found between various line and continuum luminosities that trace various subcomponents of the EGO clouds such as low dense components, dense warm cores and shock regions, which requires similarity in thermal and density structures and perhaps also in shock properties among all EGO clouds to explain. However, evidence is also found for progressive de-correlation of line luminosities across larger and larger size-scales of the cloud subcomponents.

6.5. Line width correlations

6.5.1. Dense gas and shock tracer lines

Aside from line opacity effect, millimeter line widths observed in interstellar clouds usually reflect gas kinematics in the clouds, including thermal motion of the observed molecules, turbulence,

internal motion of subcomponents of the clouds, systematic motion of gas such as infall, outflow and rotation.

The line widths (FWHM) of our dense gas and shock tracers are compared in Fig. 5. All the lines are significantly broader than their typical thermal line width at representative temperatures, including the usually optically thin warm core tracer H^{13}CO^+ 3-2. Thus, non-thermal motion is ubiquitous in the high density part of the EGO clouds. Note that in several cases where broad line wings are evident and two Gaussian profiles are fit to the broad and narrow components separately, only the central narrow component is used.

The H^{13}CO^+ lines are always the narrowest in Fig. 5, while none of them are strongly correlated with each other. The results are reminiscent of what Sakai et al. (2010) found among 20 massive clumps. To quantitatively illustrate the lack of correlation in these plots, a Kendall rank correlation test is performed to each pair of quantities in these plots by ignoring the error bars. The null hypothesis is ‘no correlation’, which is equivalent to Kendall tau coefficient $\tau = 0$. If the probability to reject the null hypothesis is $p < 0.05$, the null hypothesis is rejected and the opposite is accepted. The resulting τ and p are shown in the top left corner of each panel of the figure. The large probability p in the top row of the figure clearly demonstrate the lack of correlations. Although marginal correlations can be concluded from the smaller p values in the bottom row of the figure, the correlations become questionable when the large error bars in these plots are taken back into account.

The single dish H^{13}CO^+ 3-2 line data should not be dominated by outflows due to its high critical density and low optical depth, as indicated by the dominant disk like morphology and kinematics in the H^{13}CO^+ 1-0 line map of an outflow source by Takahashi et al. (2006). Unless outflow powered turbulence is functioning in the EGO clouds, gravity induced systematic motions such as infall, cloud rotation, and the motion of multiple protostars should be the most probable contributors to the observed H^{13}CO^+ line widths.

The lack of correlation with SiO line, which is also true if the broader component of the two-Gaussian fit of SiO lines is used, rules out outflow as a major contributor to the line width of the SO and CH_3OH lines. The latter two species could

be strongly affected by large errors in the data (the large error bars in the figure) and opacity effect which has veiled their correlation with SiO line width. Reiter et al. (2011) also found that the widths of molecular line tracers such as $\text{SO } 6_7-5_6$ are significantly affected by line opacity in high mass star forming clumps.

6.5.2. Low density gas tracers

To check if the non-thermal motion in the small scale dense cloud cores is linked to that in larger size-scale low density parts of the EGO clouds, the H^{13}CO^+ 3-2 line width are compared with that of the three isotopic CO 1-0 lines in Fig. 6. The C^{18}O 1-0 line widths are comparable to that of the H^{13}CO^+ 3-2 lines and show a rough positive correlation, while the ^{13}CO and ^{12}CO 1-0 lines are progressively broader and show no correlation. Similarly, a Kendall rank correlation test is performed to each plot in the figure. The resulting p values shown in the top left corner of each plot demonstrate a clear correlation in the left panel, a marginal correlation in the middle panel and no correlation in the right panel. It indicates that, although the non-thermal velocity fields are still correlated to some degree across the different size-scales traced by the H^{13}CO^+ and C^{18}O lines, the correlation is already very loose and progressively worse from C^{18}O to ^{13}CO to ^{12}CO 1-0 lines.

However, the line width correlations among the three isotopic CO 1-0 line themselves are much better, as shown in Fig. 7 (in linear scales in the top row and logarithmic scales in the bottom row). The data scatter looks more homogeneous in the log-log plots and a log-linear fit yields (see the solid line)

$$\begin{aligned} \lg \Delta V_{^{13}\text{CO}} &= \lg \Delta V_{\text{C}^{18}\text{O}} + 0.098(0.008), \\ R &= 0.77, \sigma = 0.07. \end{aligned} \quad (16)$$

The equations for the other two worse correlations are omitted. Hereafter, we use ΔV to represent the FWHM of line profiles. Eq. (16) is equivalent to $\Delta V(^{13}\text{CO}) \approx 1.25(\pm 0.02) \times \Delta V(\text{C}^{18}\text{O})$.

The broader ^{13}CO 1-0 lines than the C^{18}O 1-0 lines are clearly not caused by higher opacity in the former lines, because the opacities in the ^{13}CO 1-0 lines are not much larger than unity, which can be verified by multiplying a factor of 7.3 to the C^{18}O 1-0 opacities in the Table 7 of Chen et al.

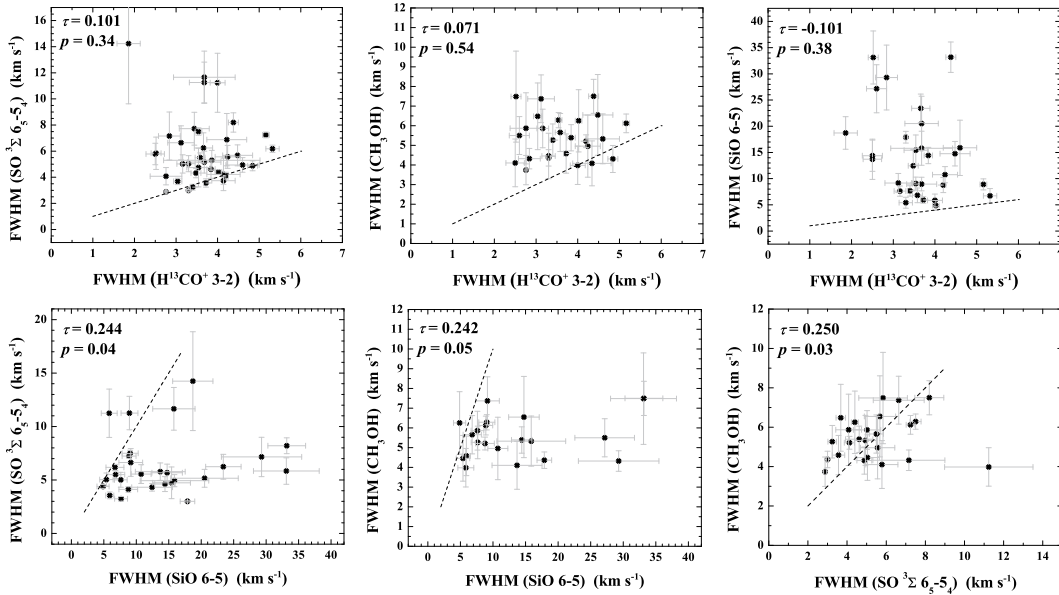


Fig. 5.— The comparison of line widths among the four dense warm gas and shock tracers observed in this survey. Only those line width data with $S/N > 3$ are used and henceforth. The dashed lines show where the two compared line widths are just equal. The parameters τ and p in the top left corner of each panel are the Kendall tau coefficient and the probability to reject the null hypothesis (see in the text).

(2010). Instead, it should be understood as the property of interstellar turbulent velocity fields. According to Solomon et al. (1987), turbulence dominated line width scales with cloud size (l in pc) and mass (M in M_{\odot}) as ΔV (km s^{-1}) = $1.0 \times l^{0.5}$ and $M = 2000 \times \Delta V^4$ in interstellar clouds in virial equilibrium and it is also applicable to substructures of a single molecular cloud (Larson 1981). Thus, the above log-linear line width correlation also suggests that the ^{13}CO 1-0 emission regions are universally $1.56(\pm 0.05)$ times larger in size and $2.4(\pm 0.2)$ times larger in mass than the C^{18}O 1-0 emission regions. This holds over a large cloud size range of 2–49 pc and a large cloud mass range of $7.7 \times 10^3 - 4.8 \times 10^6 M_{\odot}$, corresponding to the C^{18}O 1-0 line width range of 1.4–7.0 km s^{-1} .

The data scatter in the line width correlations can not be explained by observational errors. Instead, they could reflect some randomness in the velocity fields across cloud substructures of different size-scales, similar to the randomness in the luminosity correlations discussed in Sect. 6.4.2. The progressively worse line width correlations

with the H^{13}CO^+ from C^{18}O to ^{13}CO to ^{12}CO 1-0 lines and the similar trends among the three isotopic CO 1-0 lines themselves further hint that the randomness is stronger across larger substructure size-scales.

6.5.3. The inter-cloud randomness in the line width correlations

The log-linear nature of the line width correlations among the three isotopic CO 1-0 lines (increasing data scatter toward broader lines in the top row of Fig. 7) is surprising, because such behavior is expected usually when the quantities vary across several orders of magnitude, while the line widths shown here vary by merely a factor of about five. The isotopic CO 1-0 line widths are dominated by turbulence velocity fields at the whole cloud size-scale, therefore the data scatter in these line width correlations can be understood as some kind of randomness in the turbulence velocity fields. The increase of data scatter toward broader line widths thus means the increase of the randomness among more massive and bigger

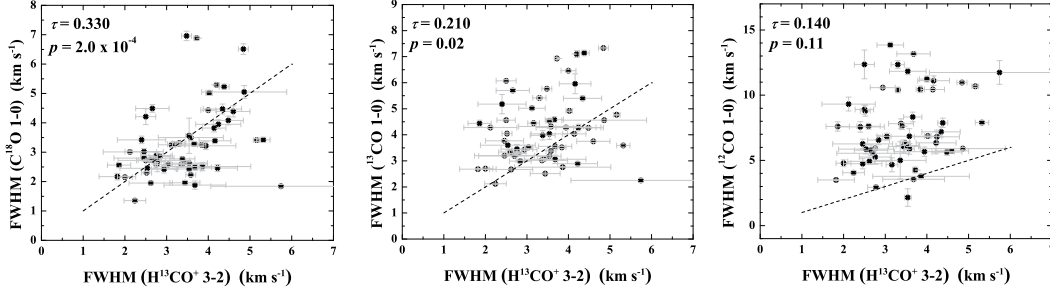


Fig. 6.— The same as Fig. 5 but between the dense warm gas tracer line ($\text{H}^{13}\text{CO}^+ 3-2$) and the three lower density tracer lines (isotopic CO 1-0). The parameters τ and p in the top left corner of each panel are the Kendall tau coefficient and the probability to reject the null hypothesis (see in the text).

EGO clouds. Because the trends are manifested by comparing EGO clouds of different size-scales (line widths), we call it inter-cloud randomness, in contrast to the randomness revealed by comparing molecular lines of very different critical densities.

To quantify the trends, we compute local sample standard deviation (with respect to the fitted log-linear correlation with fixed slope of unity) for smaller velocity sub-ranges and investigate how it varies with the mean line width. (Fig. 8). After some tests, the velocity sub-range is chosen to be 0.3 dex in the logarithmic scale, which gives the best presentation in Fig. 8 (our conclusions are not sensitive to the choice, however).

The computed local standard deviations ($\sigma_{\Delta V}$) show up as linear functions of relevant line widths (ΔV) in Fig. 8, or

$$\sigma_{\Delta V,^{13}\text{CO}} = 0.232(0.008) \Delta V_{\text{C}^{18}\text{O}} - 0.03(0.02), R = 0.95; \quad (17)$$

$$\sigma_{\Delta V,^{12}\text{CO}} = 0.29(0.03) \Delta V_{^{13}\text{CO}} + 1.4(0.1), R = 0.67; \quad (18)$$

$$\sigma_{\Delta V,^{12}\text{CO}} = 0.28(0.03) \Delta V_{\text{C}^{18}\text{O}} + 2.1(0.1), R = 0.65. \quad (19)$$

The interception of Eq. (17) is comparable to its uncertainty and much smaller than the linear term and thus can be treated as zero. Therefore, Eq. (17) demonstrates that the scatter of data points is exactly proportional to the $\text{C}^{18}\text{O} 1-0$ line width, which exactly agrees to a proportionality

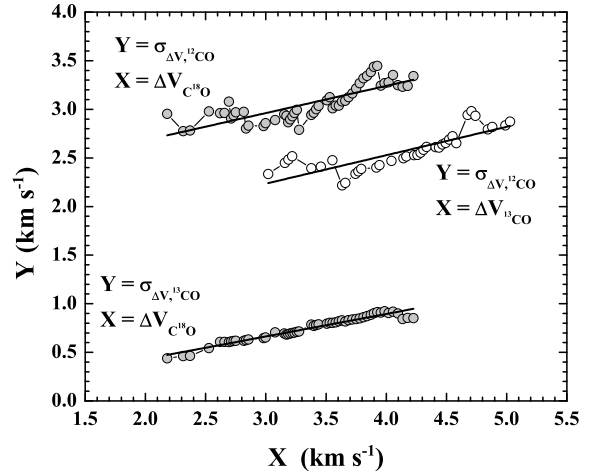


Fig. 8.— The data scatter ($\sigma_{\Delta V}$) of the line width correlations as a function of the FWHM line width (ΔV) itself. The thick solid lines are linear fits to the points (see Eqs. 17, 18 and 19).

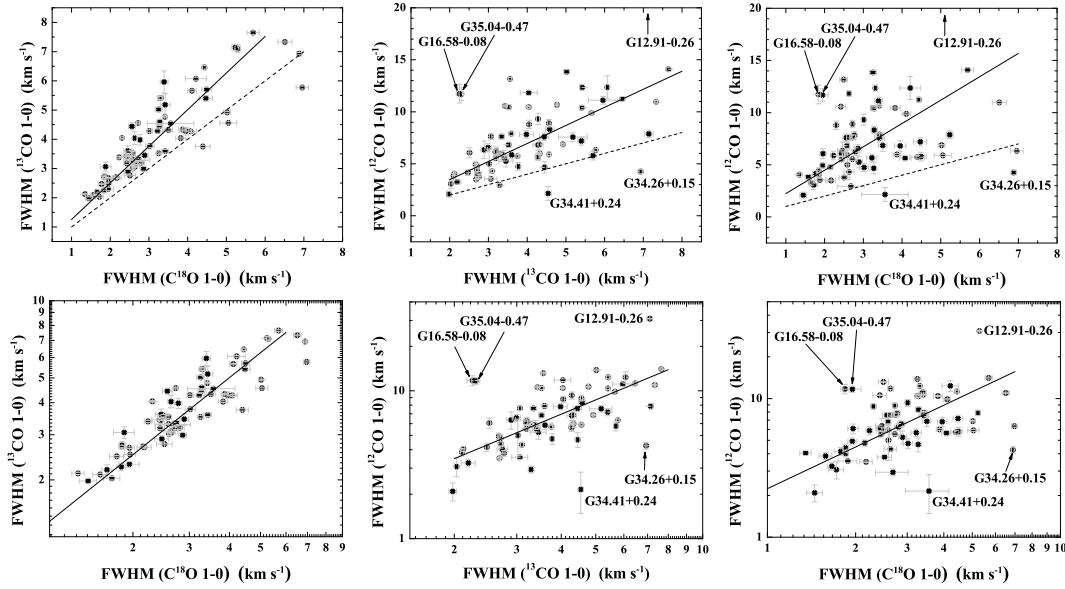


Fig. 7.— The same as Fig. 5 but among the three lower density tracer isotopic CO 1-0 lines in linear (top row) and logarithmic (bottom row) scales. The solid lines are linear fits in logarithmic space to the bottom row with a fixed slope of unity. Several objects whose ^{12}CO 1-0 line widths are abnormally too broad or too narrow and thus are excluded from the fittings are marked with their object names. The object G12.91-0.26 is outside of the plot limit in the top middle and top right panels.

between the ^{13}CO and C^{18}O 1-0 line widths in logarithmic space, instead of in linear space. In another word, the correlation between the two lines has a constant relative error of 0.232 ± 0.008 .

The slopes in the other two equations that involve the ^{12}CO 1-0 line are about 0.3, not too different from that in Eq. (17). However, the latter two equations both possess a non-zero constant term. This constant term actually becomes progressively larger from Eq. (17) to (18) to (19), which just corresponds the progressive worsening of the line width correlations among the three isotopic CO 1-0 lines in Fig. 7 (from left to right). Interpretation of this term may need a more detailed investigation of line blending and non-Gaussianity in the original CO line profiles, which is beyond the scope of this paper.

Combining the inter-cloud randomness of the turbulence velocity fields with earlier discussed progressive worsening trends of luminosity (Sect. 6.4.2) and line width (Sect. 6.5.2) correlations that suggests the increase of randomness across larger cloud subcomponent size-scales, we envision a full

view of the randomness: despite of the ubiquitous similarity of cloud thermal and density structure and shock properties, the density and thermal structure and velocity fields in the EGO clouds all possess some degree of randomness that increases over larger cloud substructure size-scales and increases toward larger EGO clouds. The better correlations among line luminosities than among line widths hints that the growth of the randomness might be faster in velocity fields than in the thermal and density structures. The nice linear relation between the line widths and their data scatter, as discussed in this subsection, further reveals some regularity in this randomness. Our EGO sample are biased to molecular clouds/clumps that harbor massive YSOs and outflows. It is interesting to check with further observations whether these properties (similarity and randomness) still hold for more general molecular clouds.

6.6. Line width – luminosity relations

The different behavior between the line width and luminosity correlations can be double checked

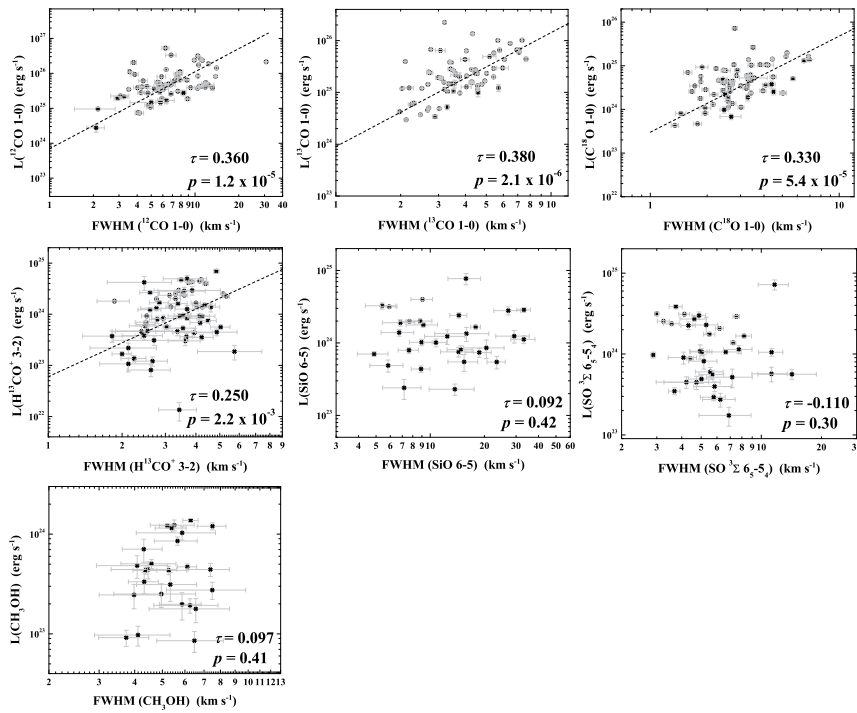


Fig. 9.— The comparison of line luminosities to line widths for all discussed lines. The dashed line in some panels shows an arbitrarily positioned straight line with a fixed slope of 2.2 in logarithmic space for the ease of comparison. The parameters τ and p in the bottom right corner of each panel are the Kendall tau coefficient and the probability to reject the null hypothesis (see in the text).

by directly comparing the line luminosities with their corresponding line widths, as shown in Fig. 9. Diverse degrees of correlation are found in the figure. Thus, a similar Kendall rank correlation test is performed to each plot. The resulting p values in the bottom right corner of each panel indicate strong correlations in the first four panels and the lack of correlation in the rest three panels. An arbitrarily placed dashed straight line with a fixed slope of 2.2 in logarithmic space is drawn in those panels with correlation to ease qualitative comparison. The figure simply confirms that, the line luminosities of the three isotopic CO 1-0 lines are clearly correlated with their line widths (top panels), as expected in turbulence dominated clouds under virial equilibrium (Solomon et al. 1987). A similar correlation of H^{13}CO^+ 3-2 line looks worse and seems to have a slightly steeper slope than the dashed line (middle left panel). The other three shock-related tracer lines (SO, SiO and CH_3OH) have their luminosities totally uncorrelated with their line widths, which confirms our previous argument that their line widths could be either broadened by outflows or dominated by observational errors and opacity effects, but not by canonical interstellar turbulence.

The diverse degrees of line width-luminosity correlations support that the different lines trace different dynamical subcomponents of the EGO clouds.

Multi-tracer multi-cloud intercomparison study has been systematically discussed by Goodman et al. (1998). However, they only discussed the study of cloud size-velocity dispersion relation with single dish mapping data, and thus is not directly applicable to our study of line width and luminosity correlations with single dish single pointing observations. Future extension of their discussion to the kind of analysis done in this work will be helpful, but will involve more physics such as energy level excitation, randomness in line widths and luminosities, and probably also the astrochemistry of the various species in various cloud subcomponents. Extension of the current study to single dish mapping could be another direction of further steps.

7. Summary

We have surveyed two 1-GHz bands in 1.1 mm toward a northern subsample of 89 *Spitzer GLIMPSE* extended green objects (EGOs) using a single dish and present a comprehensive catalog of observed molecular line data (Sect. 5.2). Eight molecular species are undoubtedly detected: H^{13}CO^+ , SiO, SO, CH_3OH , CH_3OCH_3 , $\text{CH}_3\text{CH}_2\text{CN}$, HCOOCH_3 , and HN^{13}C . Line of sight velocity is determined for 70 EGOs and kinematic distance is estimated for 80 EGOs (with the help of literature C^{18}O observations from Chen et al. 2010). The main conclusions are

1. The high detection rate of 79 per cent of H^{13}CO^+ 3-2 line demonstrates the detection of dense cores toward most of the EGOs. All of these detected lines are broader than the thermal line width, suggesting the common existence of non-thermal supersonic motions in the EGO clouds.
2. The high detection rate of 53 per cent of SiO 6-5 line among the H^{13}CO^+ detected EGOs supports the idea that these EGOs are experiencing active outflow shocks.
3. The line luminosities are found to be strongly log-linearly correlated among all considered lines, including our four high density or shock tracers and three lower density tracer isotopic CO 1-0 lines. Distinctively, diverse degrees of correlations are found among the line widths, which supports that they trace quite different dynamical components of the clouds. Such ubiquitous luminosity correlations require *a universal similarity of density and thermal structures and perhaps of shock properties among all EGO clouds. This is possible if all the observed shocks are produced within the natal clouds of the forming stars in the EGOs.*
4. The data scatter in the line width and luminosity correlations are interpreted by randomness in the density and thermal structures and velocity fields in the EGO clouds. Both the line width and luminosity correlations are found to be progressively worse when the pairs of compared lines trace more different cloud subcomponent size-scales,

which indicates the increase of the randomness across larger cloud subcomponent size-scales.

5. The data scatters in the line widths correlations among the three isotopic CO 1-0 lines appear as nice linear functions of line width itself, which hints both the increase of velocity randomness toward larger whole-cloud sizes and some regularity behind.

J.H. thanks Dr. Tatsuhiko Hasegawa for some comments on the chemistry of the detected species and Dr. Robert Simon for some helpful discussions upon the kinematic distances. J.H. also thanks the support of the ‘Western Light’ project of China and the Chinese National Science Foundation (Grant No. 11173056). S.T. is financially supported by a postdoctoral fellowship at the Institute of Astronomy and Astrophysics, Academia Sinica, Taiwan. X.C. acknowledges the financial support from the Chinese National Science Foundation (Grants No. 11073041 and 11133008).

Facilities: HHT ()

Table 4: Line parameters.

Object	Transition ^a	ν (MHz)	σ_ν ^b (MHz)	FWHM (km s ⁻¹)	σ_{FWHM}^c (km s ⁻¹)	T_{MB} (mK)	σ_{Tmb} (mK)	I_{int}^d (K km s ⁻¹)	σ_I^d (K km s ⁻¹)	SNR ^e Note ^e
(1)	(2)	(3)	(4)	(5)	(6)	(7)	(8)	(9)	(10)	(11) (12)
G10.29-0.13	H ¹³ CO ⁺ ,3-2	260255.34	0.14	2.66	0.40	176	23	0.488	0.068	7.2
G10.34-0.14	CH ₃ OH,7 _{3,4} - 7 _{2,5} - +	251641.74	0.28	3.80	0.70	91	20	0.317	0.075	4.2
	CH ₃ OH,6 _{3,3} - 6 _{2,4} - +	251738.39	0.38	5.14	1.08	78	19	0.401	0.079	5.1
	CH ₃ OH,5 _{3,2} - 5 _{2,3} - +	251812.21	0.31	2.22	0.78	56	18	1.042	0.109	9.6
	CH ₃ OH,5 _{3,2} - 5 _{2,3} - +	251812.21		23.46	5.18	52	18			s
	SO, ³ Σ,6 ₅ - 5 ₄	251825.99	0.23	6.24	1.16	164	20	1.242	0.089	14.0
	CH ₃ OH,4 _{3,1} - 4 _{2,2} - +	251866.85	0.26	4.58	0.86	104	20	0.568	0.079	7.2
	CH ₃ OH,5 _{3,3} - 5 _{2,4} + -	251890.90		6.24	0.54	86	20	0.574	0.074	7.8 p
	CH ₃ OH,6 _{3,4} - 6 _{2,5} + -	251895.73		6.24		72	20	0.480	0.079	6.1 p
	CH ₃ OH,4 _{3,2} - 4 _{2,3} + -	251900.49		6.24		124	20	0.826	0.082	10.1 p
	CH ₃ OH,3 _{3,0} - 3 _{2,1} - +	251905.81		6.24		63	20	0.416	0.068	6.1 p
	CH ₃ OH,3 _{3,1} - 3 _{2,2} + -	251917.04		6.50	0.74	69	22	0.477	0.081	5.9 p
	CH ₃ OH,7 _{3,5} - 7 _{2,6} + -	251923.63		6.50		47	22	0.323	0.075	4.3 p
	CH ₃ OH,8 _{3,6} - 8 _{2,7} + -	251983.71	0.70	5.94	2.04	50	21	0.326	0.089	3.7
	CH ₃ OH,9 _{3,7} - 9 _{2,8} + -	252089.14	2.66	25.16	7.92	25	21	0.607	0.163	3.7
	H ¹³ CO ⁺ ,3-2	260255.31	0.07	3.66	0.22	401	23	1.644	0.091	18.1
	SiO,6-5	260517.27	0.82	23.42	2.72	96	23	2.473	0.194	12.7
G11.11-0.11	SO, ³ Σ,6 ₅ - 5 ₄	251825.36	0.28	2.18	1.12	119	33	0.383	0.103	3.7
	H ¹³ CO ⁺ ,3-2	260255.38	0.09	2.60	0.28	424	38	1.859	0.188	9.9
	H ¹³ CO ⁺ ,3-2	260255.38		31.66	18.58	30	38			s
G11.92-0.61	CH ₃ OH,8 _{3,5} - 8 _{2,6} - +	251517.35	0.70	7.64	1.70	70	21	0.530	0.094	5.6
	CH ₃ OH,7 _{3,4} - 7 _{2,5} - +	251642.54	0.44	7.22	1.22	76	19	0.568	0.094	6.0
	CH ₃ OH,6 _{3,3} - 6 _{2,4} - +	251738.27	0.34	7.10	0.82	98	20	0.675	0.091	7.4
	CH ₃ OH,5 _{3,2} - 5 _{2,3} - +	251811.89	0.42	9.24	1.06	93	19	0.902	0.088	10.3
	SO, ³ Σ,6 ₅ - 5 ₄	251826.16	0.25	21.12	5.12	37	18	1.383	0.091	15.2
	SO, ³ Σ,6 ₅ - 5 ₄	251826.16		6.64	1.30	112	18			s
	CH ₃ OH,4 _{3,1} - 4 _{2,2} - +	251866.38	0.30	6.08	1.08	101	19	0.708	0.088	8.0
	CH ₃ OH,5 _{3,3} - 5 _{2,4} + -	251890.90		6.22	0.50	94	20	0.620	0.072	8.6 p
	CH ₃ OH,6 _{3,4} - 6 _{2,5} + -	251895.73		6.22		108	20	0.715	0.081	8.8 p
	CH ₃ OH,4 _{3,2} - 4 _{2,3} + -	251900.49		6.22		52	20	0.345	0.079	4.4 p
	CH ₃ OH,3 _{3,0} - 3 _{2,1} - +	251905.81		6.22		80	20	0.528	0.073	7.2 p
	CH ₃ OH,3 _{3,1} - 3 _{2,2} + -	251917.04		5.14	0.34	101	20	0.551	0.067	8.2 p
	CH ₃ OH,7 _{3,5} - 7 _{2,6} + -	251923.63		5.14		80	20	0.438	0.063	7.0 p
	CH ₃ OH,8 _{3,6} - 8 _{2,7} + -	251985.15	0.39	6.42	1.30	80	19	0.564	0.091	6.2
	CH ₃ OH,9 _{3,7} - 9 _{2,8} + -	252088.69	0.87	11.20	1.92	54	19	0.570	0.110	5.2
	CH ₃ OH,10 _{3,8} - 10 _{2,9} + -	252252.36	0.66	8.28	1.48	54	19	0.430	0.097	4.4
	CH ₃ OH,11 _{3,9} - 11 _{2,10} + -	252485.31	0.41	6.56	0.98	82	21	0.474	0.091	5.2
	H ¹³ CO ⁺ ,3-2	260255.33	0.05	3.12	0.32	520	24	3.040	0.117	26.0
	H ¹³ CO ⁺ ,3-2	260255.33		8.32	1.98	146	24			s
	SiO,6-5	260518.21	0.41	9.16	1.82	91	23	2.294	0.158	14.5
	SiO,6-5	260518.21		26.94	4.66	53	23			s
G12.02-0.21	H ¹³ CO ⁺ ,3-2	260255.34	0.24	2.46	0.72	103	23	0.264	0.081	3.3
G12.20-0.03	CH ₃ OH,8 _{3,5} - 8 _{2,6} - +	251515.65	0.47	5.08	1.30	87	28	0.531	0.138	3.8
	CH ₃ OH,6 _{3,3} - 6 _{2,4} - +	251738.71	0.32	3.08	0.96	124	33	0.427	0.113	3.8
	SO, ³ Σ,6 ₅ - 5 ₄	251825.87	0.43	4.48	1.74	119	37	0.636	0.132	4.8
	CH ₃ OH,6 _{3,4} - 6 _{2,5} + -	251893.26		4.76		114	36	0.577	0.107	5.4 p

^aThe string '(E+A)' after the transition CH₃OCH₃,10_{2,9} - 9_{1,8} means it is a blending of four transitions: EA, AE, EE, and AA.

^bIf the value of σ_ν is missing, it means the line is either fit with fixed catalogue frequency or fit with fix line frequency increment in a multi-Gaussian profile fitting.

^cIf the value of σ_{HWHM} is missing, it means the line is fit with the same line width as other lines in a multi-Gaussian profile fitting.

^dIf the values of I_{int} , σ_I and SNR are missing, it means the line is the second component of a double Gaussian fit to the wide line wing of a broad line feature.

^e**p** = partially blended with neighbouring lines of which blended lines are fit together by a multi-Gaussian profile with fix catalogue frequencies and identical line width; **b** = totally blended lines of which member lines are fit independently with a single Gaussian profile, so that the contribution from other blended lines are not separated yet. **s** = the second Gaussian component of the double-Gaussian fit to a line with broad line wings.

Table 4: (continued) Line parameters.

Object (1)	Transition ^a (2)	ν (MHz) (3)	σ_ν ^b (MHz) (4)	FWHM (km s ⁻¹) (5)	σ_{FWHM} ^c (km s ⁻¹) (6)	T_{MB} (mK) (7)	σ_{Tmb} (mK) (8)	I_{int} ^d (K km s ⁻¹) (9)	σ_I ^d (K km s ⁻¹) (10)	SNR ^d (11)	Note ^e (12)	
G12.42+0.50	CH ₃ OH,3 _{3,0} - 3 _{2,1} - +	251903.34		4.76		75	36	0.382	0.109	3.5	p	
	CH ₃ OH,7 _{3,5} - 7 _{2,6} + -	251917.04		3.58		90	39	0.342	0.099	3.5	p	
	CH ₃ OH,3 _{3,1} - 3 _{2,2} + -	251923.63		3.58		91	39	0.347	0.099	3.5	p	
	H ¹³ CO ⁺ ,3-2	260255.17	0.17		4.34	0.46	301	38	1.350	0.143	9.4	
	CH ₃ OH,8 _{3,5} - 8 _{2,6} - +	251517.47	0.42		4.58	1.20	55	17	0.298	0.061	4.9	
	c-HCCCH,6 _{2,5} - 5 _{1,4}	251527.51	0.24		2.86	0.56	82	18	0.187	0.052	3.6	
	CH ₃ OH,6 _{3,3} - 6 _{2,4} - +	251738.94	0.28		3.24	1.04	64	16	0.259	0.055	4.7	
	CH ₃ OH,5 _{3,2} - 5 _{2,3} - +	251811.52	0.22		3.62	0.56	92	16	0.399	0.058	6.9	
	SO, ³ Σ,6 ₅ - 5 ₄	251825.85	0.02		2.88	0.08	856	17	3.310	0.076	43.6	
	SO, ³ Σ,6 ₅ - 5 ₄	251825.85			11.58	2.66	57	17				s
	CH ₃ OH,4 _{3,1} - 4 _{2,2} - +	251866.35	0.17		3.08	0.56	107	16	0.346	0.052	6.7	
	CH ₃ OH,5 _{3,3} - 5 _{2,4} + -	251890.90			4.20	0.24	74	17	0.332	0.048	6.9	p
	CH ₃ OH,6 _{3,4} - 6 _{2,5} + -	251895.73			4.20		48	17	0.216	0.046	4.7	p
	CH ₃ OH,4 _{3,2} - 4 _{2,3} + -	251900.49			4.20		63	17	0.283	0.046	6.2	p
	CH ₃ OH,3 _{3,0} - 3 _{2,1} - +	251905.81			4.20		75	17	0.338	0.046	7.3	p
CH ₃ OH,3 _{3,1} - 3 _{2,2} + -	251917.04			3.70	0.36	84	17	0.333	0.052	6.4	p	
H ¹³ CO ⁺ ,3-2	260255.33	0.01		2.76	0.02	2261	20	6.752	0.071	95.1		
SiO,6-5	260518.08	0.31		3.06	1.04	77	20	0.270	0.067	4.0		
G12.68-0.18	CH ₃ OH,8 _{3,5} - 8 _{2,6} - +	251517.52	0.36			190	39	1.200	0.154	7.8		
	CH ₃ OCH ₃ ,10 _{2,9} - 9 _{1,8} (E+A)	251584.64	0.64			101	39	0.476	0.137	3.5		
	CH ₃ OH,7 _{3,4} - 7 _{2,5} - +	251641.44	0.38		6.40	1.20	161	38	1.164	0.154	7.6	
	CH ₃ CH ₂ CN,28 _{4,25} - 27 _{4,24}	251674.47	0.59		5.32	1.60	96	38	0.513	0.143	3.6	
	CH ₃ OH,6 _{3,3} - 6 _{2,4} - +	251739.33	0.49		7.30	1.86	127	36	1.058	0.165	6.4	
	CH ₃ OH,5 _{3,2} - 5 _{2,3} - +	251812.50	0.88		11.38	4.48	100	34	1.191	0.193	6.2	
	SO, ³ Σ,6 ₅ - 5 ₄	251825.80	0.23		4.08	0.66	188	33	0.771	0.130	5.9	
	CH ₃ OH,4 _{3,1} - 4 _{2,2} - +	251866.02	0.24		2.56	0.54	156	34	0.425	0.109	3.9	
	CH ₃ OH,5 _{3,3} - 5 _{2,4} + -	251890.90			4.50	0.24	162	35	0.779	0.105	7.4	p
	CH ₃ OH,6 _{3,4} - 6 _{2,5} + -	251895.73			4.50		183	35	0.880	0.103	8.5	p
	CH ₃ OH,4 _{3,2} - 4 _{2,3} + -	251900.49			4.50		142	35	0.683	0.102	6.7	p
	CH ₃ OH,3 _{3,0} - 3 _{2,1} - +	251905.81			4.50		138	35	0.661	0.102	6.5	p
	CH ₃ OH,3 _{3,1} - 3 _{2,2} + -	251917.04			5.58	0.38	167	34	0.993	0.114	8.7	p
	CH ₃ OH,7 _{3,5} - 7 _{2,6} + -	251923.63			5.58		167	34	0.994	0.116	8.6	p
	CH ₃ OH,8 _{3,6} - 8 _{2,7} + -	251984.75	0.33		4.42	1.62	149	37	0.834	0.137	6.1	
	CH ₃ OH,9 _{3,7} - 9 _{2,8} + -	252090.18	0.63		8.10	2.22	115	36	1.004	0.170	5.9	
	CH ₃ OH,10 _{3,8} - 10 _{2,9} + -	252252.59	0.25		3.26	0.80	166	34	0.676	0.116	5.8	
	CH ₃ OH,11 _{3,9} - 11 _{2,10} + -	252484.64	0.40		5.08	1.08	126	32	0.648	0.142	4.6	
	H ₂ CCO,13 _{1,13} - 12 _{1,12}	260190.05	0.63		8.74	1.30	96	31	0.825	0.185	4.5	
	H ¹³ CO ⁺ ,3-2	260255.38	0.11		2.76	0.38	354	37	1.121	0.123	9.1	
	U260365	260365.38	0.20		1.50	0.58	202	38	0.414	0.107	3.9	
	HCOOCH ₃ ,21 _{8,13} - 20 _{8,12} E	260386.50	4.84		12.32	7.80	119	35	1.055	0.218	4.8	
	SiO,6-5	260513.95	0.80		4.14	3.28	58	35	1.057	0.269	3.9	
	CH ₃ CH ₂ CN,29 _{4,26} - 28 _{4,25}	260663.72	0.26		1.48	0.44	178	39	0.332	0.097	3.4	b
	CH ₃ CH ₂ CN,29 _{5,26} - 28 _{5,25}	260663.72	0.25		1.48	0.42	178	38	0.332	0.097	3.4	b
CH ₃ OCH ₃ ,6 _{3,3} - 5 _{2,4} EE	260761.49	0.24		1.86	0.60	149	38	0.371	0.115	3.2		
G12.91-0.03	SO, ³ Σ,6 ₅ - 5 ₄	251825.98	0.78			59	27	0.439	0.112	3.9		
	CH ₃ OH,5 _{3,3} - 5 _{2,4} + -	251890.90				62	24	0.283	0.068	4.2	p	
	H ¹³ CO ⁺ ,3-2	260255.31	0.07		2.84	0.26	359	24	1.431	0.115	12.4	
	H ¹³ CO ⁺ ,3-2	260255.31			12.98	7.74	24	24				s
	SiO,6-5	260519.95	2.26		29.30	6.18	36	23	1.052	0.208	5.1	
G12.91-0.26	CH ₃ OH,8 _{3,5} - 8 _{2,6} - +	251516.80	0.14			275	23	1.723	0.091	18.9		
	c-HCCCH,6 _{2,5} - 5 _{1,4}	251526.71	0.30			95	23	0.417	0.075	5.6		
	CH ₃ OCH ₃ ,10 _{2,9} - 9 _{1,8} (E+A)	251582.71	0.29		7.34	0.84	126	21	0.990	0.097	10.2	
	CH ₃ CH ₂ CN,28 _{5,23} - 27 _{5,22}	251609.89	0.43		4.20	1.08	66	20	0.271	0.083	3.3	
	CH ₃ OH,7 _{3,4} - 7 _{2,5} - +	251640.92			4.54	0.50	254	20				s
	CH ₃ OH,7 _{3,4} - 7 _{2,5} - +	251640.92	0.10		16.68	5.94	43	20	1.908	0.115	16.6	
	CH ₃ OH,6 _{3,3} - 6 _{2,4} - +	251737.72	0.09		4.90	0.26	290	18	1.521	0.083	18.3	
	CH ₃ OH,5 _{3,2} - 5 _{2,3} - +	251811.53	0.09		5.54	0.26	329	19	2.013	0.091	22.1	
	SO, ³ Σ,6 ₅ - 5 ₄	251825.63	0.06		4.12	0.26	397	20	4.141	0.118	35.1	
	SO, ³ Σ,6 ₅ - 5 ₄	251825.63			14.40	1.38	161	20				s
	CH ₃ OH,4 _{3,1} - 4 _{2,2} - +	251866.03	0.12		5.80	0.36	290	22	1.841	0.091	20.2	

Table 4: (continued) Line parameters.

Object (1)	Transition ^a (2)	ν (MHz) (3)	σ_ν^b (MHz) (4)	FWHM (km s ⁻¹) (5)	σ_{FWHM}^c (km s ⁻¹) (6)	T_{MB} (mK) (7)	σ_{Tmb} (mK) (8)	I_{int}^d (K km s ⁻¹) (9)	σ_I^d (K km s ⁻¹) (10)	SNR ^d Note ^e (11)	(12)
	CH ₃ OH,5 _{3,3} - 5 _{2,4} + -	251890.90		5.48	0.14	317	24	1.847	0.082	22.5	p
	CH ₃ OH,6 _{3,4} - 6 _{2,5} + -	251895.73		5.48		273	24	1.593	0.080	19.9	p
	CH ₃ OH,4 _{3,2} - 4 _{2,3} + -	251900.49		5.48		277	24	1.612	0.078	20.7	p
	CH ₃ OH,3 _{3,0} - 3 _{2,1} - +	251905.81		5.48		241	24	1.405	0.078	18.0	p
	CH ₃ OH,3 _{3,1} - 3 _{2,2} + -	251917.04		6.00	0.16	239	24	1.524	0.082	18.6	p
	CH ₃ OH,7 _{3,5} - 7 _{2,6} + -	251923.63		6.00		271	24	1.731	0.081	21.4	p
	CH ₃ OH,8 _{3,6} - 8 _{2,7} + -	251984.13	0.12	5.56	0.34	286	24	1.732	0.091	19.0	
	CH ₃ OH,9 _{3,7} - 9 _{2,8} + -	252089.58	0.11	5.02	0.30	277	22	1.479	0.087	17.0	
	CH ₃ OH,10 _{3,8} - 10 _{2,9} + -	252252.04	0.12	4.52	0.34	247	22	1.176	0.083	14.2	
	CH ₃ OH,11 _{3,9} - 11 _{2,10} + -	252484.67	0.11	4.10	0.30	256	22	1.106	0.079	14.0	
	H ₂ CCO,13 _{1,13} - 12 _{1,12}	260188.97	0.35	6.18	0.80	100	22	0.636	0.105	6.1	
	CH ₃ CH ₂ CN,29 _{6,24} - 28 _{6,23}	260221.66		5.92	0.58	64	22	0.407	0.074	5.5	
	CH ₃ CH ₂ CN,29 _{6,23} - 28 _{6,22}	260229.16		5.92		51	22	0.321	0.074	4.3	
	HCOOCH ₃ ,21 _{3,18} - 20 _{3,17} E	260244.84	1.01	6.80	2.12	51	22	0.683	0.109	6.3	
	HCOOCH ₃ ,21 _{3,18} - 20 _{3,17} A	260255.56	0.02	4.20	0.06	1334	23	6.358	0.097	65.5	b
	H ¹³ CO ⁺ ,3-2	260255.56	0.02	4.20	0.06	1334	23	6.358	0.097	65.5	b
	CH ₃ OCH ₃ ,19 _{5,15} - 19 _{4,16} EE	260327.64	0.75	9.70	3.32	70	23	0.805	0.129	6.2	
	HCOOCH ₃ ,21 _{8,13} - 20 _{8,12} E	260381.39	0.37	5.60	0.86	117	25	0.632	0.101	6.3	
	CH ₃ OCH ₃ ,16 _{5,11} - 16 _{4,12} EE	260403.53	0.54	7.30	1.64	87	25	0.566	0.112	5.1	
	HCOOCH ₃ ,21 _{8,14} - 20 _{8,13} E	260403.53	0.54	7.30	1.64	87	25	0.566	0.112	5.1	
	SiO,6-5	260518.03	0.44	8.78	1.44	124	27	2.673	0.188	14.2	
	SiO,6-5	260518.03		38.48	7.48	43	27				s
	CH ₃ OCH ₃ ,18 _{5,14} - 18 _{4,15} EE	260726.82	0.65	8.20	1.52	65	23	0.546	0.116	4.7	
	CH ₃ OCH ₃ ,6 _{3,3} - 5 _{2,4} EE	260757.02	0.49	7.12	1.30	89	24	0.664	0.112	5.9	
	U260797	260796.44	0.33	3.30	0.96	87	23	0.297	0.084	3.5	
	U260865	260865.37	0.52	4.56	1.72	62	23	0.343	0.097	3.5	
	HCOOCH ₃ ,21 _{5,17} - 20 _{5,16} E	261148.04	0.45	5.00	1.82	90	26	0.476	0.097	4.9	
	CH ₃ OCH ₃ ,17 _{5,13} - 17 _{4,14} EE	261148.04	0.45	5.00	1.82	90	26	0.476	0.097	4.9	
G14.33-0.64	CH ₃ OH,8 _{3,5} - 8 _{2,6} - +	251517.14	0.12	4.38	0.36	236	21	1.139	0.089	12.8	
	CH ₃ OCH ₃ ,10 _{2,9} - 9 _{1,8} (E+A)	251582.75	0.88	10.62	2.42	53	22	0.587	0.123	4.8	
	CH ₃ OH,7 _{3,4} - 7 _{2,5} - +	251641.76	0.14	4.56	0.40	219	23	1.049	0.089	11.8	
	CH ₃ OH,6 _{3,3} - 6 _{2,4} - +	251738.42	0.09	4.00	0.26	353	24	1.530	0.085	18.0	
	CH ₃ OH,5 _{3,2} - 5 _{2,3} - +	251812.00	0.08	4.20	0.22	423	25	1.855	0.085	21.8	
	SO, ³ Σ,6 ₅ - 5 ₄	251825.85		13.98	1.00	289	22				s
	SO, ³ Σ,6 ₅ - 5 ₄	251825.85	0.02	3.00	0.06	1528	22	9.259	0.136	68.1	
	CH ₃ OH,4 _{3,1} - 4 _{2,2} - +	251866.63	0.09	4.32	0.28	353	23	1.722	0.089	19.3	
	CH ₃ OH,5 _{3,3} - 5 _{2,4} + -	251890.90		4.18	0.06	352	23	1.566	0.065	24.1	p
	CH ₃ OH,6 _{3,4} - 6 _{2,5} + -	251895.73		4.18		368	23	1.635	0.064	25.5	p
	CH ₃ OH,4 _{3,2} - 4 _{2,3} + -	251900.49		4.18		369	23	1.643	0.064	25.7	p
	CH ₃ OH,3 _{3,0} - 3 _{2,1} - +	251905.81		4.18		323	23	1.438	0.065	22.1	p
	CH ₃ OH,3 _{3,1} - 3 _{2,2} + -	251917.04		4.26	0.12	285	23	1.297	0.071	18.3	p
	CH ₃ OH,7 _{3,5} - 7 _{2,6} + -	251923.63		4.26		282	23	1.280	0.072	17.8	p
	CH ₃ OH,8 _{3,6} - 8 _{2,7} + -	251984.67	0.14	4.38	0.46	220	23	1.061	0.089	11.9	
	CH ₃ OH,9 _{3,7} - 9 _{2,8} + -	252090.03	0.19	4.24	0.48	171	25	0.745	0.089	8.4	
	CH ₃ OH,10 _{3,8} - 10 _{2,9} + -	252252.50	0.26	4.00	0.66	124	24	0.510	0.084	6.1	
	CH ₃ OH,11 _{3,9} - 11 _{2,10} + -	252485.33	0.26	5.48	0.74	109	19	0.634	0.092	6.9	
	H ₂ CCO,13 _{1,13} - 12 _{1,12}	260192.03	0.45	4.20	1.04	77	26	0.311	0.093	3.3	
	H ¹³ CO ⁺ ,3-2	260255.32	0.01	3.30	0.04	2088	23	7.436	0.097	76.7	
	SiO,6-5	260518.63	0.35	17.90	1.12	227	28	4.876	0.203	24.0	
	CH ₃ OCH ₃ ,6 _{3,3} - 5 _{2,4} EE	260758.74	0.73	7.54	2.04	79	27	0.674	0.117	5.8	
	HCOOCH ₃ ,21 _{5,17} - 20 _{5,16} A	261165.06	0.17	2.46	0.52	153	25	0.377	0.083	4.5	
G14.63-0.58	SO, ³ Σ,6 ₅ - 5 ₄	251825.97	0.07	3.68	0.24	329	20	1.380	0.077	17.9	
	CH ₃ OH,4 _{3,1} - 4 _{2,2} - +	251864.38	0.63	6.48	1.70	55	21	0.385	0.095	4.1	
	CH ₃ OH,6 _{3,4} - 6 _{2,5} + -	251895.73		4.64		46	21	0.229	0.061	3.8	p
	CH ₃ OH,4 _{3,2} - 4 _{2,3} + -	251900.49		4.64		66	21	0.326	0.061	5.3	p
	CH ₃ OH,7 _{3,5} - 7 _{2,6} + -	251923.63		5.62		69	23	0.413	0.081	5.1	p
	H ¹³ CO ⁺ ,3-2	260255.30	0.04	3.04	0.10	684	22	2.249	0.076	29.6	
	SiO,6-5	260518.52	0.28	2.12	1.02	70	21	1.224	0.119	10.3	
	SiO,6-5	260518.52		17.84	2.60	57	21				s
G16.58-0.08	H ¹³ CO ⁺ ,3-2	260255.36	0.60	5.74	1.68	49	19	0.292	0.092	3.2	

Table 4: (continued) Line parameters.

Object (1)	Transition ^a (2)	ν (MHz) (3)	σ_ν ^b (MHz) (4)	FWHM (km s ⁻¹) (5)	σ_{FWHM} ^c (km s ⁻¹) (6)	T_{MB} (mK) (7)	σ_{Tmb} (mK) (8)	I_{int} ^d (K km s ⁻¹) (9)	σ_I ^d (K km s ⁻¹) (10)	SNR ^d Note ^e (11) (12)	
G16.59-0.05	CH ₃ OH,8 _{3,5} - 8 _{2,6} - +	251517.23	0.20	5.36	0.56	153	19	0.876	0.086	10.2	
	c-HCCCH,6 _{2,5} - 5 _{1,4}	251526.80	0.50	4.78	1.80	54	19	0.318	0.082	3.9	
	CH ₃ OCH ₃ ,10 _{2,9} - 9 _{1,8} (E+A)	251587.28	0.45	4.16	1.84	64	19	0.308	0.078	3.9	
	CH ₃ OH,7 _{3,4} - 7 _{2,5} - +	251641.63	0.18	4.54	0.50	148	20	0.711	0.082	8.7	
	CH ₃ OH,6 _{3,3} - 6 _{2,4} - +	251738.14	0.19	5.48	0.52	163	20	0.961	0.086	11.2	
	CH ₃ OH,5 _{3,2} - 5 _{2,3} - +	251811.30	0.18	5.36	0.54	176	22	1.020	0.086	11.9	
	SO, ³ Σ _g ,6 ₅ - 5 ₄	251825.77	0.12	5.50	0.36	276	22	1.703	0.089	19.1	
	CH ₃ OH,4 _{3,1} - 4 _{2,2} - +	251866.28	0.16	4.68	0.52	175	20	0.930	0.086	10.8	
	CH ₃ OH,5 _{3,3} - 5 _{2,4} + -	251890.90		4.64	0.12	190	20	0.937	0.059	15.9	p
	CH ₃ OH,6 _{3,4} - 6 _{2,5} + -	251895.73		4.64		190	20	0.936	0.058	16.1	p
	CH ₃ OH,4 _{3,2} - 4 _{2,3} + -	251900.49		4.64		183	20	0.901	0.058	15.5	p
	CH ₃ OH,3 _{3,0} - 3 _{2,1} - +	251905.81		4.64		166	20	0.820	0.058	14.1	p
	CH ₃ OH,3 _{3,1} - 3 _{2,2} + -	251917.04		5.04	0.18	173	20	0.926	0.065	14.2	p
	CH ₃ OH,7 _{3,5} - 7 _{2,6} + -	251923.63		5.04		128	20	0.687	0.062	11.1	p
	CH ₃ OH,8 _{3,6} - 8 _{2,7} + -	251984.06	0.31	5.88	0.78	110	22	0.614	0.089	6.9	
	CH ₃ OH,9 _{3,7} - 9 _{2,8} + -	252090.25	0.32	5.94	1.10	111	21	0.756	0.093	8.1	
	CH ₃ OH,10 _{3,8} - 10 _{2,9} + -	252252.95	0.59	8.24	2.34	63	20	0.601	0.102	5.9	
	CH ₃ OH,11 _{3,9} - 11 _{2,10} + -	252485.94	0.37	7.04	1.26	88	19	0.707	0.096	7.4	
	H ₂ CCO,13 _{1,13} - 12 _{1,12}	260193.25	0.42	3.62	1.68	65	22	0.286	0.084	3.4	
	H ¹³ CO ⁺ ,3-2	260255.43	0.05	3.58	0.12	600	22	2.275	0.084	27.1	
SiO,6-5	260518.31		37.10	9.32	31	23				s	
SiO,6-5	260518.31	0.39	6.82	1.40	99	23	1.836	0.183	10.0		
CH ₃ OCH ₃ ,6 _{3,3} - 5 _{2,4} EE	260761.52	0.61	5.84	1.48	63	24	0.355	0.101	3.5		
G16.61-0.24	H ¹³ CO ⁺ ,3-2	260255.39	0.20	3.62	0.54	129	21	0.433	0.085	5.1	
G17.96+0.08	H ¹³ CO ⁺ ,3-2	260255.34	0.21	2.62	0.52	103	21	0.306	0.077	4.0	
G18.67+0.03	H ¹³ CO ⁺ ,3-2	260255.34	0.25	3.58	0.78	106	22	0.420	0.078	5.4	
G18.89-0.47	CH ₃ OH,5 _{3,2} - 5 _{2,3} - +	251810.04	0.48	5.50	1.38	51	16	0.318	0.081	3.9	
	SO, ³ Σ _g ,6 ₅ - 5 ₄	251826.04	0.73	11.24	2.26	48	16	0.534	0.109	4.9	
	CH ₃ OH,4 _{3,1} - 4 _{2,2} - +	251866.74	0.33	4.08	0.66	69	17	0.234	0.074	3.2	
	CH ₃ OH,6 _{3,4} - 6 _{2,5} + -	251895.73		3.58		53	18	0.202	0.045	4.5	p
	CH ₃ OH,3 _{3,0} - 3 _{2,1} - +	251905.81		3.58		45	18	0.171	0.045	3.8	p
	CH ₃ OH,9 _{3,7} - 9 _{2,8} + -	252092.37	0.22	2.36	0.72	85	19	0.229	0.062	3.7	
	H ¹³ CO ⁺ ,3-2	260255.23	0.06	4.00	0.18	365	17	1.550	0.079	19.6	
	SiO,6-5	260517.33	0.43	5.84	1.22	69	19	0.457	0.086	5.3	
	G19.01-0.03	CH ₃ OH,8 _{3,5} - 8 _{2,6} - +	251518.08	0.67	6.22	2.38	40	15	0.338	0.058	5.8
		CH ₃ OH,5 _{3,2} - 5 _{2,3} - +	251812.16	0.26	3.00	0.64	53	13	0.159	0.044	3.6
SO, ³ Σ _g ,6 ₅ - 5 ₄		251828.49	0.86	14.24	4.62	41	12	0.598	0.081	7.4	
CH ₃ OH,4 _{3,1} - 4 _{2,2} - +		251866.31	0.56	6.40	1.92	41	13	0.288	0.058	5.0	
CH ₃ OH,5 _{3,3} - 5 _{2,4} + -		251890.90		4.76		50	13	0.255	0.039	6.5	p
CH ₃ OH,6 _{3,4} - 6 _{2,5} + -		251895.73		4.76		41	13	0.207	0.039	5.3	p
CH ₃ OH,4 _{3,2} - 4 _{2,3} + -		251900.49		4.76		50	13	0.256	0.039	6.6	p
CH ₃ OH,3 _{3,0} - 3 _{2,1} - +		251905.81		4.76		36	13	0.181	0.039	4.6	p
CH ₃ OH,3 _{3,1} - 3 _{2,2} + -		251917.04		4.94	0.56	37	13	0.196	0.041	4.8	p
CH ₃ OH,7 _{3,5} - 7 _{2,6} + -		251923.63		4.94		28	13	0.146	0.040	3.6	p
CH ₃ OH,8 _{3,6} - 8 _{2,7} + -		251983.84	0.82	8.10	2.24	32	13	0.269	0.064	4.2	
CH ₃ OH,10 _{3,8} - 10 _{2,9} + -		252252.58	1.44	10.54	3.42	22	13	0.237	0.071	3.3	
CH ₃ OH,11 _{3,9} - 11 _{2,10} + -		252486.30	1.04	6.50	2.58	30	12	0.220	0.060	3.7	
H ₂ CCO,13 _{1,13} - 12 _{1,12}	260193.08	0.56	7.66	1.26	45	13	0.330	0.076	4.3		
H ¹³ CO ⁺ ,3-2	260255.33		5.52	0.96	191	14				s	
H ¹³ CO ⁺ ,3-2	260255.33	0.03	1.86	0.28	392	14	1.914	0.064	29.9		
SiO,6-5	260523.99	1.21	18.72	3.10	41	16	0.785	0.113	6.9		
G19.36-0.03	CH ₃ OH,8 _{3,5} - 8 _{2,6} - +	251517.25	0.41	4.36	1.30	66	21	0.349	0.076	4.6	
	CH ₃ OH,7 _{3,4} - 7 _{2,5} - +	251642.11	0.30	4.36	0.84	86	20	0.369	0.076	4.9	
	CH ₃ OH,6 _{3,3} - 6 _{2,4} - +	251738.64	0.41	4.40	1.06	65	19	0.285	0.076	3.7	
	CH ₃ OH,5 _{3,2} - 5 _{2,3} - +	251812.74	0.49	6.24	1.12	69	20	0.451	0.086	5.2	
	SO, ³ Σ _g ,6 ₅ - 5 ₄	251826.06	0.23	5.78	0.82	141	21	0.926	0.082	11.3	
	CH ₃ OH,4 _{3,1} - 4 _{2,2} - +	251866.59	0.21	2.18	0.48	93	20	0.197	0.060	3.3	
	CH ₃ OH,5 _{3,3} - 5 _{2,4} + -	251890.90		4.76		54	21	0.271	0.063	4.3	p
	CH ₃ OH,6 _{3,4} - 6 _{2,5} + -	251895.73		4.76		74	21	0.374	0.064	5.8	p
CH ₃ OH,4 _{3,2} - 4 _{2,3} + -	251900.49		4.76		74	21	0.373	0.064	5.8	p	

Table 4: (continued) Line parameters.

Object (1)	Transition ^a (2)	ν (MHz) (3)	σ_ν^b (MHz) (4)	FWHM (km s ⁻¹) (5)	σ_{FWHM}^c (km s ⁻¹) (6)	T_{MB} (mK) (7)	σ_{Tmb} (mK) (8)	I_{int}^d (K km s ⁻¹) (9)	σ_I^d (K km s ⁻¹) (10)	SNR ^d (11)	Note ^e (12)
	CH ₃ OH,3 _{3,0} - 3 _{2,1} - +	251905.81		4.76		52	21	0.264	0.063	4.2	p
	CH ₃ OH,3 _{3,1} - 3 _{2,2} + -	251917.04		3.42	0.36	66	21	0.240	0.058	4.1	p
	CH ₃ OH,7 _{3,5} - 7 _{2,6} + -	251923.63		3.42		85	21	0.311	0.058	5.4	p
	CH ₃ OH,8 _{3,6} - 8 _{2,7} + -	251984.77	0.49	3.78	2.28	49	20	0.226	0.072	3.1	
	H ¹³ CO ⁺ ,3-2	260255.32		7.20	1.86	90	21				s
	H ¹³ CO ⁺ ,3-2	260255.32	0.04	2.50	0.22	468	21	1.999	0.083	24.1	
	SiO,6-5	260518.31	1.01	13.70	3.84	47	19	0.730	0.127	5.7	
G19.61-0.12	H ¹³ CO ⁺ ,3-2	260255.35	0.17	4.24	0.54	211	26	1.052	0.092	11.4	
G19.61-0.14	H ¹³ CO ⁺ ,3-2	260255.39	0.18	5.04	0.46	135	17	0.647	0.069	9.4	
	SiO,6-5	260518.11	0.81	5.64	2.44	39	17	0.241	0.071	3.4	
G19.88-0.53	CH ₃ OH,8 _{3,5} - 8 _{2,6} - +	251517.24	0.24	4.82	0.72	113	19	0.635	0.071	8.9	
	c-HCCCH,6 _{2,5} - 5 _{1,4}	251526.35	0.62	4.14	1.30	52	20	0.302	0.071	4.3	
	CH ₃ OCH ₃ ,10 _{2,9} - 9 _{1,8} (E+A)	251581.29	0.48	4.86	1.78	67	19	0.375	0.071	5.3	
	CH ₃ OH,7 _{3,4} - 7 _{2,5} - +	251641.71	0.20	5.68	0.64	135	17	0.854	0.078	10.9	
	CH ₃ OH,6 _{3,3} - 6 _{2,4} - +	251738.46	0.16	5.22	0.46	162	17	0.926	0.074	12.5	
	CH ₃ OH,5 _{3,2} - 5 _{2,3} - +	251812.11	0.19	7.28	0.78	160	17	1.084	0.068	15.9	
	SO, ³ Σ _g ,6 ₅ - 5 ₄	251825.63	0.04	3.24	0.22	432	17	4.173	0.098	42.6	
	SO, ³ Σ _g ,6 ₅ - 5 ₄	251825.63		11.04	1.00	207	17				s
	CH ₃ OH,4 _{3,1} - 4 _{2,2} - +	251866.67	0.15	4.96	0.42	183	19	0.975	0.074	13.2	
	CH ₃ OH,5 _{3,3} - 5 _{2,4} + -	251890.90		4.08	0.10	190	21	0.824	0.057	14.5	p
	CH ₃ OH,6 _{3,4} - 6 _{2,5} + -	251895.73		4.08		193	21	0.838	0.056	15.0	p
	CH ₃ OH,4 _{3,2} - 4 _{2,3} + -	251900.49		4.08		177	21	0.772	0.056	13.8	p
	CH ₃ OH,3 _{3,0} - 3 _{2,1} - +	251905.81		4.08		148	21	0.643	0.057	11.3	p
	CH ₃ OH,3 _{3,1} - 3 _{2,2} + -	251917.04		4.34	0.22	134	21	0.616	0.064	9.6	p
	CH ₃ OH,7 _{3,5} - 7 _{2,6} + -	251923.63		4.34		144	21	0.666	0.063	10.6	p
	CH ₃ OH,8 _{3,6} - 8 _{2,7} + -	251984.20	0.21	4.40	0.60	127	20	0.587	0.071	8.3	
	CH ₃ OH,9 _{3,7} - 9 _{2,8} + -	252088.57	0.41	6.96	1.06	73	17	0.487	0.083	5.9	
	CH ₃ OH,10 _{3,8} - 10 _{2,9} + -	252252.17	0.50	5.20	1.60	73	18	0.424	0.074	5.7	
	CH ₃ OH,11 _{3,9} - 11 _{2,10} + -	252485.45	0.43	4.98	1.20	65	18	0.349	0.074	4.7	
	H ₂ CCO,13 _{1,13} - 12 _{1,12}	260192.14	0.26	3.24	0.62	76	17	0.258	0.072	3.6	
	H ¹³ CO ⁺ ,3-2	260255.35	0.02	3.40	0.06	1293	19	4.841	0.080	60.5	
	SiO,6-5	260517.49		49.64	8.74	52	22				s
	SiO,6-5	260517.49	0.24	7.66	1.00	183	22	3.267	0.143	22.8	
G20.24+0.07	H ¹³ CO ⁺ ,3-2	260255.34	0.29	3.94	0.72	96	21	0.398	0.078	5.1	
G21.24+0.19	H ¹³ CO ⁺ ,3-2	260255.34	0.08	2.00	0.18	267	21	0.626	0.063	9.9	
G22.04+0.22	CH ₃ OH,8 _{3,5} - 8 _{2,6} - +	251517.20	1.43	12.38	4.90	48	16	0.562	0.108	5.2	
	CH ₃ OH,7 _{3,4} - 7 _{2,5} - +	251641.68	0.34	4.84	0.82	76	18	0.378	0.072	5.3	
	CH ₃ OH,6 _{3,3} - 6 _{2,4} - +	251738.67	0.56	6.70	1.42	57	19	0.377	0.083	4.5	
	CH ₃ OH,5 _{3,2} - 5 _{2,3} - +	251812.34	0.34	4.40	0.84	80	20	0.361	0.068	5.3	
	SO, ³ Σ _g ,6 ₅ - 5 ₄	251826.11	0.39	5.84	1.24	82	20	0.570	0.078	7.3	
	CH ₃ OH,4 _{3,1} - 4 _{2,2} - +	251865.87	0.60	6.32	1.94	51	19	0.337	0.081	4.2	
	CH ₃ OH,5 _{3,3} - 5 _{2,4} + -	251890.90		5.96		72	19	0.456	0.064	7.1	p
	CH ₃ OH,6 _{3,4} - 6 _{2,5} + -	251895.73		5.96		61	19	0.388	0.067	5.8	p
	CH ₃ OH,4 _{3,2} - 4 _{2,3} + -	251900.49		5.96		51	19	0.322	0.066	4.9	p
	CH ₃ OH,3 _{3,0} - 3 _{2,1} - +	251905.81		5.96		65	19	0.409	0.063	6.5	p
	CH ₃ OH,3 _{3,1} - 3 _{2,2} + -	251917.04		5.22	0.48	46	17	0.254	0.054	4.7	p
	CH ₃ OH,7 _{3,5} - 7 _{2,6} + -	251923.63		5.22		68	17	0.379	0.056	6.8	p
	CH ₃ OH,8 _{3,6} - 8 _{2,7} + -	251984.41	0.45	6.14	0.98	59	17	0.331	0.081	4.1	
	CH ₃ OH,9 _{3,7} - 9 _{2,8} + -	252090.99	1.20	13.88	3.26	37	19	0.577	0.112	5.2	
	H ¹³ CO ⁺ ,3-2	260255.33	0.04	2.52	0.12	471	19	1.325	0.067	19.8	
	SiO,6-5	260519.03	1.80	33.12	5.06	45	22	1.605	0.200	8.0	
G23.01-0.41	CH ₃ OH,8 _{3,5} - 8 _{2,6} - +	251517.79	0.43	8.74	1.18	120	15	1.216	0.083	14.7	
	CH ₃ OH,7 _{3,4} - 7 _{2,5} - +	251641.43	0.20	6.58	0.48	133	16	0.899	0.071	12.7	
	CH ₃ OH,6 _{3,3} - 6 _{2,4} - +	251738.44	0.20	13.56	2.60	58	16	1.123	0.081	13.9	
	CH ₃ OH,6 _{3,3} - 6 _{2,4} - +	251738.44		3.60	0.80	88	16				s
	CH ₃ OH,5 _{3,2} - 5 _{2,3} - +	251811.57	0.25	8.66	0.94	134	17	1.269	0.076	16.7	
	SO, ³ Σ _g ,6 ₅ - 5 ₄	251825.13	0.22	8.20	0.74	153	18	1.429	0.078	18.3	
	CH ₃ OH,4 _{3,1} - 4 _{2,2} - +	251867.04	0.17	5.42	0.54	161	19	0.980	0.066	14.8	
	CH ₃ OH,5 _{3,3} - 5 _{2,4} + -	251890.90		7.44	0.46	118	20	0.931	0.083	11.2	p
	CH ₃ OH,6 _{3,4} - 6 _{2,5} + -	251895.73		7.44		127	20	1.003	0.097	10.3	p

Table 4: (continued) Line parameters.

Object (1)	Transition ^a (2)	ν (MHz) (3)	σ_ν ^b (MHz) (4)	FWHM (km s ⁻¹) (5)	σ_{FWHM} ^c (km s ⁻¹) (6)	T_{MB} (mK) (7)	σ_{Tmb} (mK) (8)	I_{int} ^d (K km s ⁻¹) (9)	σ_I ^d (K km s ⁻¹) (10)	SNR ^d Note ^e (11)	(12)
	CH ₃ OH,4 _{3,2} - 4 _{2,3} + -	251900.49		7.44		107	20	0.847	0.095	8.9	p
	CH ₃ OH,3 _{3,0} - 3 _{2,1} - +	251905.81		7.44		137	20	1.088	0.090	12.1	p
	CH ₃ OH,3 _{3,1} - 3 _{2,2} + -	251917.04		8.34		123	20	1.095	0.082	13.4	p
	CH ₃ OH,7 _{3,5} - 7 _{2,6} + -	251923.63		8.34		123	20	1.094	0.082	13.3	p
	CH ₃ OH,8 _{3,6} - 8 _{2,7} + -	251984.58	0.37	8.70	1.22	98	19	0.896	0.081	11.1	
	CH ₃ OH,9 _{3,7} - 9 _{2,8} + -	252090.15	0.28	8.66	0.68	116	17	1.021	0.081	12.6	
	CH ₃ OH,10 _{3,8} - 10 _{2,9} + -	252252.64	0.26	7.84	0.82	115	17	1.010	0.078	12.9	
	CH ₃ OH,11 _{3,9} - 11 _{2,10} + -	252484.88	0.34	9.34	1.10	92	16	0.955	0.083	11.5	
	H ₂ CCO,13 _{1,13} - 12 _{1,12}	260192.76	1.41	13.88	6.94	39	21	0.645	0.123	5.2	
	CH ₃ CH ₂ CN,29 _{6,24} - 28 _{6,23}	260221.66		9.26	2.10	33	21	0.322	0.092	3.5	
	CH ₃ CH ₂ CN,29 _{6,23} - 28 _{6,22}	260229.16		9.26		39	21	0.387	0.100	3.9	
	H ¹³ CO ⁺ ,3-2	260255.40	0.04	4.38	0.12	700	21	3.411	0.082	41.6	
	HCOOCH ₃ ,21 _{8,13} - 20 _{8,12} E	260383.99	0.20	1.94	0.54	104	21	0.321	0.063	5.1	
	SiO,6-5	260520.92	1.16	33.18	2.90	70	21	2.453	0.187	13.1	
	CH ₃ OCH ₃ ,6 _{3,3} - 5 _{2,4} EE	260757.72	1.25	9.56	2.38	35	22	0.325	0.108	3.0	
	OC ³⁴ S,22-21	260986.46	0.66	4.96	1.90	48	21	0.250	0.082	3.0	
G23.82+0.38	H ¹³ CO ⁺ ,3-2	260255.34	0.22	3.36	0.62	107	20	0.404	0.070	5.8	
G23.96-0.11	CH ₃ OH,5 _{3,2} - 5 _{2,3} - +	251812.79	0.84	8.28	3.00	45	19	0.293	0.091	3.2	
	SO, ³ Σ _g ,6 ₅ - 5 ₄	251825.85	0.30	5.56	0.88	93	19	0.574	0.075	7.7	
	CH ₃ OH,4 _{3,1} - 4 _{2,2} - +	251866.81	0.35	4.10	0.78	73	19	0.233	0.068	3.4	
	CH ₃ OH,5 _{3,3} - 5 _{2,4} + -	251890.90		4.70	0.44	57	19	0.285	0.059	4.8	p
	CH ₃ OH,6 _{3,4} - 6 _{2,5} + -	251895.73		4.70		39	19	0.197	0.059	3.3	p
	CH ₃ OH,4 _{3,2} - 4 _{2,3} + -	251900.49		4.70		57	19	0.285	0.060	4.8	p
	CH ₃ OH,3 _{3,0} - 3 _{2,1} - +	251905.81		4.70		42	19	0.208	0.057	3.6	p
	CH ₃ OH,3 _{3,1} - 3 _{2,2} + -	251917.04		2.76	0.48	59	19	0.174	0.049	3.6	p
	U252478	252477.92	0.54	3.82	1.56	53	17	0.251	0.068	3.7	
	U252557	252556.71	1.36	9.98	2.96	29	17	0.296	0.096	3.1	
	H ¹³ CO ⁺ ,3-2	260254.96	0.10	4.24	0.30	280	21	1.316	0.084	15.7	
	SiO,6-5	260518.63	0.52	10.76	1.54	86	21	0.967	0.119	8.1	
G24.00-0.10	CH ₃ OH,6 _{3,3} - 6 _{2,4} - +	251737.70	1.01	7.70	2.40	42	18	0.317	0.090	3.5	
	CH ₃ OH,5 _{3,2} - 5 _{2,3} - +	251813.47	0.31	2.74	0.90	57	17	0.184	0.058	3.2	
	SO, ³ Σ _g ,6 ₅ - 5 ₄	251825.08	0.44	3.86	1.34	85	18	0.345	0.069	5.0	
	CH ₃ OH,4 _{3,1} - 4 _{2,2} - +	251866.61	0.82	6.40	2.64	37	19	0.269	0.082	3.3	
	CH ₃ OH,6 _{3,4} - 6 _{2,5} + -	251895.73		5.26		45	20	0.249	0.064	3.9	p
	CH ₃ OH,4 _{3,2} - 4 _{2,3} + -	251900.49		5.26		38	20	0.210	0.062	3.4	p
	CH ₃ OH,3 _{3,0} - 3 _{2,1} - +	251905.81		5.26		36	20	0.201	0.061	3.3	p
	H ¹³ CO ⁺ ,3-2	260255.47	0.15	4.16	0.38	160	18	0.673	0.083	8.1	
G24.11-0.17	H ¹³ CO ⁺ ,3-2	260255.34	0.18	2.54	0.66	136	24	0.391	0.077	5.1	
G24.33+0.14	CH ₃ OH,8 _{3,5} - 8 _{2,6} - +	251516.71	0.51	6.64	1.48	109	32	0.647	0.147	4.4	
	CH ₃ CH ₂ CN,28 _{5,23} - 27 _{5,22}	251606.32	0.34	3.10	0.86	67	20	0.256	0.067	3.8	
	CH ₃ OH,7 _{3,4} - 7 _{2,5} - +	251640.98	0.23	4.00	0.68	116	21	0.550	0.070	7.9	
	CH ₃ CH ₂ CN,28 _{4,25} - 27 _{4,24}	251667.67	0.68	5.56	1.70	44	20	0.241	0.080	3.0	
	CH ₃ OH,6 _{3,3} - 6 _{2,4} - +	251738.12	0.14	3.34	0.40	153	19	0.549	0.067	8.2	
	CH ₃ OH,5 _{3,2} - 5 _{2,3} - +	251811.76	0.23	5.56	0.74	128	19	0.805	0.080	10.1	
	SO, ³ Σ _g ,6 ₅ - 5 ₄	251826.04	0.31	2.70	1.02	56	18	0.980	0.099	9.9	
	SO, ³ Σ _g ,6 ₅ - 5 ₄	251826.04		16.84	4.34	50	18				s
	CH ₃ OH,4 _{3,1} - 4 _{2,2} - +	251866.46	0.28	6.18	0.72	108	19	0.657	0.080	8.2	
	CH ₃ OH,5 _{3,3} - 5 _{2,4} + -	251890.90		4.72	0.18	126	19	0.631	0.056	11.3	p
	CH ₃ OH,6 _{3,4} - 6 _{2,5} + -	251895.73		4.72		133	19	0.665	0.055	12.1	p
	CH ₃ OH,4 _{3,2} - 4 _{2,3} + -	251900.49		4.72		161	19	0.806	0.057	14.1	p
	CH ₃ OH,3 _{3,0} - 3 _{2,1} - +	251905.81		4.72		95	19	0.478	0.055	8.7	p
	CH ₃ OH,3 _{3,1} - 3 _{2,2} + -	251917.04		4.60	0.26	108	20	0.527	0.061	8.6	p
	CH ₃ OH,7 _{3,5} - 7 _{2,6} + -	251923.63		4.60		130	20	0.638	0.064	10.0	p
	CH ₃ OH,8 _{3,6} - 8 _{2,7} + -	251984.12	0.22	4.72	0.60	115	19	0.562	0.074	7.6	
	CH ₃ OH,9 _{3,7} - 9 _{2,8} + -	252089.08	0.36	6.90	1.12	92	20	0.705	0.086	8.2	
	CH ₃ OH,10 _{3,8} - 10 _{2,9} + -	252253.11	0.63	8.02	1.98	79	19	0.704	0.091	7.7	
	CH ₃ OH,11 _{3,9} - 11 _{2,10} + -	252485.19	0.33	5.84	0.88	86	18	0.541	0.080	6.8	
	HCOOCH ₃ ,21 _{3,18} - 20 _{3,17} A	260255.67	0.08	2.60	0.24	468	37	1.356	0.122	11.1	b
	H ¹³ CO ⁺ ,3-2	260255.67	0.08	2.60	0.24	468	37	1.356	0.122	11.1	b
	CH ₃ OCH ₃ ,16 _{5,11} - 16 _{4,12} EE	260403.85	0.81	6.00	2.36	50	20	0.394	0.094	4.2	b

Table 4: (continued) Line parameters.

Object (1)	Transition ^a (2)	ν (MHz) (3)	σ_ν ^b (MHz) (4)	FWHM (km s ⁻¹) (5)	σ_{FWHM}^c (km s ⁻¹) (6)	T_{MB} (mK) (7)	σ_{Tmb} (mK) (8)	I_{int}^d (K km s ⁻¹) (9)	σ_I^d (K km s ⁻¹) (10)	SNR ^d Note ^e (11) (12)	
	HCOOCH ₃ ,21 _{8,14} – 20 _{8,13} E	260403.85	0.81	6.00	2.38	50	20	0.394	0.094	4.2	b
	SiO,6-5	260518.07	1.37	27.16	4.58	51	20	1.427	0.181	7.9	
	HCOOCH ₃ ,21 _{5,17} – 20 _{5,16} E	261144.25	0.43	3.00	1.12	61	23	0.233	0.075	3.1	b
	CH ₃ OCH ₃ , 17 _{5,13} – 17 _{4,14} EE	261144.25	0.43	3.00	1.12	61	23	0.233	0.075	3.1	b
	HN ¹³ C,3-2	261263.39	0.10	2.72	0.28	253	23	0.821	0.071	11.6	
G24.63+0.15	SO, ³ Σ,6 ₅ – 5 ₄	251826.44	1.03	10.52	3.66	37	18	0.418	0.109	3.8	
	CH ₃ OH,5 _{3,3} – 5 _{2,4} + –	251890.90		3.58		46	21	0.176	0.052	3.4	p
	H ¹³ CO ⁺ ,3-2	260255.32	0.14	3.54	0.44	183	20	0.781	0.077	10.1	
	SiO,6-5	260519.14	2.21	17.72	6.26	30	23	0.558	0.152	3.7	
G24.94+0.07	CH ₃ OH,5 _{3,2} – 5 _{2,3} – +	251809.65	0.88	10.02	3.80	48	21	0.581	0.113	5.1	
	SO, ³ Σ,6 ₅ – 5 ₄	251825.80	0.78	6.88	2.00	47	21	0.367	0.096	3.8	
	H ¹³ CO ⁺ ,3-2	260255.33	0.18	4.22	0.48	170	23	0.747	0.089	8.4	
G25.38-0.15	CH ₃ OH,6 _{3,3} – 6 _{2,4} – +	251738.87	0.33	2.46	1.00	58	18	0.178	0.055	3.2	
	CH ₃ OH,5 _{3,2} – 5 _{2,3} – +	251813.72	0.80	7.06	1.84	43	18	0.361	0.081	4.5	
	SO, ³ Σ,6 ₅ – 5 ₄	251825.86	0.22	5.04	0.62	125	18	0.699	0.072	9.7	
	CH ₃ OH,4 _{3,1} – 4 _{2,2} – +	251867.04	0.42	4.38	0.96	57	18	0.219	0.069	3.2	
	CH ₃ OH,5 _{3,3} – 5 _{2,4} + –	251890.90		3.94	0.20	84	17	0.350	0.047	7.4	p
	CH ₃ OH,6 _{3,4} – 6 _{2,5} + –	251895.73		3.94		56	17	0.234	0.045	5.2	p
	CH ₃ OH,4 _{3,2} – 4 _{2,3} + –	251900.49		3.94		97	17	0.407	0.045	9.0	p
	CH ₃ OH,3 _{3,0} – 3 _{2,1} – +	251905.81		3.94		71	17	0.298	0.045	6.6	p
	H ¹³ CO ⁺ ,3-2	260255.29	0.06	3.30	0.16	382	20	1.340	0.070	19.1	
	SiO,6-5	260518.21		71.60	13.38	22	22				s
	SiO,6-5	260518.21	0.33	5.40	1.04	100	22	2.155	0.212	10.2	
G28.28-0.36	H ¹³ CO ⁺ ,3-2	260255.34	0.20	2.12	0.64	164	31	0.385	0.092	4.2	
G28.83-0.25	H ¹³ CO ⁺ ,3-2	260255.32	0.10	3.38	0.30	320	28	1.197	0.112	10.7	
G28.85-0.23	H ¹³ CO ⁺ ,3-2	260255.41	0.22	2.40	0.58	109	24	0.289	0.075	3.9	
G34.26+0.15	CH ₃ OH,7 _{3,4} – 7 _{2,5} – +	251642.27	0.24	3.82	0.82	118	22	0.505	0.072	7.0	
	CH ₃ OH,6 _{3,3} – 6 _{2,4} – +	251737.93	0.19	3.62	0.70	137	21	0.638	0.076	8.4	
	CH ₃ OH,5 _{3,2} – 5 _{2,3} – +	251811.59	0.38	9.18	1.72	114	22	1.345	0.105	12.8	
	SO, ³ Σ,6 ₅ – 5 ₄	251825.47	0.06	3.56	0.32	405	22	3.211	0.105	30.6	
	SO, ³ Σ,6 ₅ – 5 ₄	251825.47		11.48	2.00	137	22				s
	CH ₃ OH,4 _{3,1} – 4 _{2,2} – +	251866.49	0.19	5.10	0.76	155	21	0.932	0.083	11.2	
	CH ₃ OH,5 _{3,3} – 5 _{2,4} + –	251890.90		4.50	0.14	155	20	0.739	0.060	12.3	p
	CH ₃ OH,6 _{3,4} – 6 _{2,5} + –	251895.73		4.50		131	20	0.625	0.059	10.6	p
	CH ₃ OH,4 _{3,2} – 4 _{2,3} + –	251900.49		4.50		185	20	0.885	0.060	14.8	p
	CH ₃ OH,3 _{3,0} – 3 _{2,1} – +	251905.81		4.50		129	20	0.619	0.058	10.7	p
	CH ₃ OH,3 _{3,1} – 3 _{2,2} + –	251917.04		5.36	0.24	146	19	0.833	0.065	12.8	p
	CH ₃ OH,7 _{3,5} – 7 _{2,6} + –	251923.63		5.36		115	19	0.656	0.062	10.6	p
	CH ₃ OH,8 _{3,6} – 8 _{2,7} + –	251984.96	0.40	3.12	1.58	58	19	0.239	0.068	3.5	
	CH ₃ OH,10 _{3,8} – 10 _{2,9} + –	252252.64	0.24	1.94	0.86	79	21	0.191	0.059	3.2	
	H ₂ CCO,13 _{1,13} – 12 _{1,12}	260192.36	0.42	3.50	0.98	62	21	0.264	0.080	3.3	
	H ¹³ CO ⁺ ,3-2	260255.37	0.02	3.72	0.06	1374	25	5.598	0.084	66.6	
	SiO,6-5	260517.01	0.13	5.92	0.62	261	21	4.288	0.180	23.8	
	SiO,6-5	260517.01		42.96	7.78	67	21				s
	U260865	260864.39	0.37	3.84	0.78	77	22	0.292	0.080	3.6	
G34.28+0.18	H ¹³ CO ⁺ ,3-2	260255.34	0.07	2.50	0.24	367	26	1.029	0.081	12.7	
	SiO,6-5	260517.25	0.90	14.38	2.98	72	27	1.113	0.165	6.7	
G34.39+0.22	SO, ³ Σ,6 ₅ – 5 ₄	251825.76	0.23	5.02	0.70	122	20	0.693	0.081	8.6	
	CH ₃ OH,5 _{3,3} – 5 _{2,4} + –	251890.90		5.86	0.98	45	24	0.279	0.085	3.3	p
	H ¹³ CO ⁺ ,3-2	260255.34	0.05	3.16	0.14	572	23	1.960	0.078	25.1	
	SiO,6-5	260519.72	0.32	7.62	0.98	134	24	1.119	0.104	10.8	
G34.41+0.24	CH ₃ CH ₂ CN,28 _{5,24} – 27 _{5,23}	251503.22	0.71	8.04	2.04	62	24	0.542	0.105	5.2	
	CH ₃ OH,8 _{3,5} – 8 _{2,6} – +	251516.98	0.15	6.70	0.44	275	23	2.093	0.098	21.4	
	c-HCCCH,6 _{2,5} – 5 _{1,4}	251526.45	0.86	6.54	2.50	53	23	0.857	0.098	8.7	
	CH ₃ OCH ₃ ,10 _{2,9} – 9 _{1,8} (E+A)	251583.89	0.34	6.62	0.80	114	23	0.768	0.095	8.1	
	CH ₃ CH ₂ CN,28 _{5,23} – 27 _{5,22}	251605.76	0.80	7.88	2.60	53	23	0.455	0.101	4.5	
	CH ₃ OH,7 _{3,4} – 7 _{2,5} – +	251641.84	0.13	6.06	0.40	271	22	1.790	0.095	18.8	
	CH ₃ CH ₂ CN,28 _{4,25} – 27 _{4,24}	251667.56	1.27	8.66	2.86	38	23	0.365	0.108	3.4	
	CH ₃ OH,6 _{3,3} – 6 _{2,4} – +	251738.18	0.10	5.90	0.28	343	21	2.193	0.091	24.1	
	CH ₃ OH,5 _{3,2} – 5 _{2,3} – +	251811.82	0.09	5.74	0.28	388	23	2.475	0.091	27.2	

Table 4: (continued) Line parameters.

Object (1)	Transition ^a (2)	ν (MHz) (3)	σ_ν ^b (MHz) (4)	FWHM (km s ⁻¹) (5)	σ_{FWHM}^c (km s ⁻¹) (6)	T_{MB} (mK) (7)	σ_{Tmb} (mK) (8)	I_{int}^d (K km s ⁻¹) (9)	σ_I^d (K km s ⁻¹) (10)	SNR ^d Note ^e (11) (12)	
	SO, ³ $\Sigma_65 - 5_4$	251825.64	0.09	7.50	0.28	489	24	4.064	0.101	40.2	
	CH ₃ OH, 4 _{3,1} - 4 _{2,2} - +	251866.49	0.09	5.04	0.26	405	25	2.163	0.088	24.6	
	CH ₃ OH, 5 _{3,3} - 5 _{2,4} + -	251890.90		5.08	0.12	355	25	1.921	0.080	24.0	p
	CH ₃ OH, 6 _{3,4} - 6 _{2,5} + -	251895.73		5.08		338	25	1.829	0.079	23.2	p
	CH ₃ OH, 4 _{3,2} - 4 _{2,3} + -	251900.49		5.08		371	25	2.006	0.078	25.7	p
	CH ₃ OH, 3 _{3,0} - 3 _{2,1} - +	251905.81		5.08		334	25	1.804	0.080	22.6	p
	CH ₃ OH, 3 _{3,1} - 3 _{2,2} + -	251917.04		5.82	0.14	280	24	1.735	0.082	21.2	p
	CH ₃ OH, 7 _{3,5} - 7 _{2,6} + -	251923.63		5.82		303	24	1.877	0.082	22.9	p
	CH ₃ OH, 8 _{3,6} - 8 _{2,7} + -	251984.57	0.13	6.20	0.42	269	22	1.822	0.095	19.2	
	CH ₃ OH, 9 _{3,7} - 9 _{2,8} + -	252090.17	0.17	7.66	0.52	218	21	1.838	0.104	17.7	
	CH ₃ OH, 10 _{3,8} - 10 _{2,9} + -	252252.64	0.20	7.96	0.58	204	23	1.715	0.104	16.5	
	CH ₃ OH, 11 _{3,9} - 11 _{2,10} + -	252485.23	0.19	7.00	0.50	196	22	1.435	0.098	14.6	
	H ₂ CCO, 13 _{1,13} - 12 _{1,12}	260191.54	0.38	5.34	0.96	85	21	0.490	0.110	4.5	
	CH ₃ CH ₂ CN, 29 _{6,24} - 28 _{6,23}	260221.66		8.04	0.90	49	21	0.423	0.080	5.3	
	CH ₃ CH ₂ CN, 29 _{6,23} - 28 _{6,22}	260229.16		8.04		39	21	0.333	0.082	4.1	
	HCOOCH ₃ , 21 _{3,18} - 20 _{3,17E}	260244.50		10.08	4.80	40	21	2.152	0.140	15.4	
	HCOOCH ₃ , 21 _{3,18} - 20 _{3,17A}	260255.43	0.03	3.54	0.08	886	21	3.507	0.096	36.5	b
	H ¹³ CO ⁺ , 3-2	260255.43	0.03	3.54	0.08	886	21	3.507	0.096	36.5	b
	CH ₃ OCH ₃ , 19 _{5,15} - 19 _{4,16EE}	260328.23	0.70	8.86	1.86	68	23	0.632	0.133	4.8	
	HCOOCH ₃ , 21 _{8,13} - 20 _{8,12E}	260382.09	0.44	8.16	1.24	136	25	1.093	0.129	8.5	
	HCOOCH ₃ , 21 _{8,14} - 20 _{8,13E}	260403.39	0.46	7.40	1.46	102	24	0.725	0.122	5.9	
	CH ₃ OCH ₃ , 16 _{5,11} - 16 _{4,12EE}	260403.39	0.46	7.40	1.46	102	24	0.725	0.122	5.9	
	SiO, 6-5	260518.64	0.27	9.06	1.24	194	30	5.548	0.209	26.5	
	SiO, 6-5	260518.64		36.46	4.32	103	30				s
	CH ₃ OCH ₃ , 6 _{3,3} - 5 _{2,4EE}	260757.92	0.54	7.24	1.16	100	29	0.708	0.122	5.8	
	U260865	260866.02	0.50	5.46	1.18	76	25	0.390	0.110	3.5	
	HCOOCH ₃ , 21 _{5,17} - 20 _{5,16E}	261147.67	0.58	8.34	1.12	87	27	0.656	0.129	5.1	
	CH ₃ OCH ₃ , 17 _{5,13} - 17 _{4,14EE}	261147.67	0.58	8.34	1.12	87	27	0.656	0.129	5.1	
	HCOOCH ₃ , 21 _{5,17} - 20 _{5,16A}	261165.53	0.36	3.58	1.24	101	27	0.467	0.096	4.9	
G35.03+0.35	CH ₃ OH, 7 _{3,4} - 7 _{2,5} - +	251641.66	0.46	6.50	1.08	87	24	0.534	0.106	5.0	
	CH ₃ OH, 6 _{3,3} - 6 _{2,4} - +	251739.28	0.78	10.72	2.00	70	26	0.756	0.129	5.9	
	CH ₃ OH, 5 _{3,2} - 5 _{2,3} - +	251812.99	1.09	9.94	3.20	61	26	0.574	0.110	5.2	
	SO, ³ $\Sigma_65 - 5_4$	251826.06	0.09	6.18	0.28	485	28	3.311	0.103	32.1	
	CH ₃ OH, 4 _{3,1} - 4 _{2,2} - +	251867.22	0.41	6.12	1.02	105	27	0.661	0.103	6.4	
	CH ₃ OH, 5 _{3,3} - 5 _{2,4} + -	251890.90		6.08	0.56	65	27	0.424	0.093	4.6	p
	CH ₃ OH, 6 _{3,4} - 6 _{2,5} + -	251895.73		6.08		84	27	0.545	0.099	5.5	p
	CH ₃ OH, 4 _{3,2} - 4 _{2,3} + -	251900.49		6.08		92	27	0.594	0.095	6.3	p
	CH ₃ OH, 3 _{3,0} - 3 _{2,1} - +	251905.81		6.08		71	27	0.462	0.091	5.1	p
	CH ₃ OH, 3 _{3,1} - 3 _{2,2} + -	251917.04		3.58		95	27	0.360	0.068	5.3	p
	CH ₃ OH, 7 _{3,5} - 7 _{2,6} + -	251923.63		3.58		94	27	0.358	0.068	5.3	p
	CH ₃ OH, 8 _{3,6} - 8 _{2,7} + -	251986.91	0.56	4.98	2.12	61	24	0.332	0.095	3.5	
	CH ₃ OH, 9 _{3,7} - 9 _{2,8} + -	252088.95	2.09	17.00	6.74	27	21	0.520	0.155	3.4	
	H ¹³ CO ⁺ , 3-2	260255.18	0.06	5.32	0.16	634	25	3.596	0.109	33.0	
	SiO, 6-5	260518.42	0.44	6.72	1.38	109	29	2.220	0.241	9.2	
	SiO, 6-5	260518.42		56.54	14.90	27	29				s
G35.04-0.47	H ¹³ CO ⁺ , 3-2	260255.34	0.10	1.52	0.70	185	26	0.298	0.078	3.8	
	SiO, 6-5	260515.54	0.79	7.16	1.72	56	25	0.413	0.127	3.3	
G35.13-0.74	CH ₃ OH, 8 _{3,5} - 8 _{2,6} - +	251517.26		4.74	0.66	98	26	0.494	0.096	5.1	
	CH ₃ OH, 7 _{3,4} - 7 _{2,5} - +	251640.16	0.40	6.00	1.14	100	24	0.627	0.108	5.8	
	CH ₃ OH, 6 _{3,3} - 6 _{2,4} - +	251738.27	0.21	3.46	0.62	139	25	0.514	0.087	5.9	
	CH ₃ OH, 5 _{3,2} - 5 _{2,3} - +	251811.32	0.28	5.54	0.82	142	27	0.859	0.104	8.3	
	SO, ³ $\Sigma_65 - 5_4$	251825.35	0.06	4.40	0.18	596	27	2.903	0.096	30.2	
	CH ₃ OH, 4 _{3,1} - 4 _{2,2} - +	251866.73	0.27	4.50	0.74	137	27	0.669	0.096	7.0	
	CH ₃ OH, 5 _{3,3} - 5 _{2,4} + -	251890.90		5.22	0.30	116	29	0.642	0.091	7.1	p
	CH ₃ OH, 6 _{3,4} - 6 _{2,5} + -	251895.73		5.22		137	29	0.763	0.091	8.4	p
	CH ₃ OH, 4 _{3,2} - 4 _{2,3} + -	251900.49		5.22		142	29	0.787	0.091	8.6	p
	CH ₃ OH, 3 _{3,0} - 3 _{2,1} - +	251905.81		5.22		123	29	0.683	0.089	7.7	p
	CH ₃ OH, 3 _{3,1} - 3 _{2,2} + -	251917.04		5.78	0.44	124	29	0.764	0.102	7.5	p
	CH ₃ OH, 7 _{3,5} - 7 _{2,6} + -	251923.63		5.78		72	29	0.440	0.093	4.7	p
	CH ₃ OH, 8 _{3,6} - 8 _{2,7} + -	251984.89	0.72	6.76	2.10	64	28	0.452	0.108	4.2	

Table 4: (continued) Line parameters.

Object (1)	Transition ^a (2)	ν (MHz) (3)	σ_ν ^b (MHz) (4)	FWHM (km s ⁻¹) (5)	σ_{FWHM}^c (km s ⁻¹) (6)	T_{MB} (mK) (7)	σ_{Tmb} (mK) (8)	I_{int}^d (K km s ⁻¹) (9)	σ_I^d (K km s ⁻¹) (10)	SNR ^d Note ^e (11) (12)	
	CH ₃ OH,10 _{3,8} - 10 _{2,9} + -	252251.47	1.71	14.28	3.82	38	23	0.544	0.153	3.6	
	H ¹³ CO ⁺ ,3-2	260255.45	0.03	4.02	0.08	1094	27	4.662	0.107	43.6	b
	SiO,6-5	260518.09	0.32	4.88	0.94	106	28	2.312	0.164	14.1	
	SiO,6-5	260518.09		20.30	2.86	90	28				s
G35.15+0.80	H ¹³ CO ⁺ ,3-2	260255.34	0.16	1.82	0.44	146	25	0.328	0.084	3.9	
G35.20-0.74	CH ₃ OH,8 _{3,5} - 8 _{2,6} - +	251518.47	0.20	6.88	0.66	262	23	1.786	0.100	17.9	
	c-HCCCH,6 _{2,5} - 5 _{1,4}	251526.66	0.36	5.46	1.22	106	23	0.611	0.096	6.4	
	CH ₃ OCH ₃ ,10 _{2,9} - 9 _{1,8} (E+A)	251582.76	0.77	10.18	1.70	66	24	0.665	0.133	5.0	
	CH ₃ OH,7 _{3,4} - 7 _{2,5} - +	251643.24	0.16	6.26	0.46	257	25	1.717	0.108	15.9	
	CH ₃ OH,6 _{3,3} - 6 _{2,4} - +	251739.31	0.14	6.26	0.38	282	26	1.839	0.108	17.0	
	CH ₃ OH,5 _{3,2} - 5 _{2,3} - +	251812.45	0.17	6.70	0.56	262	26	2.144	0.112	19.1	
	SO, ³ Σ,6 ₅ - 5 ₄	251825.74	0.08	7.24	0.22	592	27	4.704	0.116	40.6	
	CH ₃ OH,4 _{3,1} - 4 _{2,2} - +	251866.91	0.14	6.50	0.38	291	25	1.988	0.108	18.4	
	CH ₃ OH,5 _{3,3} - 5 _{2,4} + -	251890.90		5.44	0.16	244	24	1.413	0.078	18.1	p
	CH ₃ OH,6 _{3,4} - 6 _{2,5} + -	251895.73		5.44		288	24	1.671	0.079	21.2	p
	CH ₃ OH,4 _{3,2} - 4 _{2,3} + -	251900.49		5.44		296	24	1.715	0.079	21.7	p
	CH ₃ OH,3 _{3,0} - 3 _{2,1} - +	251905.81		5.44		233	24	1.352	0.078	17.3	p
	CH ₃ OH,3 _{3,1} - 3 _{2,2} + -	251917.04		6.58	0.24	208	25	1.456	0.087	16.7	p
	CH ₃ OH,7 _{3,5} - 7 _{2,6} + -	251923.63		6.58		232	25	1.620	0.096	16.9	p
	CH ₃ OH,8 _{3,6} - 8 _{2,7} + -	251985.97	0.15	5.66	0.38	262	26	1.559	0.100	15.6	
	CH ₃ OH,9 _{3,7} - 9 _{2,8} + -	252091.73	0.21	6.14	0.78	198	26	1.410	0.108	13.1	
	CH ₃ OH,10 _{3,8} - 10 _{2,9} + -	252254.64	0.18	5.28	0.48	199	25	1.064	0.100	10.6	
	CH ₃ OH,11 _{3,9} - 11 _{2,10} + -	252487.06	0.17	5.62	0.44	206	23	1.206	0.100	12.1	
	H ¹³ CO ⁺ ,3-2	260255.16	0.03	5.16	0.08	1522	29	8.499	0.124	68.5	
	HCOOCH ₃ ,21 _{8,13} - 20 _{8,12} E	260384.15	0.77	6.52	1.60	129	29	0.715	0.129	5.5	
	SiO,6-5	260517.92	0.37	8.90	1.06	154	28	1.485	0.145	10.2	
	U260865	260863.80	0.41	4.26	1.12	93	27	0.422	0.105	4.0	
	HCOOCH ₃ ,21 _{5,17} - 20 _{5,16} E	261150.45	0.29	3.58	1.00	124	29	0.544	0.099	5.5	
	CH ₃ OCH ₃ , 17 _{5,13} - 17 _{4,14} EE	261150.45	0.29	3.58	1.00	124	29	0.544	0.099	5.5	
	HCOOCH ₃ ,21 _{5,17} - 20 _{5,16} A	261166.44	0.95	10.40	2.66	63	29	0.694	0.155	4.5	
G35.68-0.18	H ¹³ CO ⁺ ,3-2	260255.34	0.09	2.24	0.26	265	23	0.632	0.082	7.7	
G35.79-0.17	CH ₃ OH,8 _{3,5} - 8 _{2,6} - +	251518.42	0.36	1.78	0.76	73	27	0.270	0.071	3.8	
	CH ₃ OH,7 _{3,4} - 7 _{2,5} - +	251641.56	0.59	5.90	1.48	71	26	0.394	0.105	3.8	
	CH ₃ OH,6 _{3,3} - 6 _{2,4} - +	251738.35	0.61	6.18	1.32	68	26	0.374	0.109	3.4	
	CH ₃ OH,5 _{3,2} - 5 _{2,3} - +	251810.92	0.43	6.94	1.52	103	26	0.773	0.113	6.8	
	SO, ³ Σ,6 ₅ - 5 ₄	251825.24	0.49	11.26	1.56	113	25	1.296	0.139	9.3	
	CH ₃ OH,4 _{3,1} - 4 _{2,2} - +	251867.73	0.54	8.22	1.84	80	24	0.721	0.120	6.0	
	CH ₃ OH,5 _{3,3} - 5 _{2,4} + -	251890.90		5.46	0.44	76	22	0.440	0.071	6.2	p
	CH ₃ OH,6 _{3,4} - 6 _{2,5} + -	251895.73		5.46		86	22	0.499	0.073	6.8	p
	CH ₃ OH,4 _{3,2} - 4 _{2,3} + -	251900.49		5.46		60	22	0.351	0.073	4.8	p
	CH ₃ OH,3 _{3,0} - 3 _{2,1} - +	251905.81		5.46		83	22	0.480	0.074	6.5	p
	CH ₃ OH,3 _{3,1} - 3 _{2,2} + -	251917.04		4.98	0.48	95	22	0.504	0.077	6.5	p
	CH ₃ OH,7 _{3,5} - 7 _{2,6} + -	251923.63		4.98		49	22	0.262	0.066	4.0	p
	CH ₃ OH,8 _{3,6} - 8 _{2,7} + -	251984.15	0.41	6.26	0.90	100	26	0.584	0.109	5.4	
	CH ₃ OH,9 _{3,7} - 9 _{2,8} + -	252090.65	2.65	24.20	8.02	33	26	0.788	0.195	4.0	
	CH ₃ OH,10 _{3,8} - 10 _{2,9} + -	252251.78	0.38	2.98	1.20	75	24	0.250	0.082	3.0	
	CH ₃ OH,11 _{3,9} - 11 _{2,10} + -	252484.04	1.33	12.00	3.60	37	22	0.470	0.142	3.3	
	H ¹³ CO ⁺ ,3-2	260255.53	0.12	3.68	0.36	249	23	1.037	0.094	11.0	
	SiO,6-5	260517.94	0.39	8.96	1.30	124	25	1.257	0.129	9.7	
G37.48-0.10	H ¹³ CO ⁺ ,3-2	260255.34	0.17	2.46	0.46	180	29	0.493	0.087	5.7	
G39.10+0.49	CH ₃ OH,5 _{3,2} - 5 _{2,3} - +	251811.47	1.89	11.10	4.92	30	25	0.504	0.136	3.7	
	SO, ³ Σ,6 ₅ - 5 ₄	251826.42	0.68	11.66	2.00	82	25	1.008	0.142	7.1	
	H ¹³ CO ⁺ ,3-2	260255.26	0.22	3.68	0.74	169	30	0.688	0.107	6.4	
	SiO,6-5	260516.18	1.20	15.80	3.26	64	30	1.075	0.190	5.7	
G39.39-0.14	CH ₃ OH,5 _{3,2} - 5 _{2,3} - +	251811.89	0.41	2.98	1.36	71	27	0.274	0.089	3.1	
	SO, ³ Σ,6 ₅ - 5 ₄	251826.00	0.37	7.72	1.26	132	27	1.137	0.130	8.7	
	H ¹³ CO ⁺ ,3-2	260255.29	0.13	3.44	0.36	242	27	0.920	0.106	8.7	
G40.28-0.22	CH ₃ OH,8 _{3,5} - 8 _{2,6} - +	251517.30	0.23	5.24	0.66	131	20	0.767	0.086	8.9	
	CH ₃ OH,7 _{3,4} - 7 _{2,5} - +	251641.23	0.18	4.64	0.48	161	21	0.799	0.083	9.6	
	CH ₃ OH,6 _{3,3} - 6 _{2,4} - +	251738.18	0.20	6.04	0.56	165	21	1.057	0.090	11.7	

Table 4: (continued) Line parameters.

Object (1)	Transition ^a (2)	ν (MHz) (3)	σ_ν ^b (MHz) (4)	FWHM (km s ⁻¹) (5)	σ_{FWHM}^c (km s ⁻¹) (6)	T_{MB} (mK) (7)	σ_{Tmb} (mK) (8)	I_{int}^d (K km s ⁻¹) (9)	σ_I^d (K km s ⁻¹) (10)	SNR ^d Note ^e (11) (12)	
	CH ₃ OH,5 _{3,2} - 5 _{2,3} - +	251811.45	0.14	4.96	0.38	197	19	1.022	0.086	11.9	
	SO, ³ Σ,6 ₅ - 5 ₄	251825.76		4.62	0.70	169	19				s
	SO, ³ Σ,6 ₅ - 5 ₄	251825.76	0.14	18.08	3.78	68	19	1.971	0.119	16.6	
	CH ₃ OH,4 _{3,1} - 4 _{2,2} - +	251865.97	0.17	5.36	0.54	173	20	1.054	0.086	12.3	
	CH ₃ OH,5 _{3,3} - 5 _{2,4} + -	251890.90		4.82	0.12	180	19	0.924	0.058	15.9	p
	CH ₃ OH,6 _{3,4} - 6 _{2,5} + -	251895.73		4.82		182	19	0.938	0.058	16.2	p
	CH ₃ OH,4 _{3,2} - 4 _{2,3} + -	251900.49		4.82		203	19	1.042	0.058	18.0	p
	CH ₃ OH,3 _{3,0} - 3 _{2,1} - +	251905.81		4.82		169	19	0.868	0.058	15.0	p
	CH ₃ OH,3 _{3,1} - 3 _{2,2} + -	251917.04		5.28	0.20	164	20	0.923	0.066	14.0	p
	CH ₃ OH,7 _{3,5} - 7 _{2,6} + -	251923.63		5.28		133	20	0.746	0.064	11.7	p
	CH ₃ OH,8 _{3,6} - 8 _{2,7} + -	251984.32	0.31	6.84	0.86	118	22	0.883	0.096	9.2	
	CH ₃ OH,9 _{3,7} - 9 _{2,8} + -	252090.01	0.44	7.56	1.06	85	22	0.664	0.099	6.7	
	CH ₃ OH,10 _{3,8} - 10 _{2,9} + -	252252.57	0.33	4.82	1.04	90	21	0.480	0.086	5.6	
	CH ₃ OH,11 _{3,9} - 11 _{2,10} + -	252483.92	0.29	3.70	0.70	92	22	0.366	0.074	4.9	
	H ¹³ CO ⁺ ,3-2	260255.43	0.04	3.84	0.10	746	20	3.135	0.085	36.9	
	SiO,6-5	260520.15	0.55	14.42	1.56	113	25	1.744	0.144	12.1	
G40.28-0.27	H ¹³ CO ⁺ ,3-2	260255.34	0.35	2.86	1.16	96	24	0.300	0.087	3.4	
G40.60-0.72	H ¹³ CO ⁺ ,3-2	260254.10	0.24	2.70	0.86	88	18	0.305	0.064	4.8	
G43.04-0.45	SO, ³ Σ,6 ₅ - 5 ₄	251825.20	0.41	4.74	1.48	90	27	0.505	0.093	5.4	
	H ¹³ CO ⁺ ,3-2	260255.38	0.10	3.54	0.28	283	24	1.077	0.092	11.7	
	SiO,6-5	260515.13	1.35	15.44	2.90	44	23	0.619	0.161	3.8	
G45.47+0.05	CH ₃ OH,6 _{3,3} - 6 _{2,4} - +	251737.57	0.34	3.70	0.76	90	24	0.261	0.087	3.0	
	SO, ³ Σ,6 ₅ - 5 ₄	251825.48	0.13	4.88	0.38	286	26	1.551	0.096	16.2	
	CH ₃ OH,4 _{3,1} - 4 _{2,2} - +	251865.93	0.19	1.84	0.48	128	26	0.281	0.073	3.8	
	CH ₃ OH,5 _{3,3} - 5 _{2,4} + -	251890.90		5.72	0.56	51	26	0.309	0.087	3.6	p
	CH ₃ OH,6 _{3,4} - 6 _{2,5} + -	251895.73		5.72		50	26	0.301	0.090	3.3	p
	CH ₃ OH,4 _{3,2} - 4 _{2,3} + -	251900.49		5.72		82	26	0.499	0.089	5.6	p
	CH ₃ OH,3 _{3,0} - 3 _{2,1} - +	251905.81		5.72		78	26	0.476	0.091	5.2	p
	CH ₃ OH,3 _{3,1} - 3 _{2,2} + -	251917.04		5.96	0.88	68	26	0.433	0.104	4.2	p
	H ¹³ CO ⁺ ,3-2	260255.42	0.05	4.84	0.12	695	23	3.587	0.103	34.8	
	SiO,6-5	260518.45		18.86	3.36	65	25				s
	SiO,6-5	260518.45	0.36	2.42	1.88	79	25	1.434	0.146	9.8	
G45.47+0.13	SO, ³ Σ,6 ₅ - 5 ₄	251825.63	0.09	3.74	0.28	344	25	1.431	0.089	16.1	
	H ¹³ CO ⁺ ,3-2	260255.50	0.10	4.14	0.28	356	27	1.658	0.096	17.3	
G45.80-0.36	SO, ³ Σ,6 ₅ - 5 ₄	251825.81	0.31	4.22	1.24	74	17	0.383	0.061	6.3	
	CH ₃ OH,5 _{3,3} - 5 _{2,4} + -	251890.90		4.76		37	17	0.186	0.049	3.8	p
	CH ₃ OH,4 _{3,2} - 4 _{2,3} + -	251900.49		4.76		35	17	0.179	0.049	3.7	p
	H ¹³ CO ⁺ ,3-2	260255.42	0.13	4.14	0.40	171	17	0.787	0.070	11.2	
G49.07-0.33	H ¹³ CO ⁺ ,3-2	260255.42	0.12	2.94	0.30	154	16	0.492	0.065	7.6	
G49.27-0.34	c-HCCCH,6 _{2,5} - 5 _{1,4}	251527.04	0.23	2.94	0.68	133	29	0.431	0.082	5.3	
	SO, ³ Σ,6 ₅ - 5 ₄	251826.03	0.11	4.32	0.36	283	24	1.348	0.096	14.0	
	CH ₃ OH,9 _{3,7} - 9 _{2,8} + -	252086.63	1.18	9.54	3.22	42	25	0.432	0.129	3.3	
	H ¹³ CO ⁺ ,3-2	260255.30	0.04	3.48	0.12	735	27	2.830	0.097	29.2	
	SiO,6-5	260519.31	1.31	12.44	3.14	61	27	0.739	0.156	4.7	
G49.42+0.33	SO, ³ Σ,6 ₅ - 5 ₄	251825.45	0.39	5.30	0.76	64	17	0.277	0.067	4.1	
	H ¹³ CO ⁺ ,3-2	260255.56	0.31	3.86	1.16	75	18	0.353	0.068	5.2	
G49.91+0.37	H ¹³ CO ⁺ ,3-2	260255.35	0.24	3.42	0.60	99	19	0.343	0.069	5.0	
G50.36-0.42	H ¹³ CO ⁺ ,3-2	260255.39	0.20	2.12	0.50	85	17	0.190	0.057	3.3	
G53.92-0.07	H ¹³ CO ⁺ ,3-2	260255.34	0.08	2.78	0.20	204	15	0.581	0.060	9.7	
G54.11-0.08	CH ₃ OH,8 _{3,5} - 8 _{2,6} - +	251518.10	0.82	8.76	2.86	38	16	0.382	0.087	4.4	
	SO, ³ Σ,6 ₅ - 5 ₄	251826.00	0.22	5.68	0.80	110	16	0.690	0.074	9.3	
	CH ₃ OH,5 _{3,3} - 5 _{2,4} + -	251890.90		4.34	0.54	32	15	0.149	0.043	3.5	p
	CH ₃ OH,6 _{3,4} - 6 _{2,5} + -	251895.73		4.34		28	15	0.132	0.044	3.0	p
	CH ₃ OH,3 _{3,0} - 3 _{2,1} - +	251905.81		4.34		47	15	0.218	0.048	4.5	p
	H ¹³ CO ⁺ ,3-2	260255.27	0.13	4.48	0.36	191	19	0.927	0.074	12.5	
	SiO,6-5	260522.13	0.79	14.76	2.34	65	20	0.998	0.122	8.2	
G54.45+1.01	H ¹³ CO ⁺ ,3-2	260255.34	0.29	4.86	1.02	130	27	0.729	0.102	7.1	
G57.61+0.02	SO, ³ Σ,6 ₅ - 5 ₄	251824.74	1.08	5.48	3.28	58	25	0.355	0.100	3.5	
	H ¹³ CO ⁺ ,3-2	260255.34	0.12	2.48	0.34	201	25	0.526	0.078	6.7	
G58.78+0.64	CH ₃ OH,5 _{3,2} - 5 _{2,3} - +	251812.52	1.14	8.22	2.86	45	24	0.554	0.108	5.1	

Table 4: (continued) Line parameters.

Object (1)	Transition ^a (2)	ν (MHz) (3)	σ_ν ^b (MHz) (4)	FWHM (km s ⁻¹) (5)	σ_{FWHM}^c (km s ⁻¹) (6)	T_{MB} (mK) (7)	$\sigma_{T_{\text{MB}}}$ (mK) (8)	I_{int}^d (K km s ⁻¹) (9)	σ_I^d (K km s ⁻¹) (10)	SNR ^d Note ^e (11) (12)	
G59.79+0.63	SO, ³ Σ_6^- , 6 ₅ - 5 ₄	251826.53	0.28	5.16	0.84	133	25	0.776	0.090	8.6	
	CH ₃ OH, 4 _{3,1} - 4 _{2,2} - +	251866.17	0.81	6.72	2.28	51	24	0.370	0.098	3.8	
	H ¹³ CO ⁺ , 3-2	260255.17	0.12	3.68	0.40	265	25	1.198	0.095	12.6	
	SiO, 6-5	260518.47	1.80	20.52	5.20	39	23	0.810	0.189	4.3	
	SO, ³ Σ_6^- , 6 ₅ - 5 ₄	251825.37	0.17	4.94	0.56	192	23	1.081	0.091	11.9	
	CH ₃ OH, 4 _{3,1} - 4 _{2,2} - +	251865.97	0.45	4.10	1.30	66	23	0.299	0.083	3.6	
	CH ₃ OH, 6 _{3,4} - 6 _{2,5} + -	251895.73		5.82		44	24	0.275	0.085	3.2	p
	CH ₃ OH, 4 _{3,2} - 4 _{2,3} + -	251900.49		5.82		74	24	0.461	0.090	5.1	p
	CH ₃ OH, 3 _{3,0} - 3 _{2,1} - +	251905.81		5.82		41	24	0.254	0.079	3.2	p
	CH ₃ OH, 3 _{3,1} - 3 _{2,2} + -	251917.04		6.56	1.24	40	23	0.280	0.081	3.5	p
	H ¹³ CO ⁺ , 3-2	260255.52	0.14	4.60	0.40	278	27	1.388	0.099	14.0	
	SiO, 6-5	260518.30	1.01	15.88	5.28	71	24	1.348	0.169	8.0	

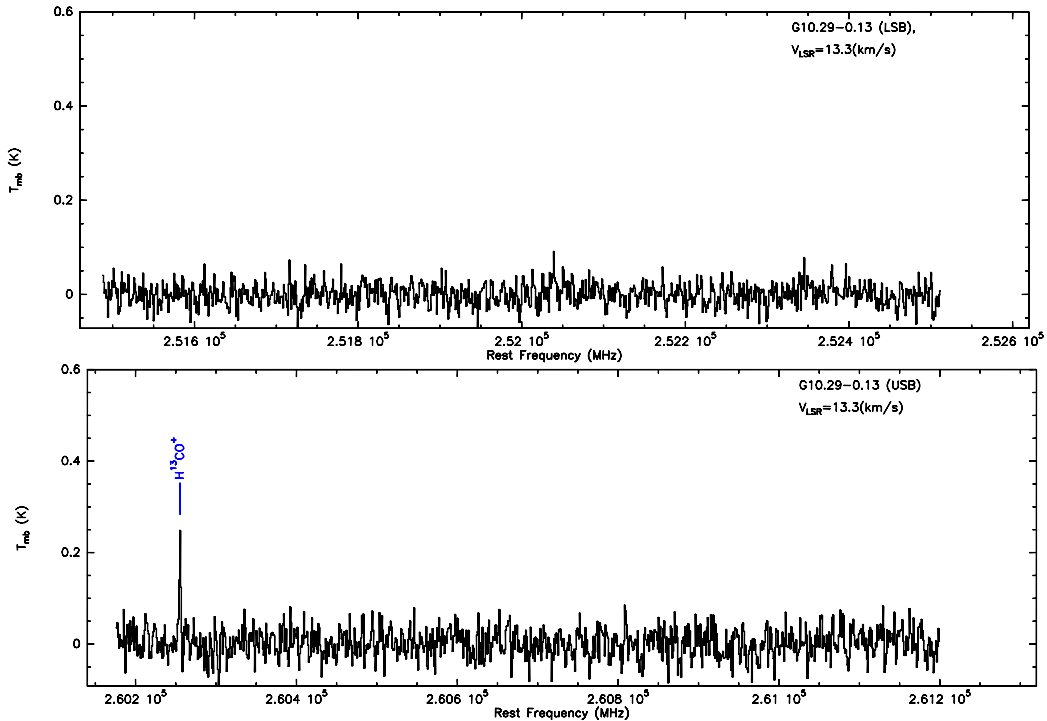


Fig. 10.— The sideband spectral plots of all observed EGOs, with identified species labelled at the catalog frequency of each identified line. The first two plots are for G10.29-0.13.

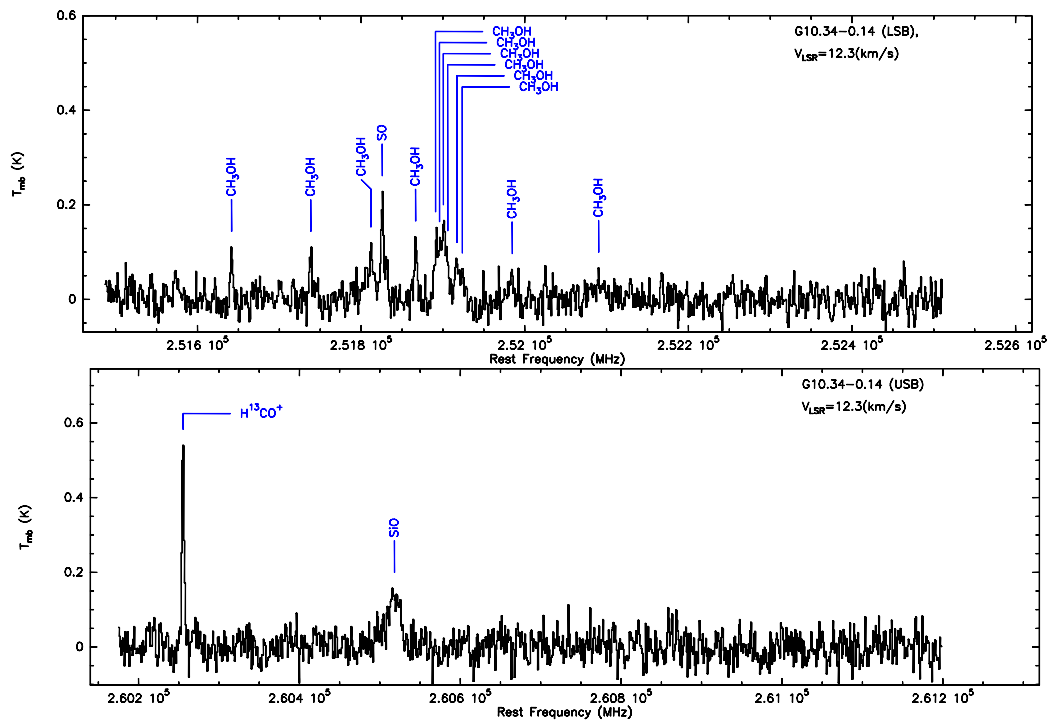


Fig. 10.— (continued) For G10.34-0.14.

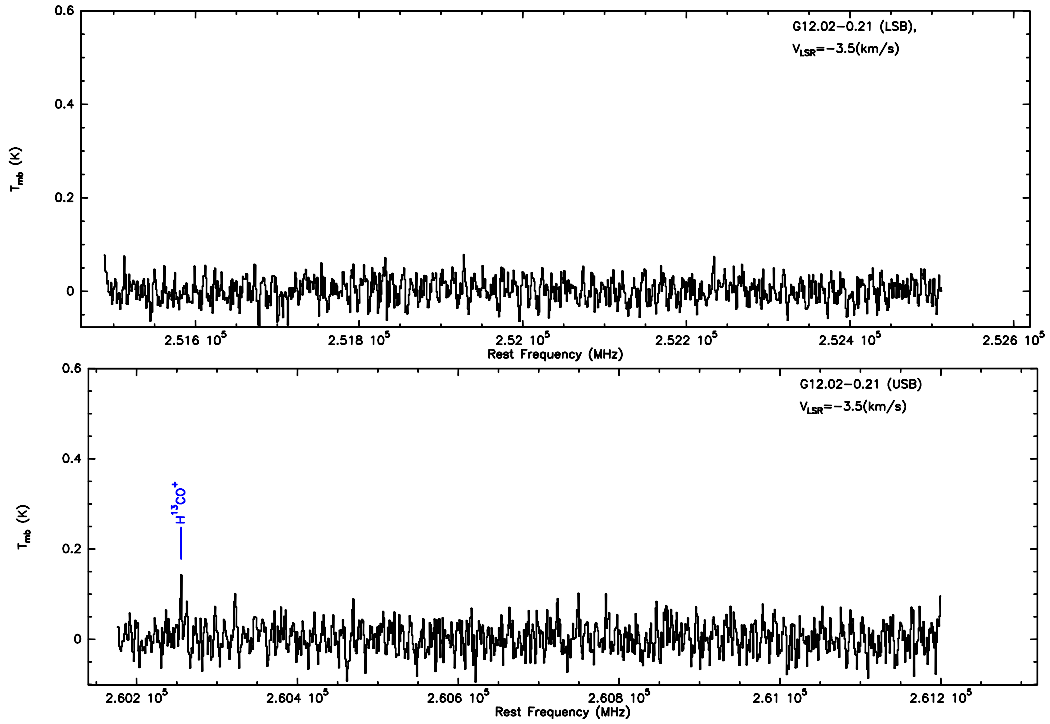


Fig. 10.— (continued) For G12.02-0.21.

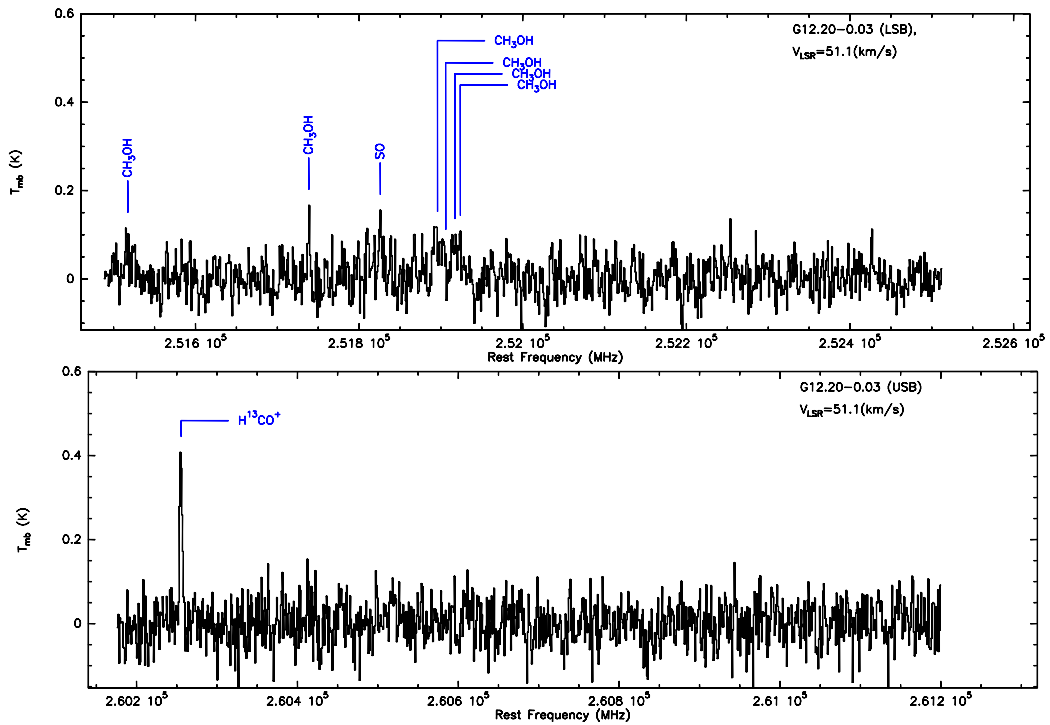


Fig. 10.— (continued) For G12.20-0.03.

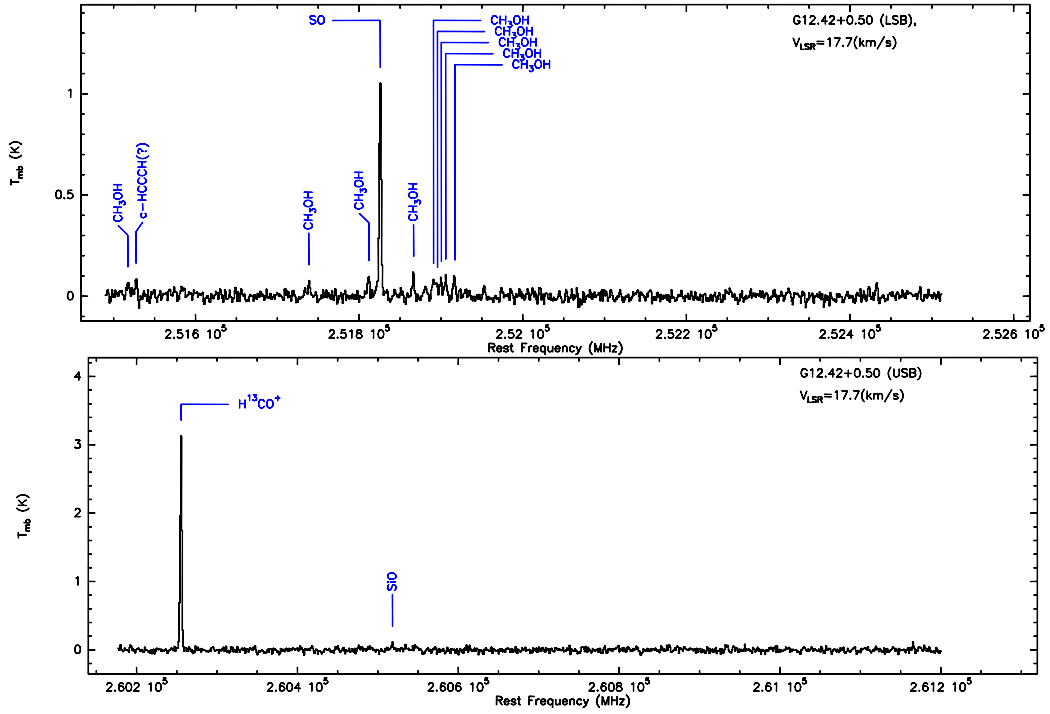


Fig. 10.— (continued) For G12.42+0.50.

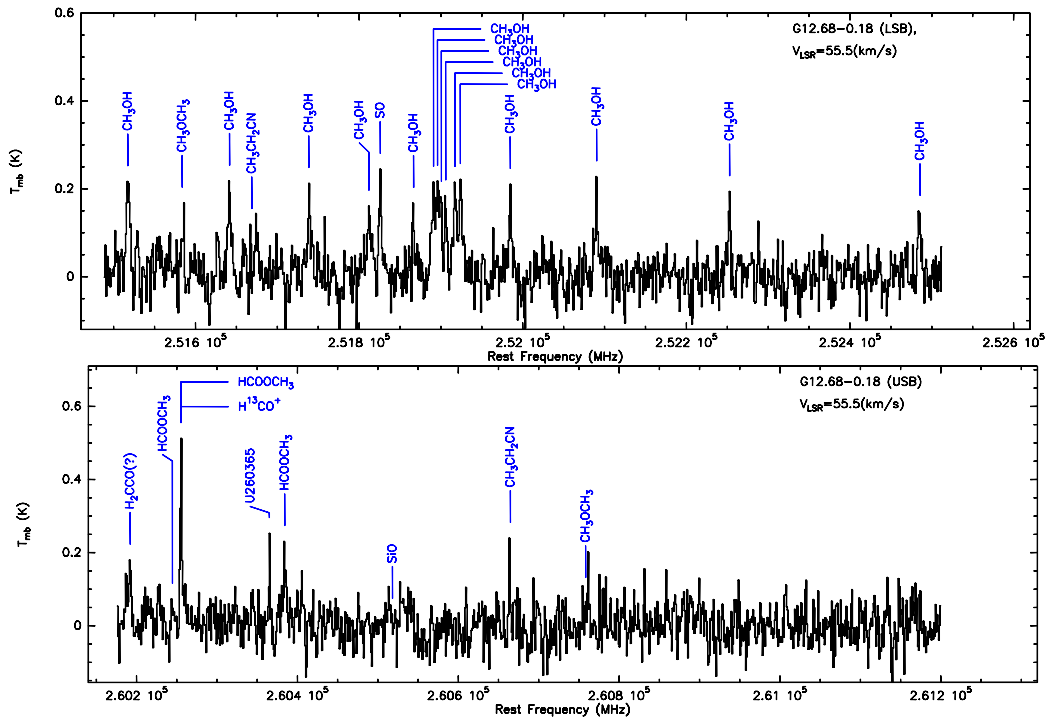


Fig. 10.— (continued) For G12.68-0.18.

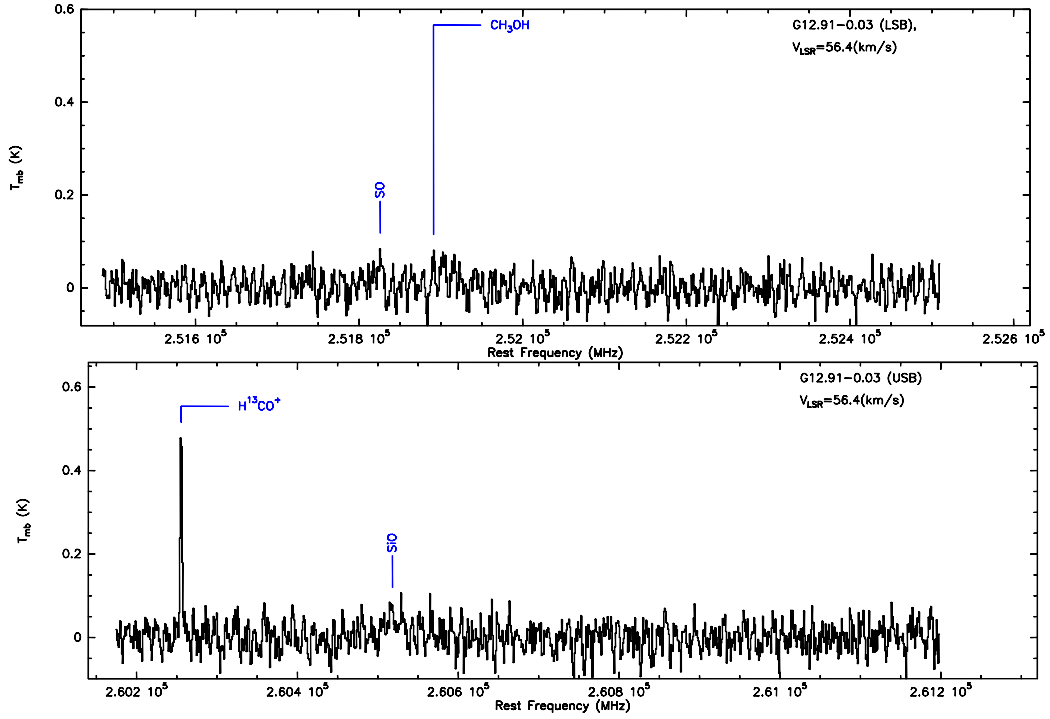


Fig. 10.— (continued) For G12.91-0.03.

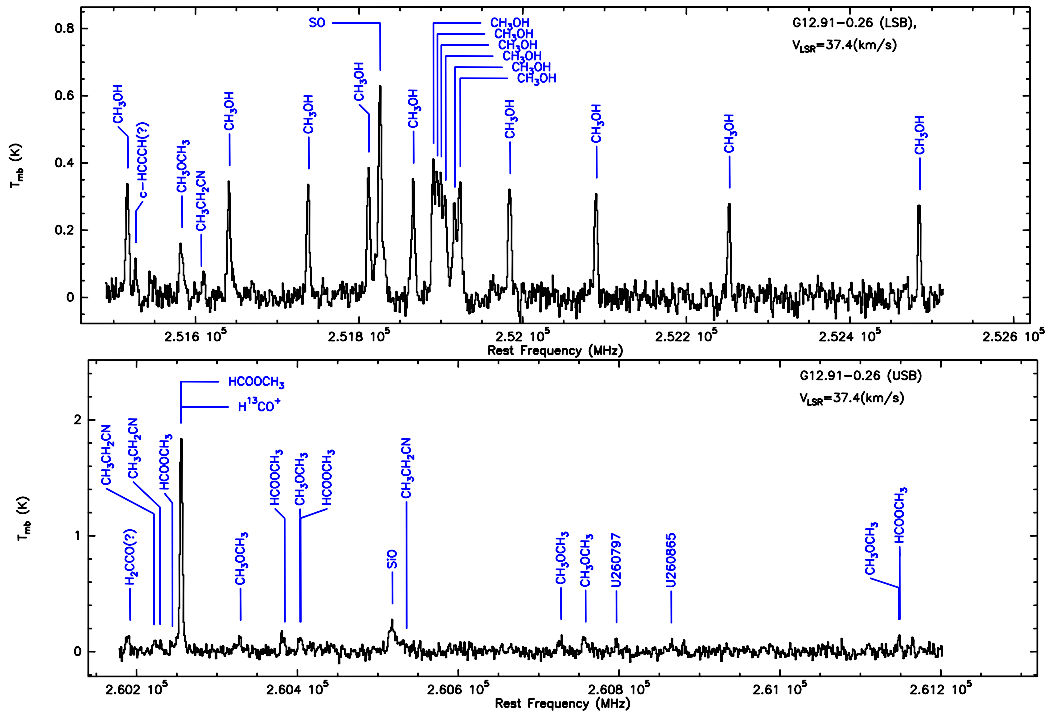


Fig. 10.— (continued) For G12.91-0.26.

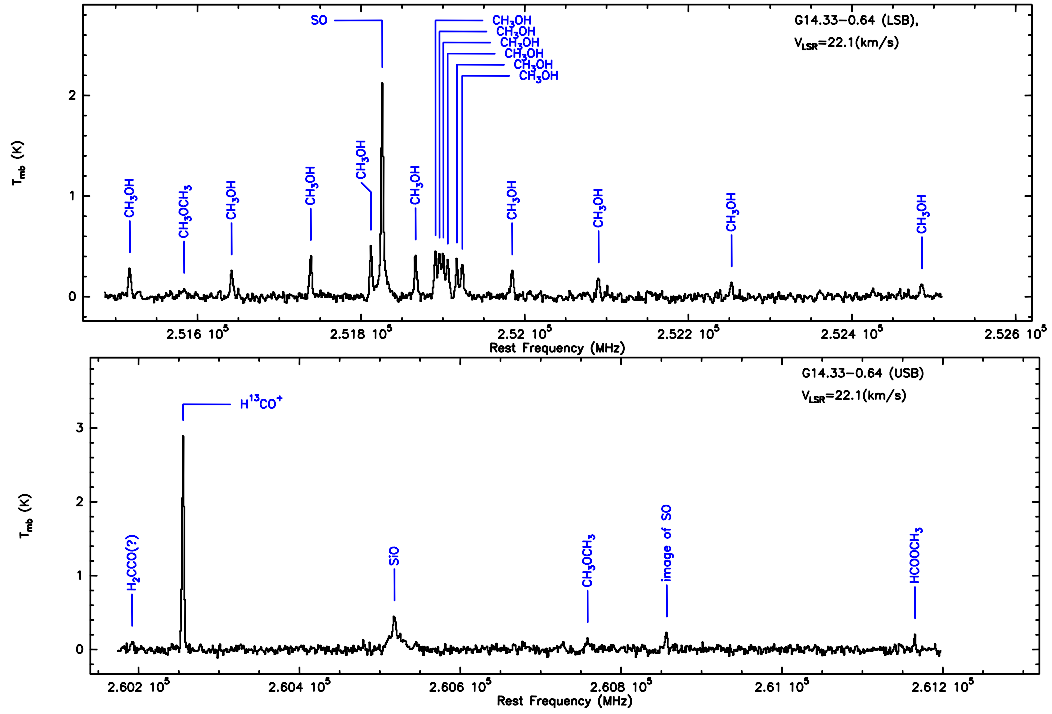


Fig. 10.— (continued) For G14.33-0.64.

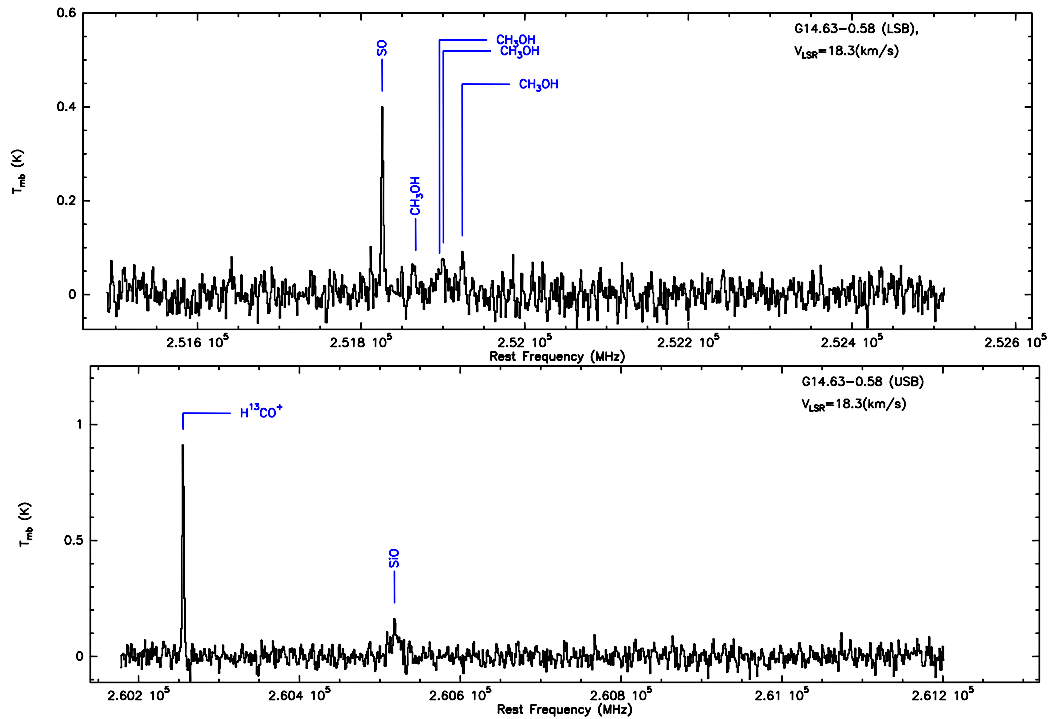


Fig. 10.— (continued) For G14.63-0.58.

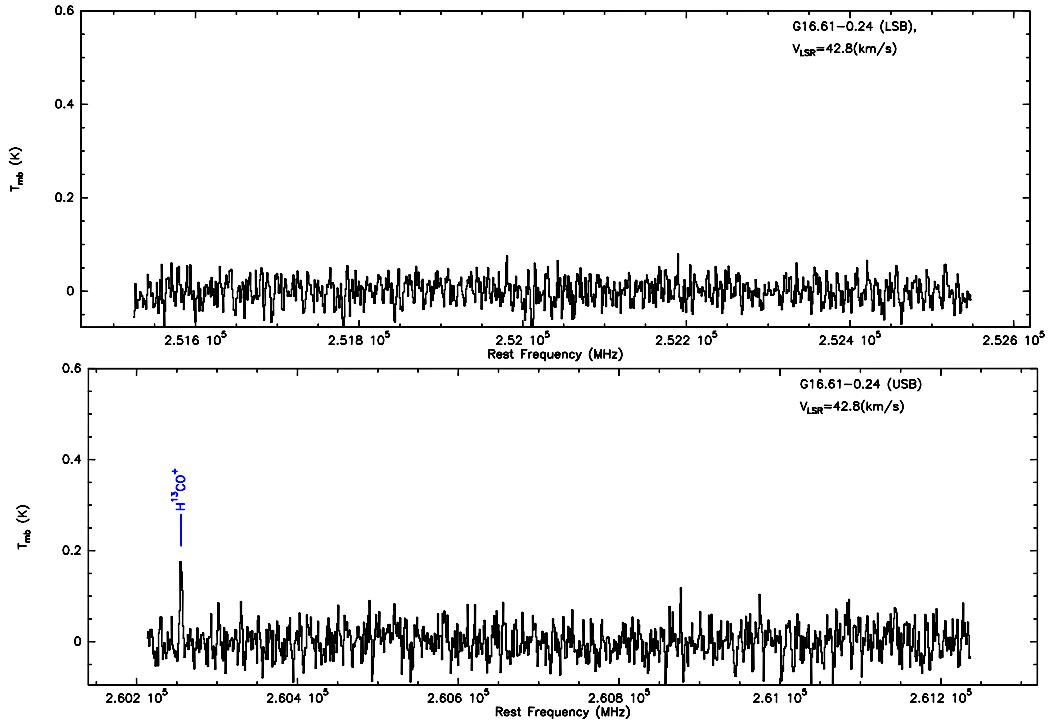


Fig. 10.— (continued) For G16.61-0.24.

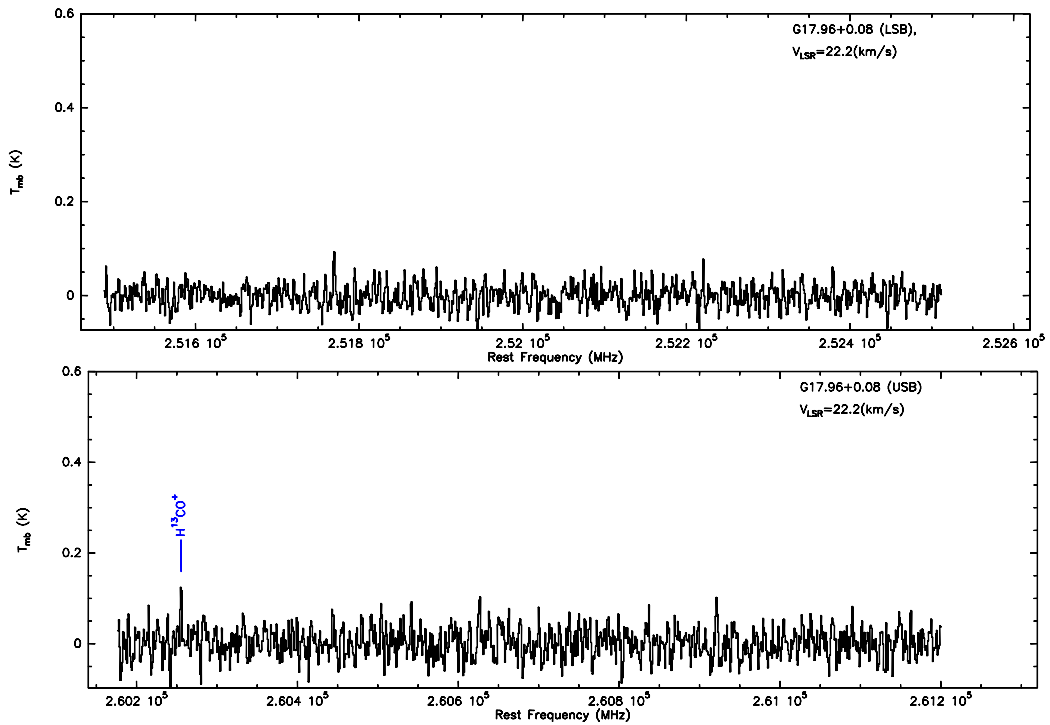


Fig. 10.— (continued) For G17.96+0.08.

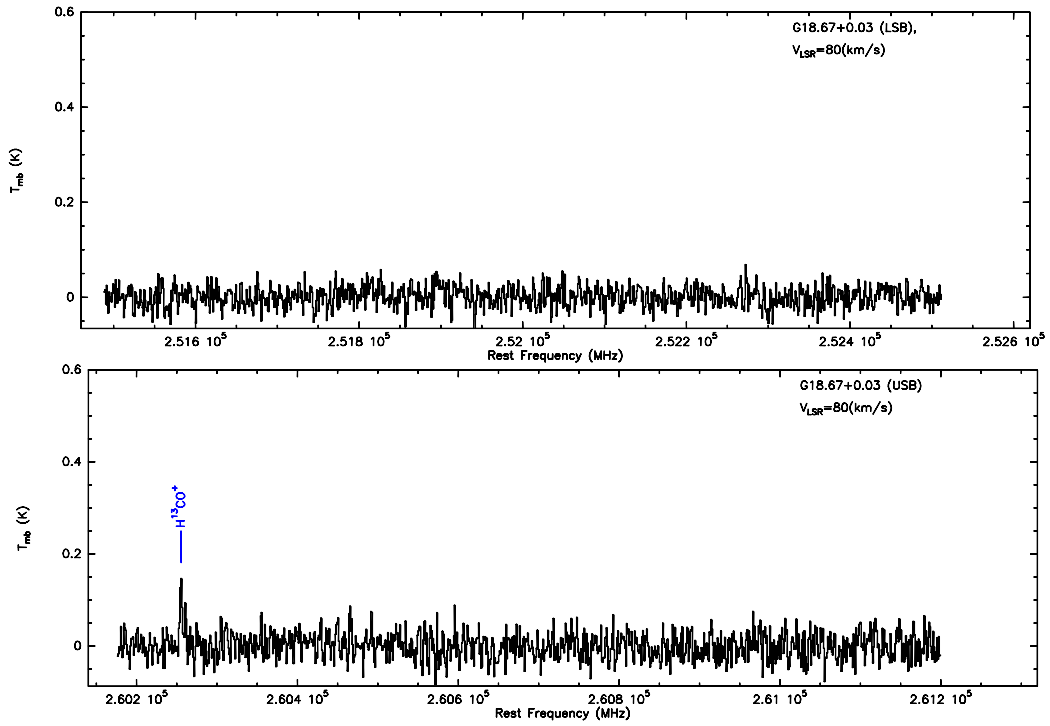


Fig. 10.— (continued) For G18.67+0.03.

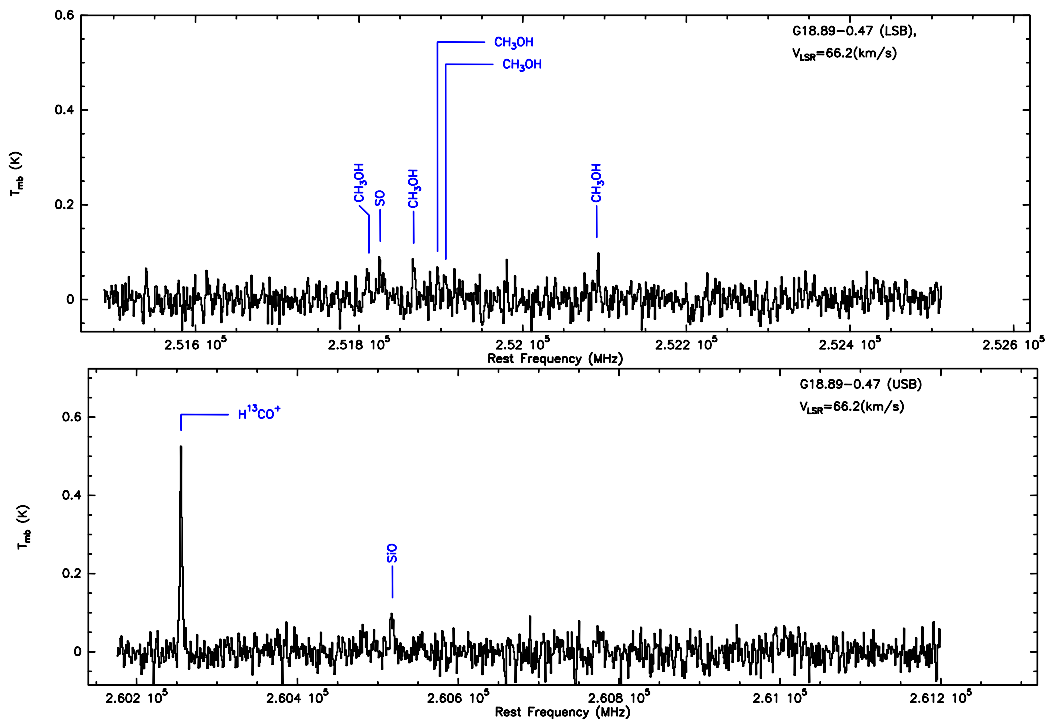


Fig. 10.— (continued) For G18.89-0.47.

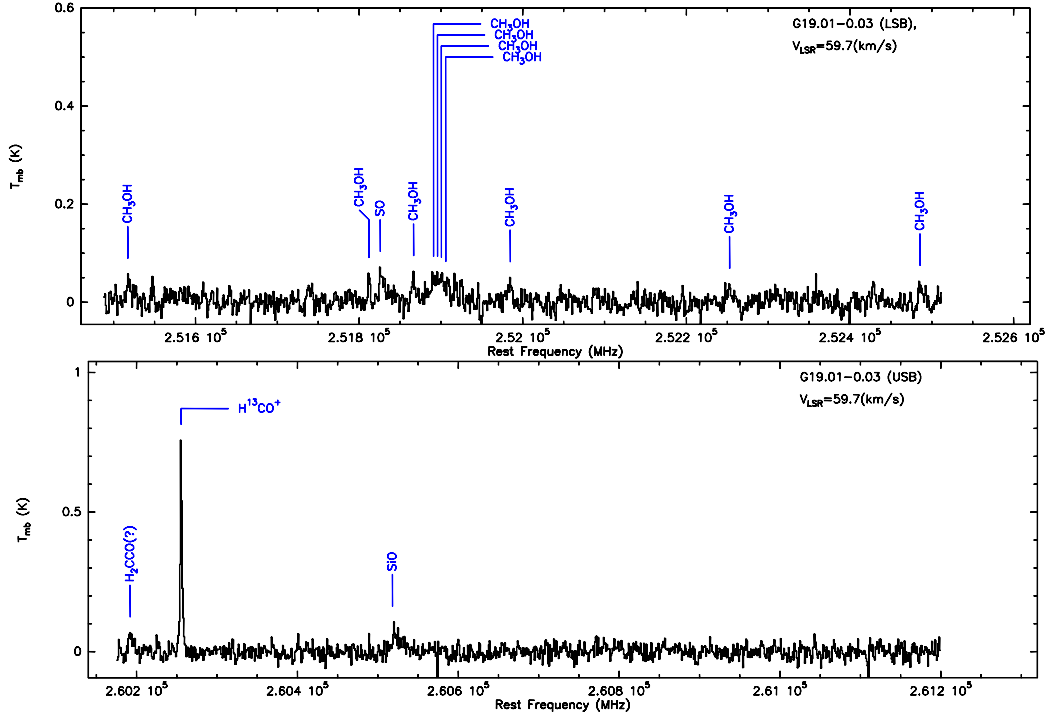


Fig. 10.— (continued) For G19.01-0.03.

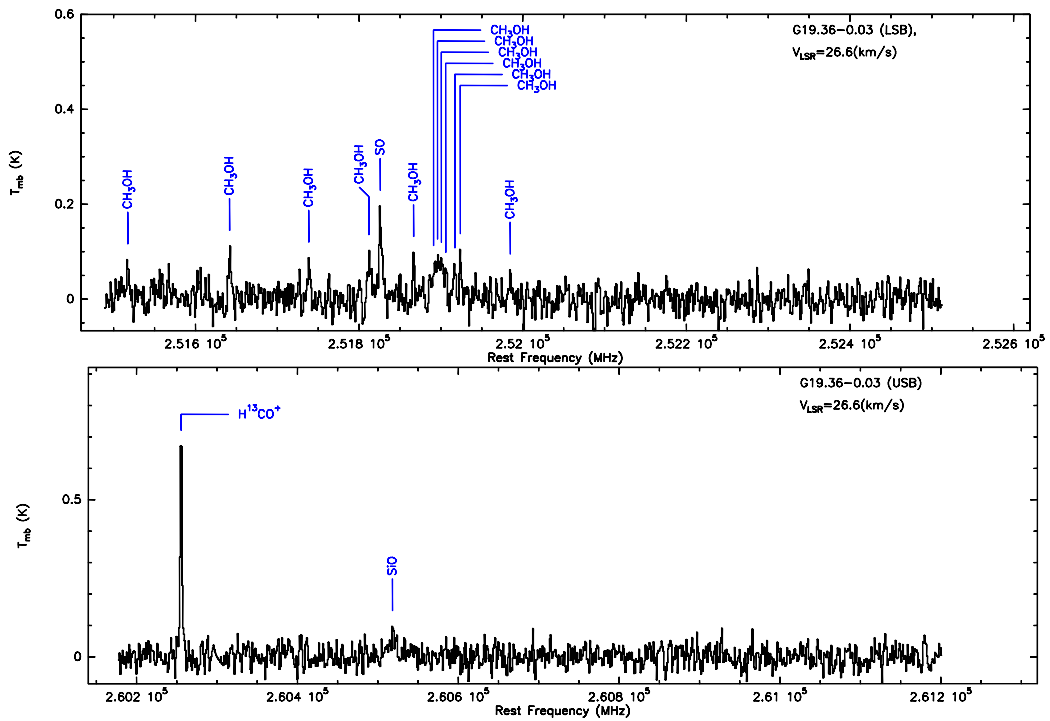


Fig. 10.— (continued) For G19.36-0.03.

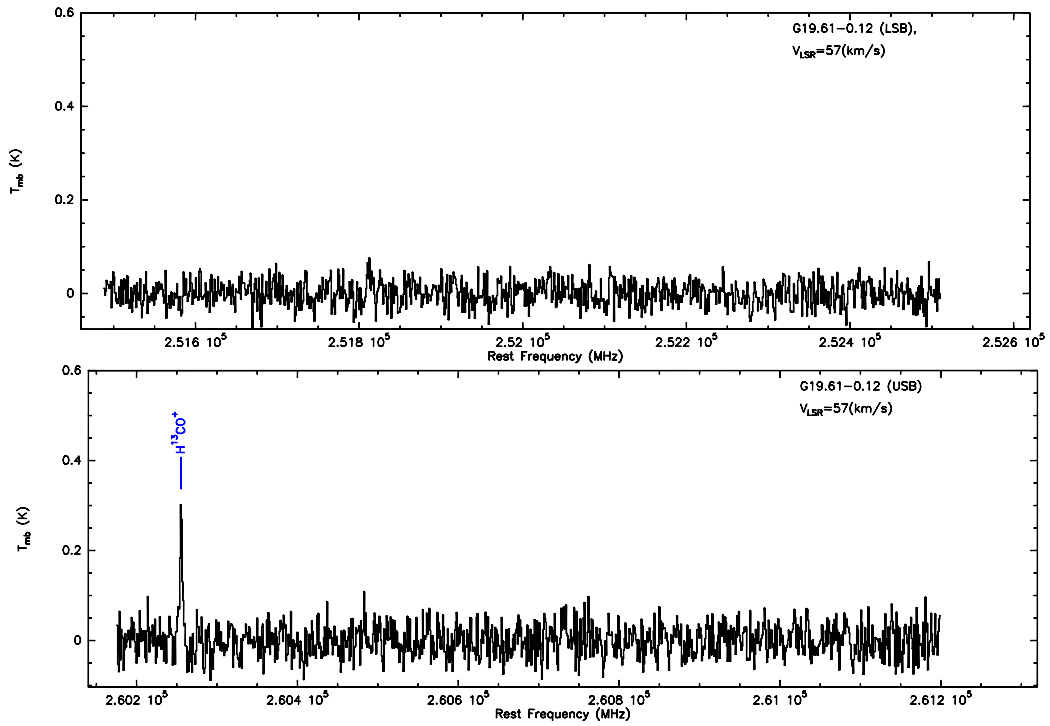


Fig. 10.— (continued) For G19.61-0.12.

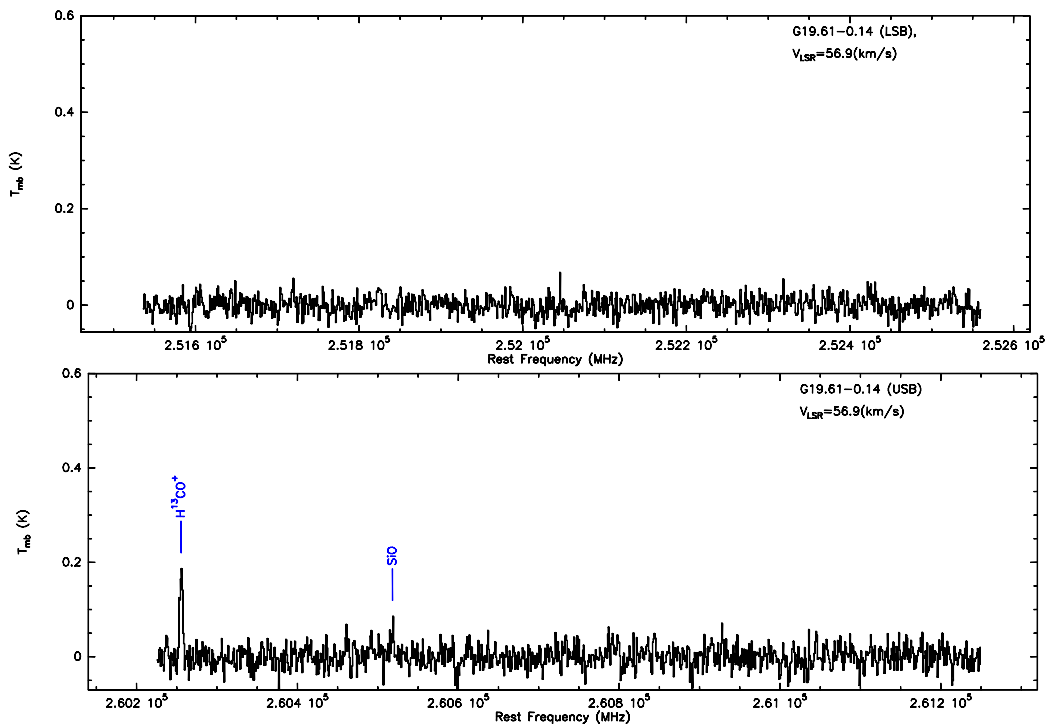


Fig. 10.— (continued) For G19.61-0.14.

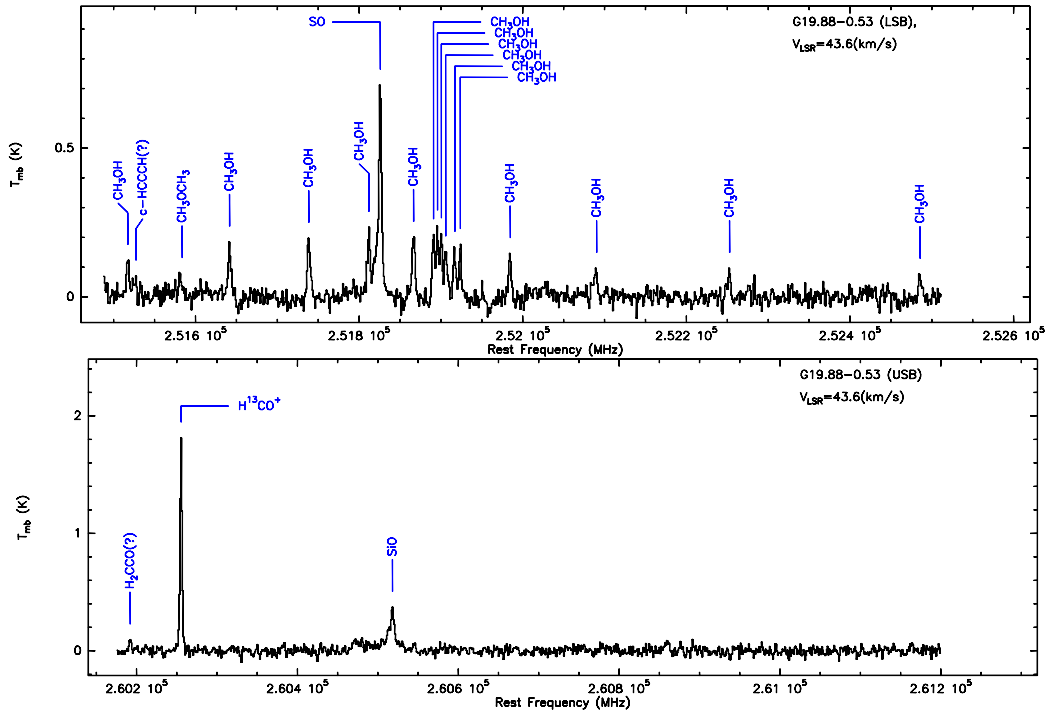


Fig. 10.— (continued) For G19.88-0.53.

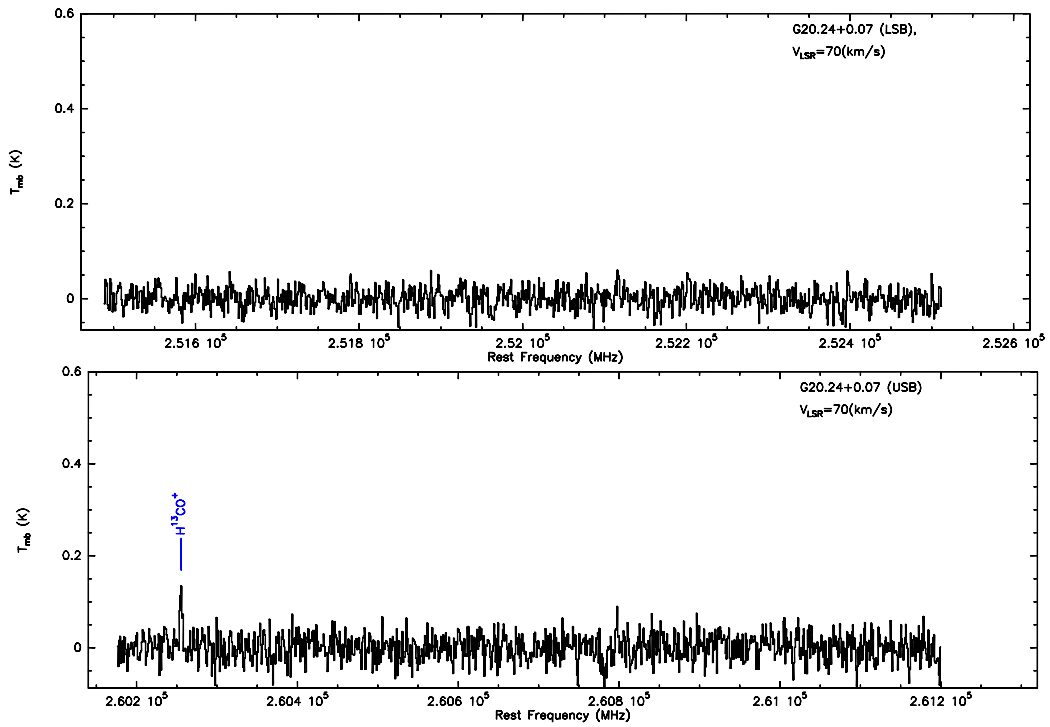


Fig. 10.— (continued) For G20.24+0.07.

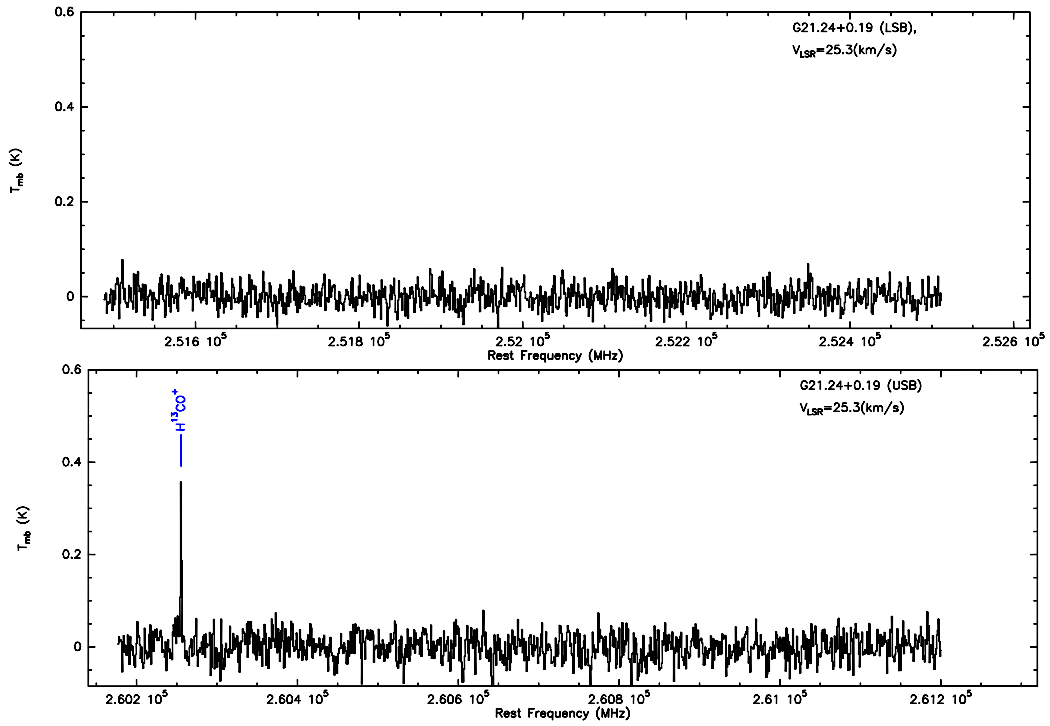


Fig. 10.— (continued) For G21.24+0.19.

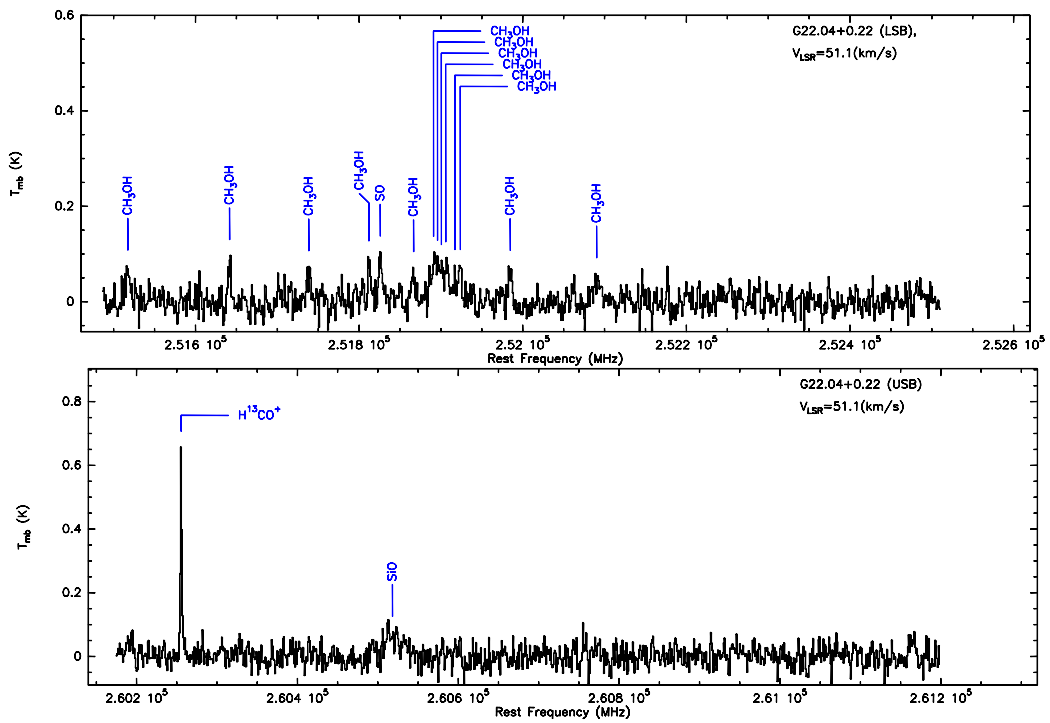


Fig. 10.— (continued) For G22.04+0.22.

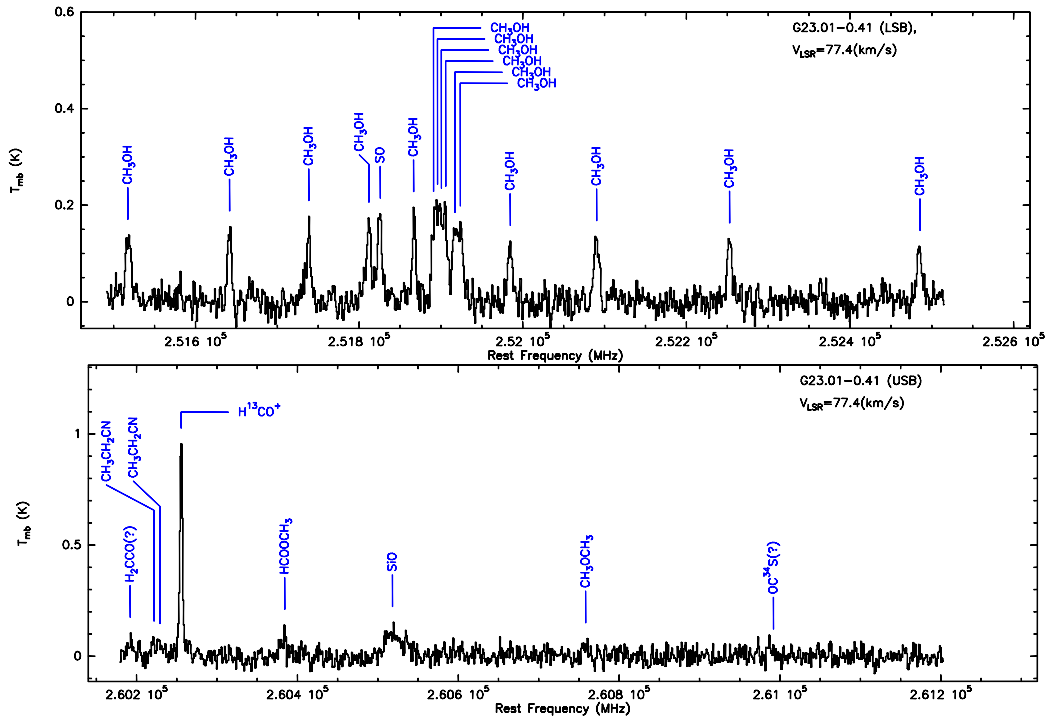


Fig. 10.— (continued) For G23.01-0.41.

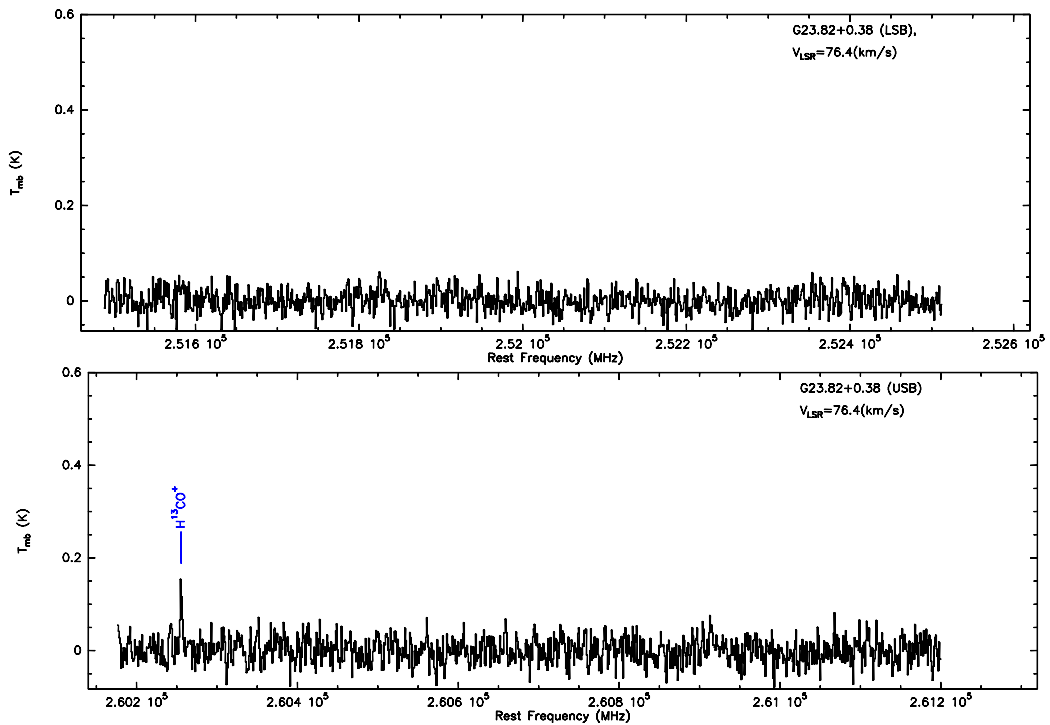


Fig. 10.— (continued) For G23.82+0.38.

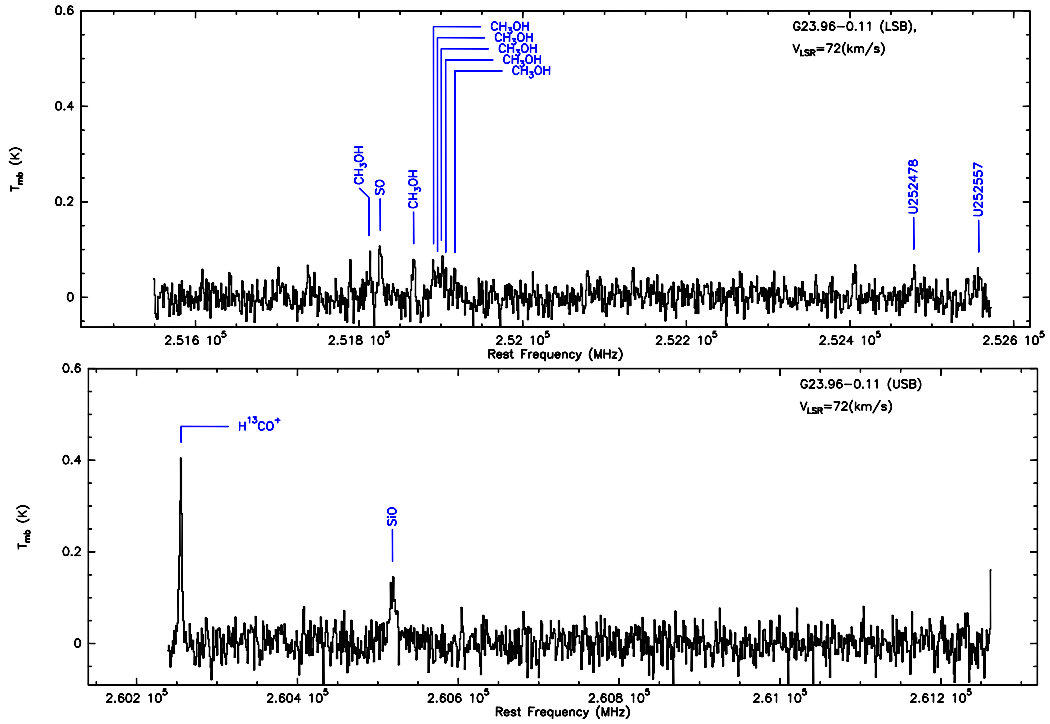


Fig. 10.— (continued) For G23.96-0.11.

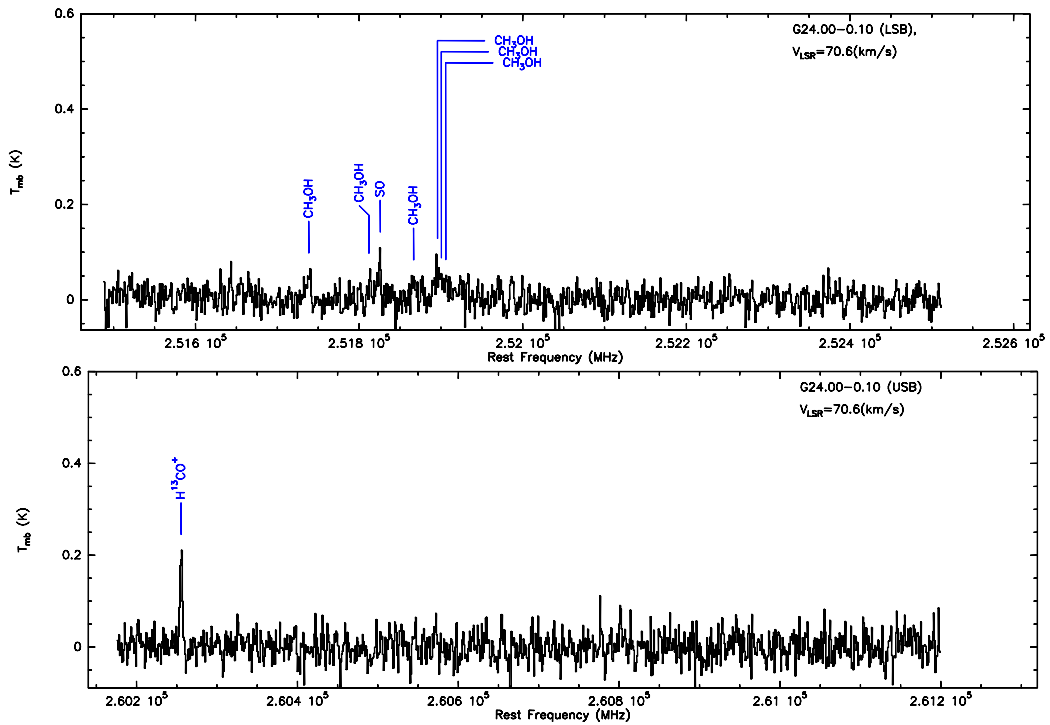


Fig. 10.— (continued) For G24.00-0.10.

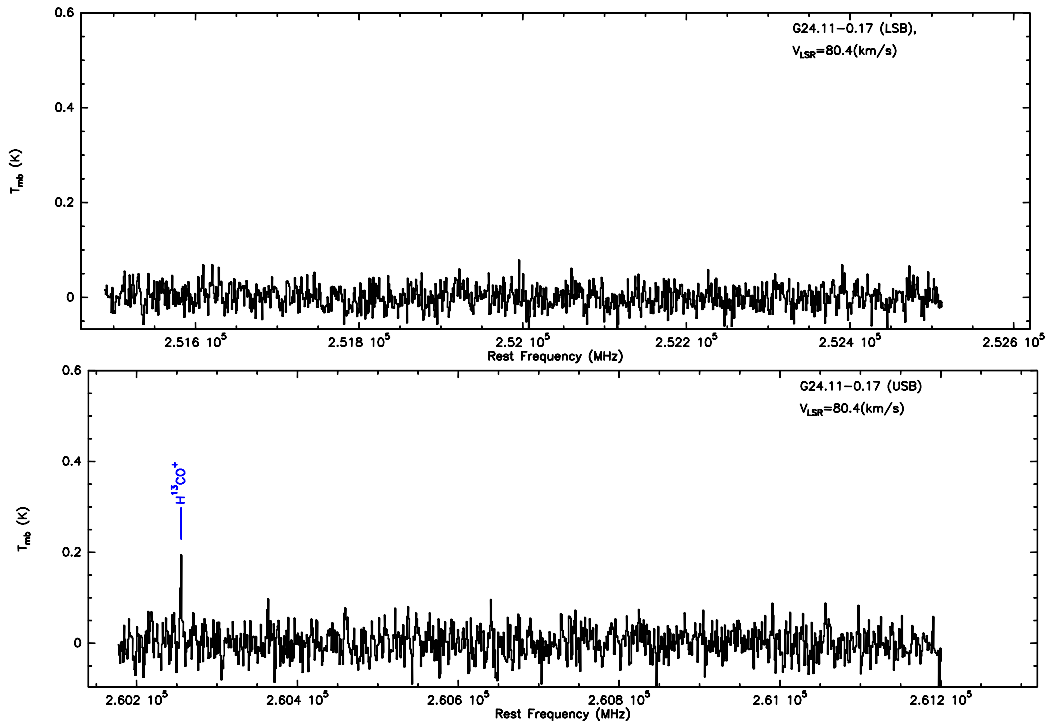


Fig. 10.— (continued) For G24.11-0.17.

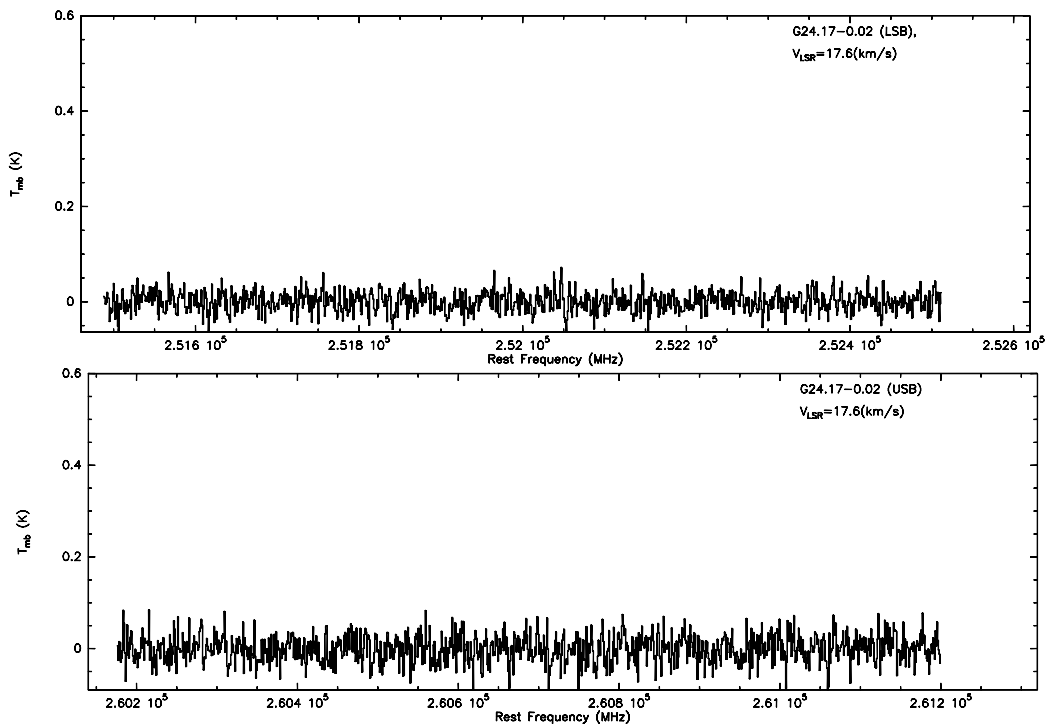


Fig. 10.— (continued) For G24.17-0.02.

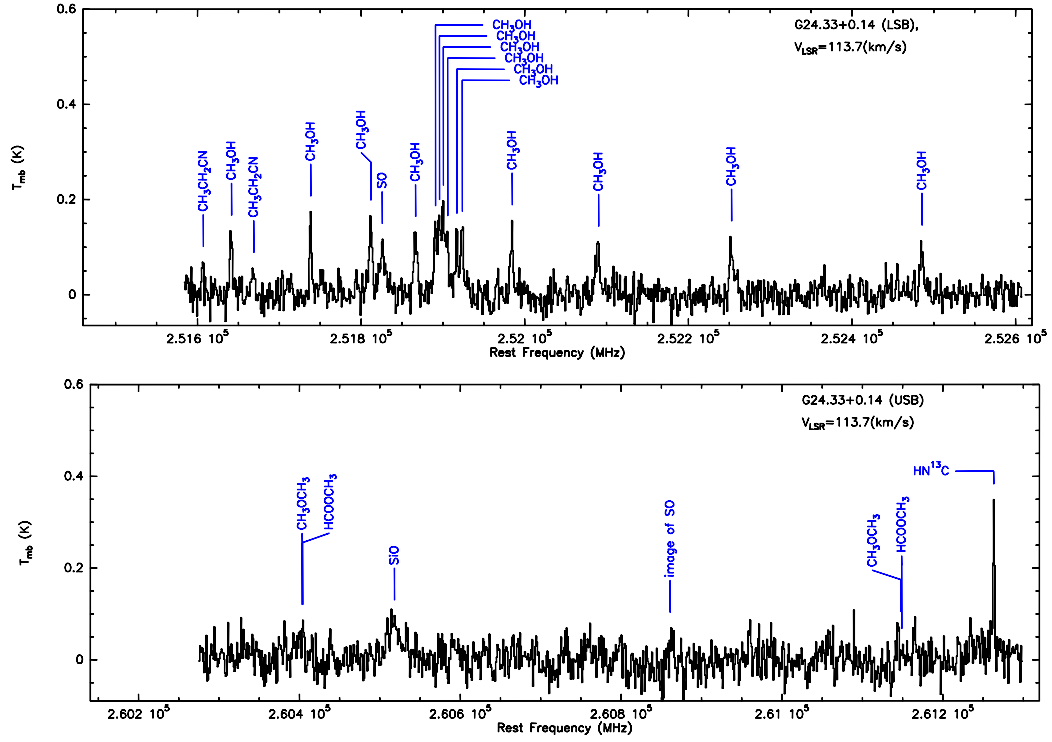


Fig. 10.— (continued) For G24.33+0.14.

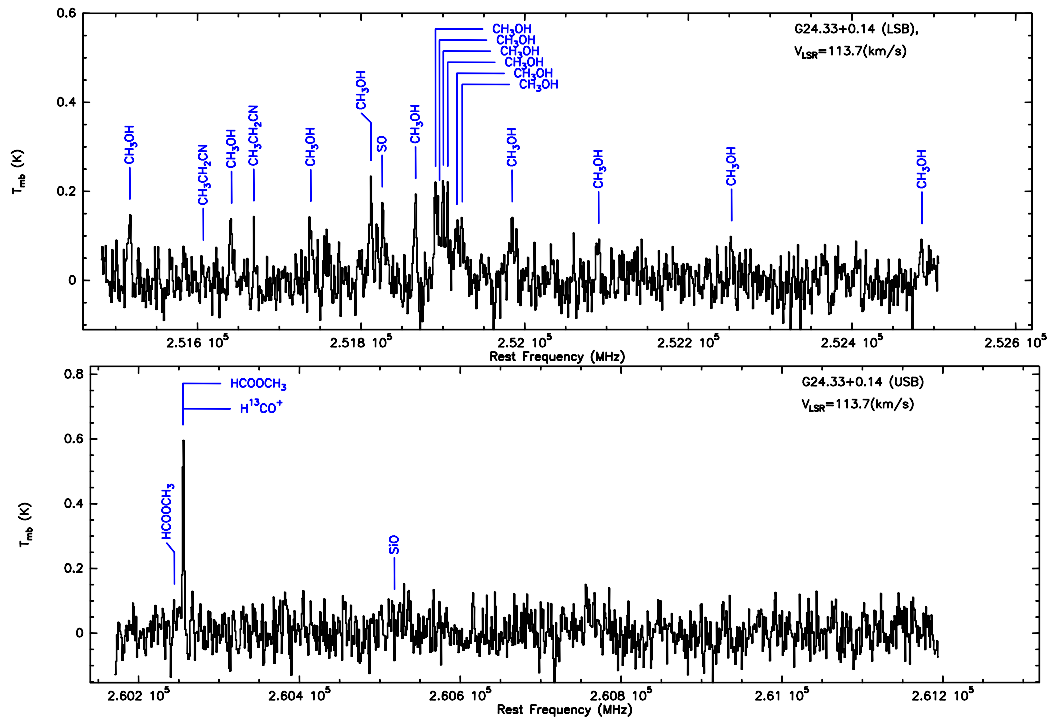


Fig. 10.— (continued) For G24.33+0.14 (different frequency coverage).

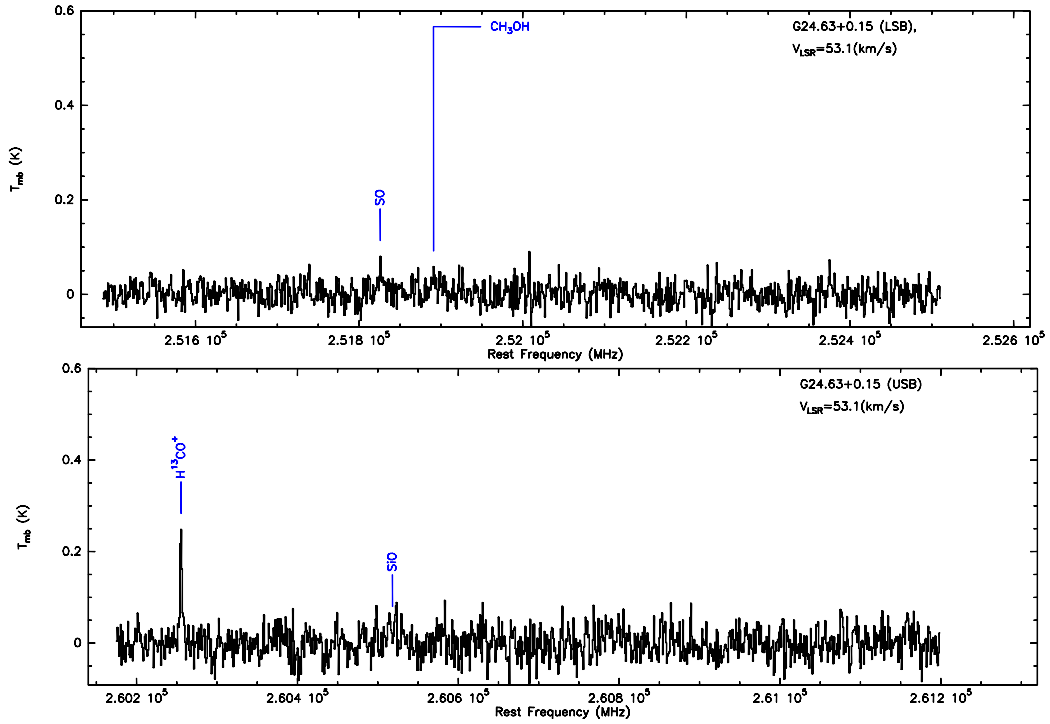


Fig. 10.— (continued) For G24.63+0.15.

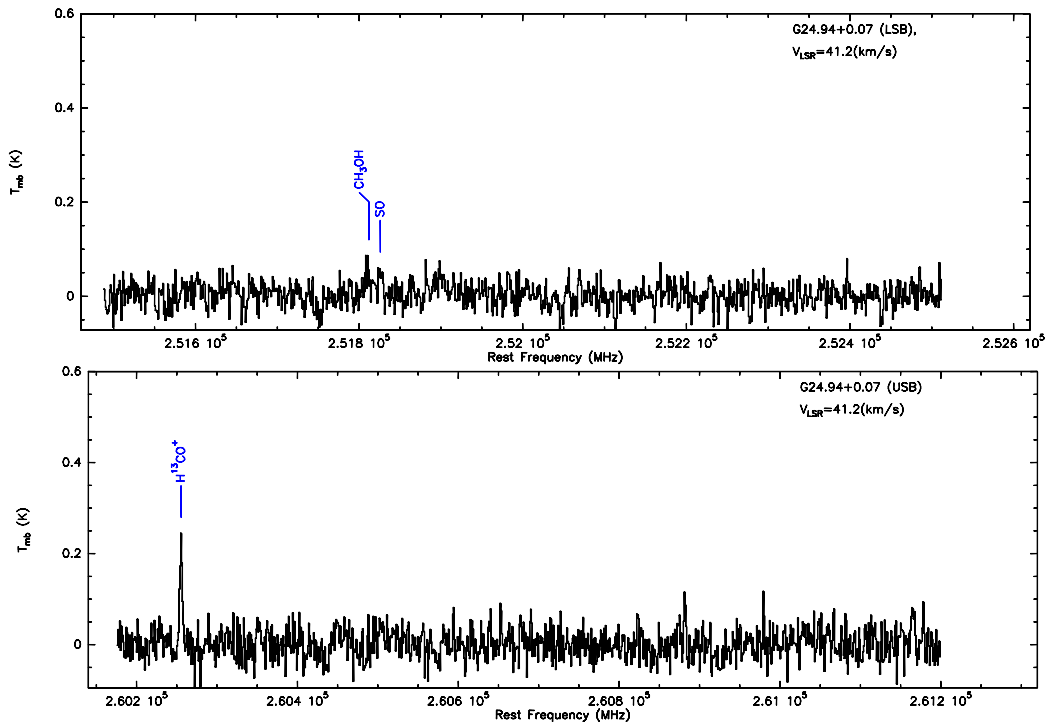


Fig. 10.— (continued) For G24.94+0.07.

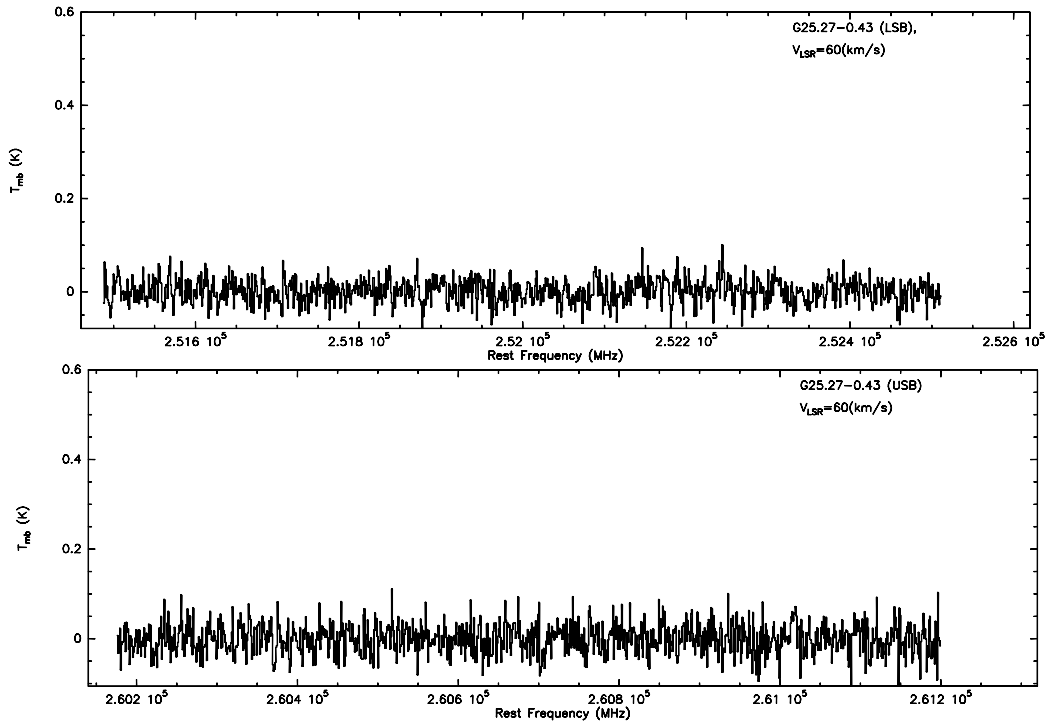


Fig. 10.— (continued) For G25.27-0.43.

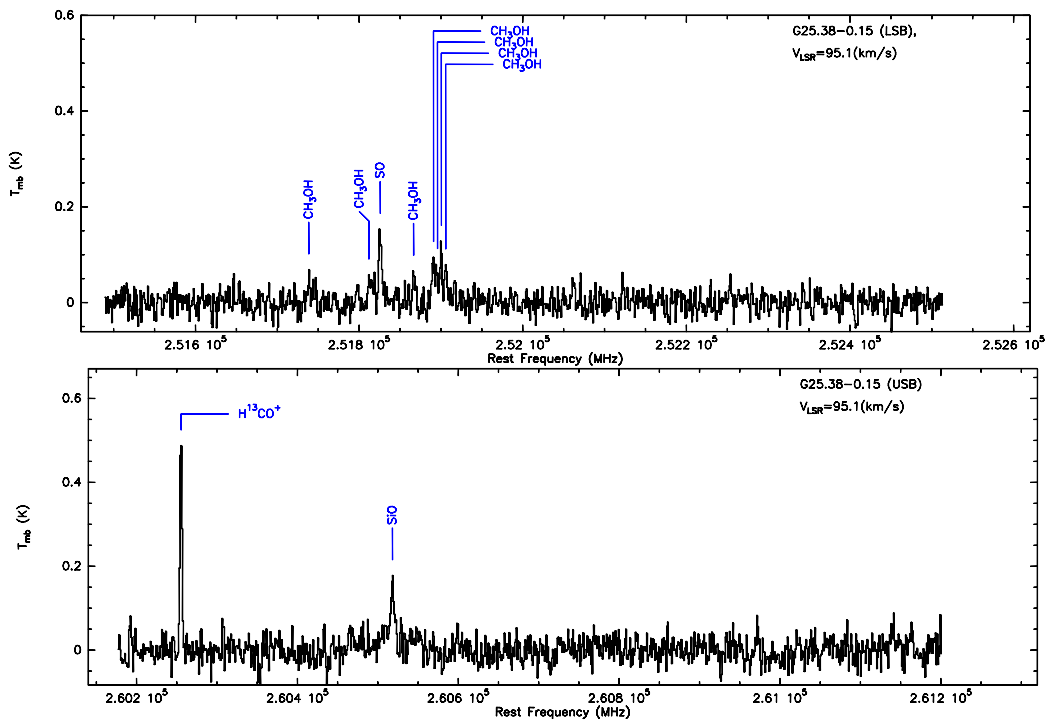


Fig. 10.— (continued) For G25.38-0.15.

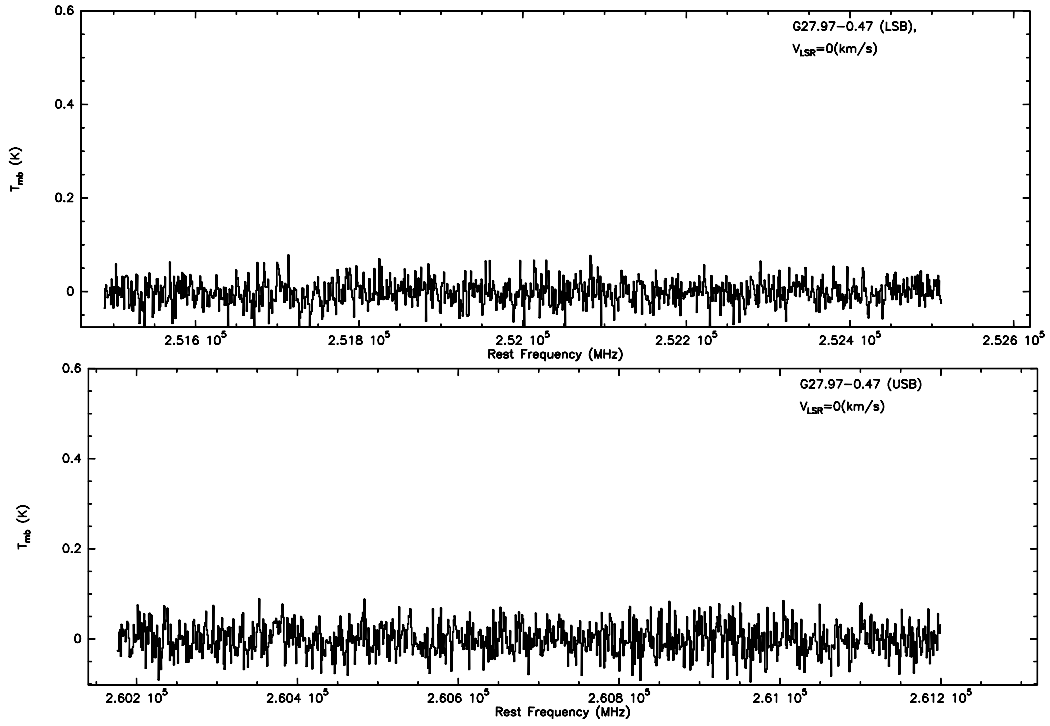


Fig. 10.— (continued) For G27.97-0.47.

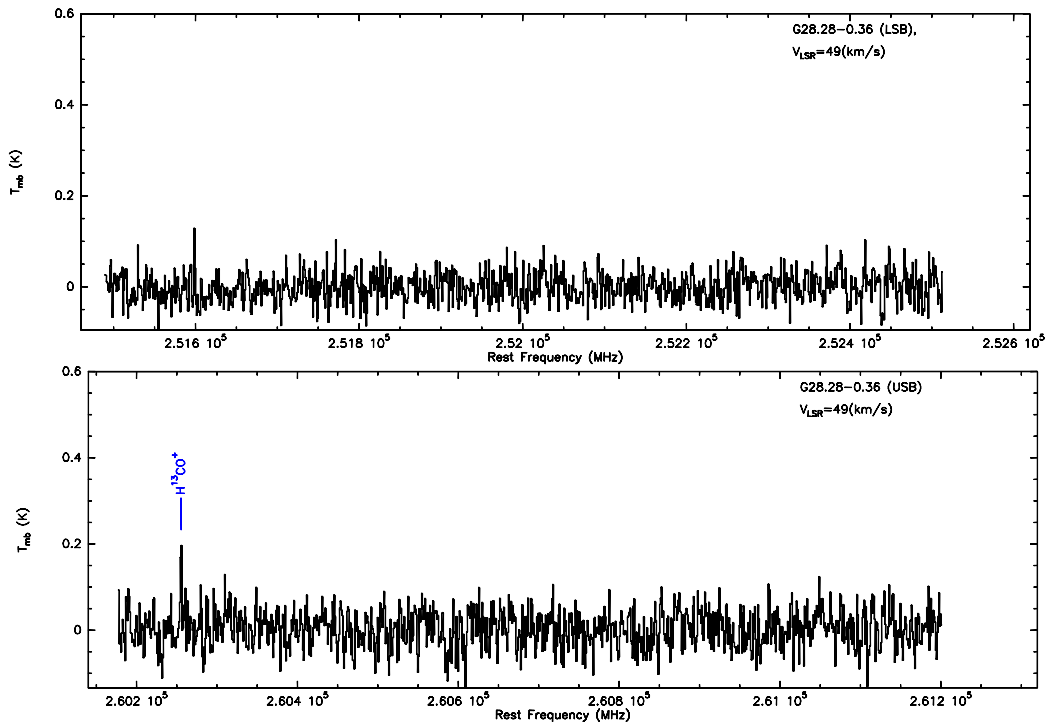


Fig. 10.— (continued) For G28.28-0.36.

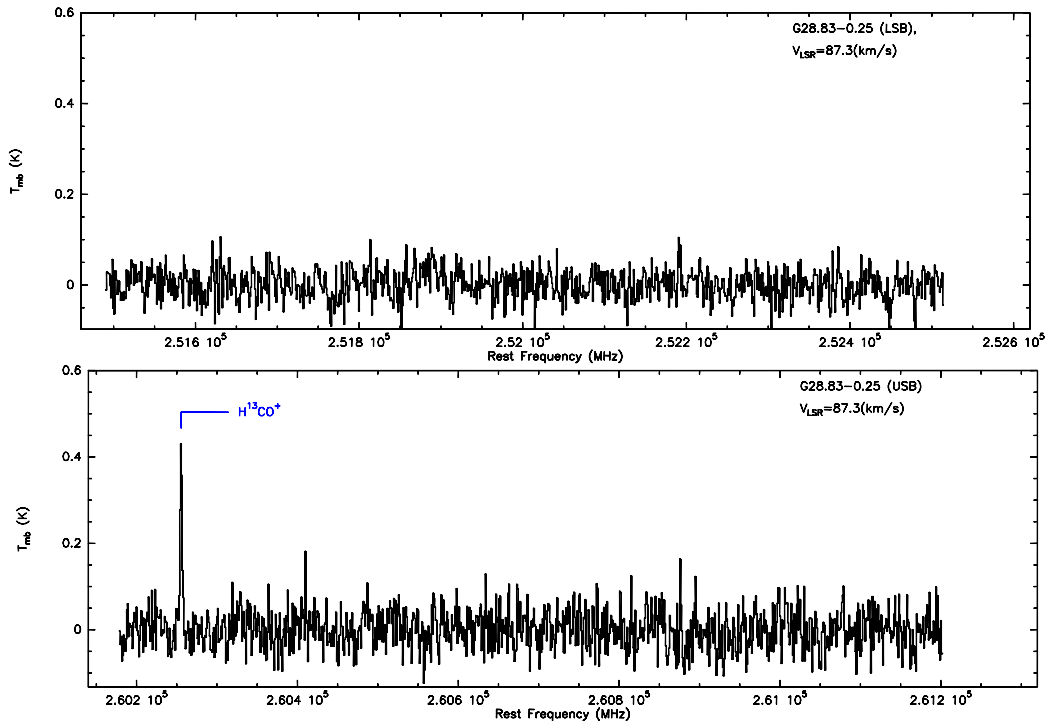


Fig. 10.— (continued) For G28.83-0.25.

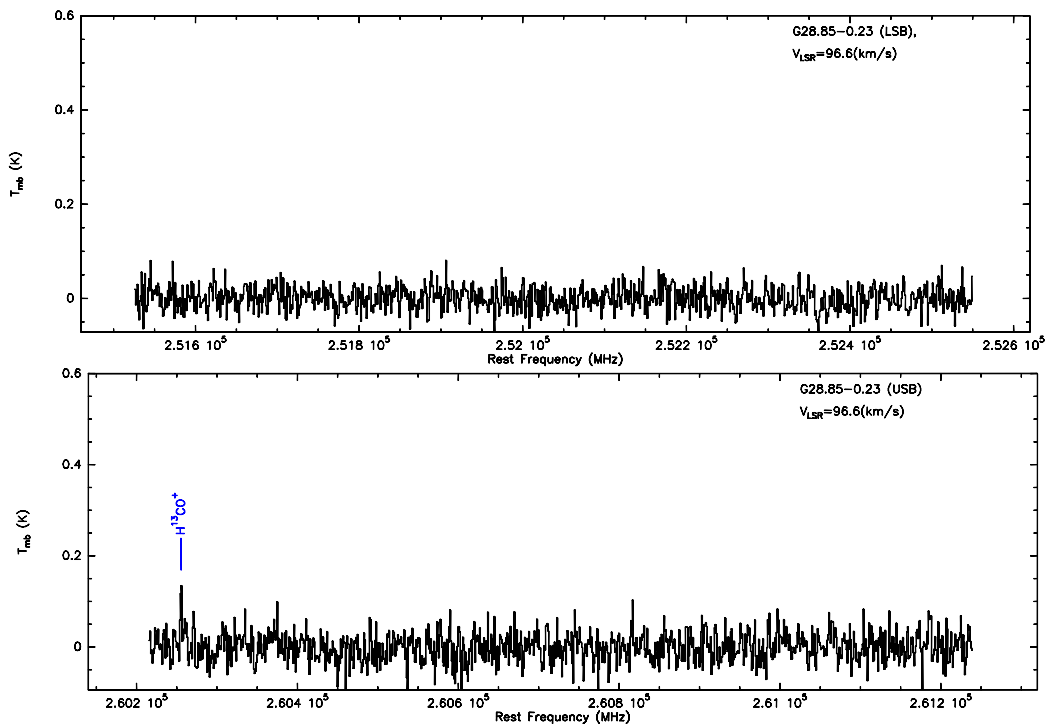


Fig. 10.— (continued) For G28.85-0.23.

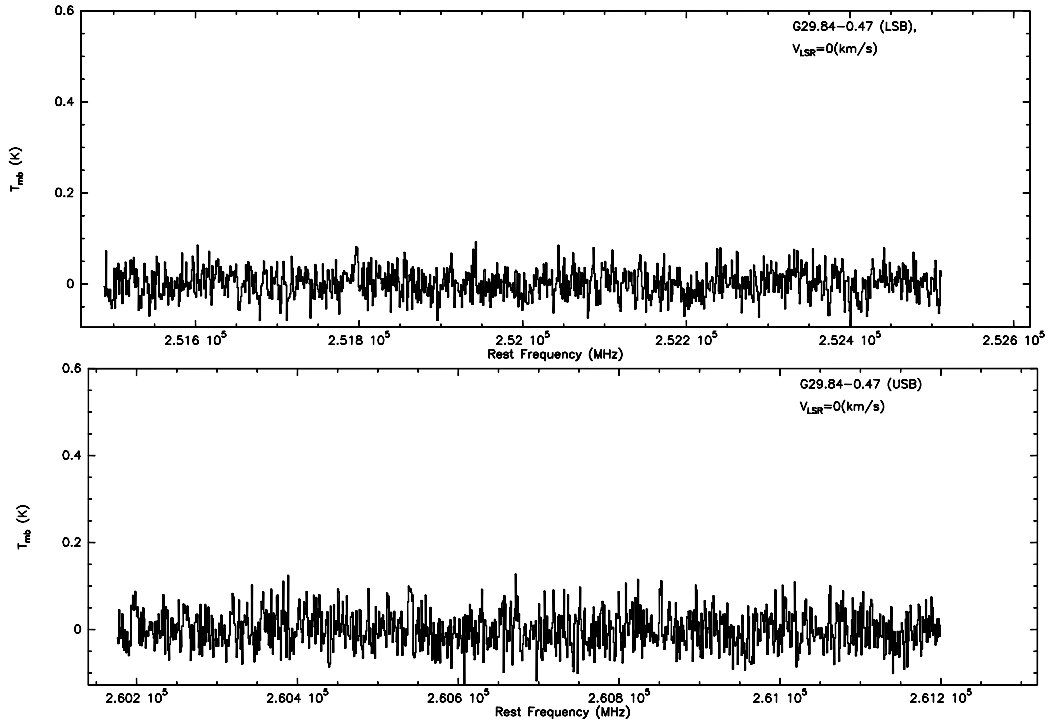


Fig. 10.— (continued) For G29.84-0.47.

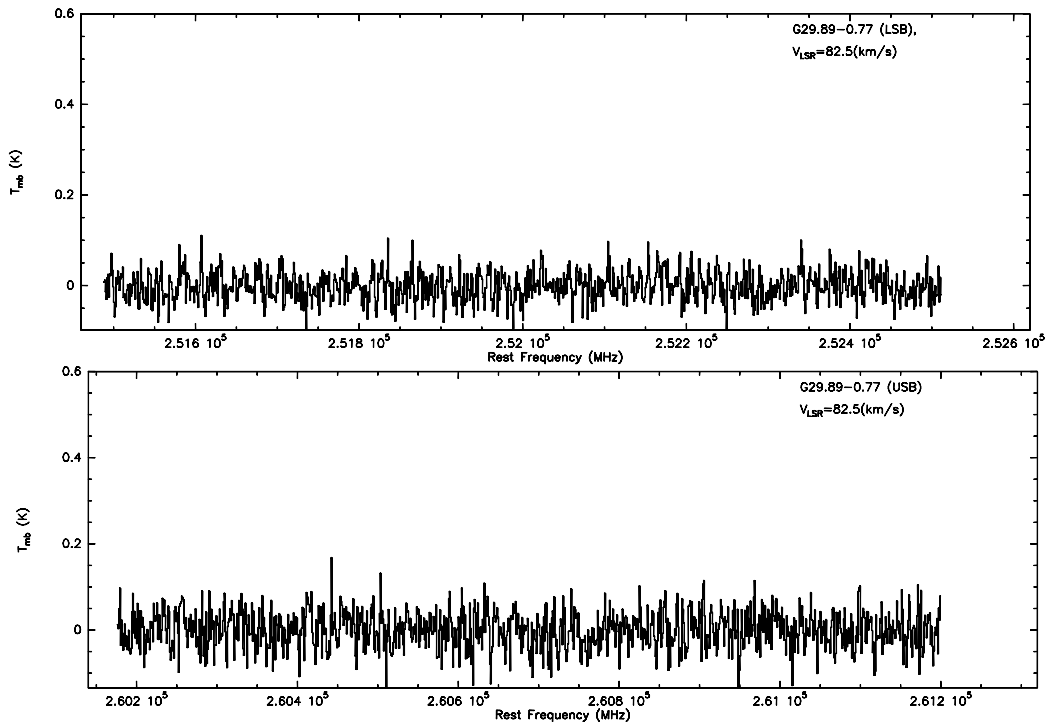


Fig. 10.— (continued) For G29.89-0.77.

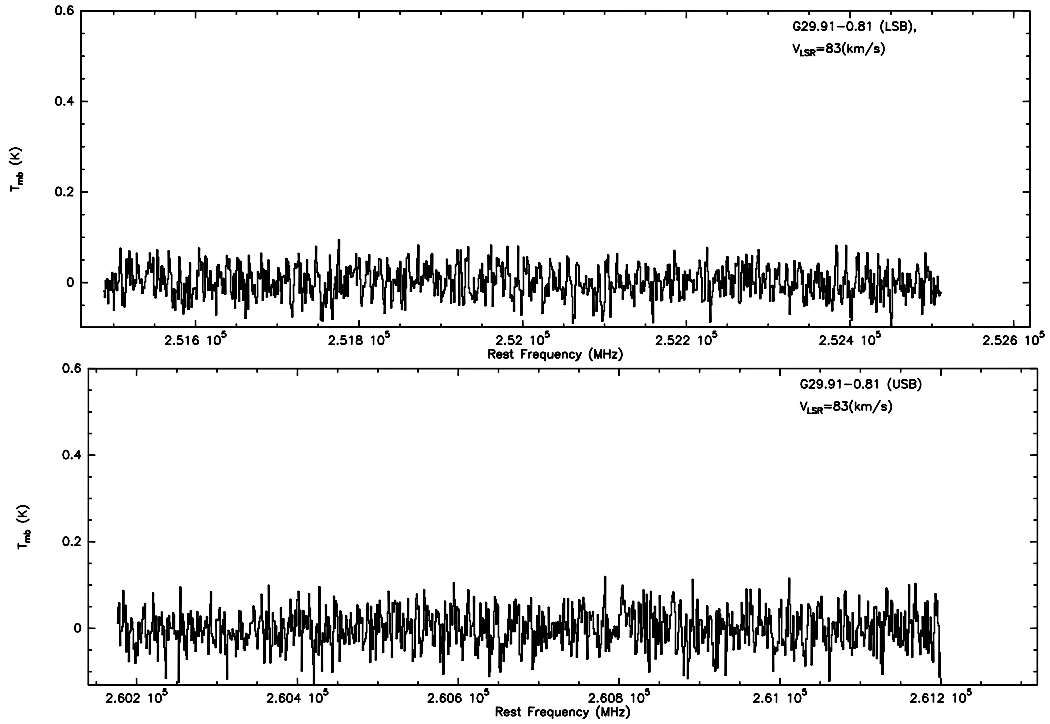


Fig. 10.— (continued) For G29.91-0.81.

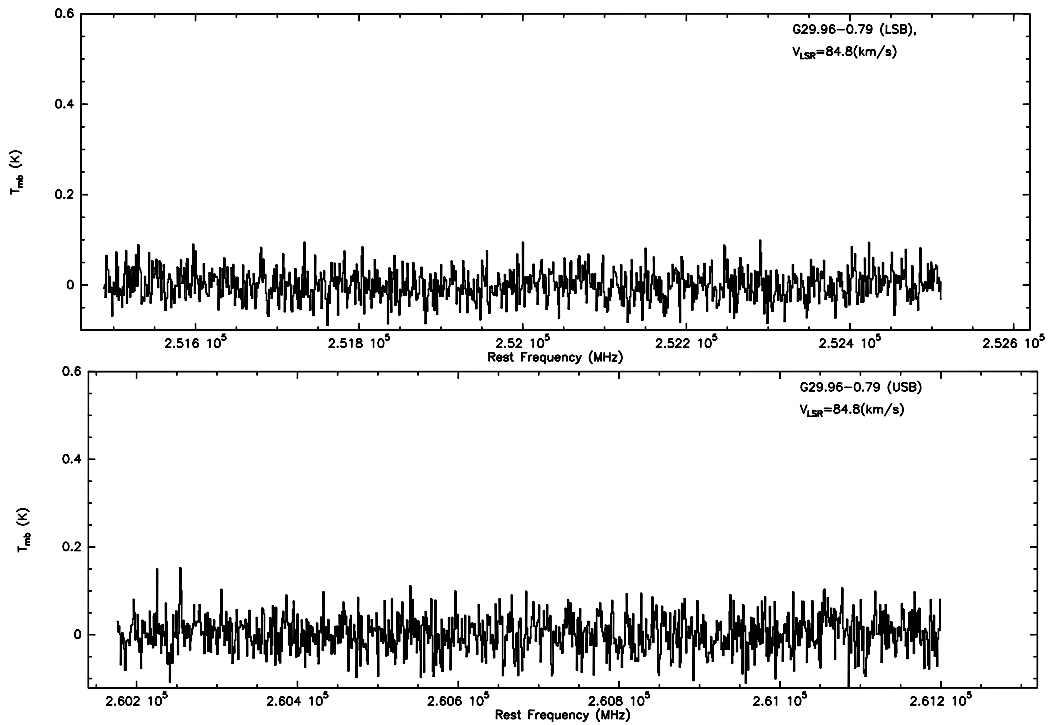


Fig. 10.— (continued) For G29.96-0.79.

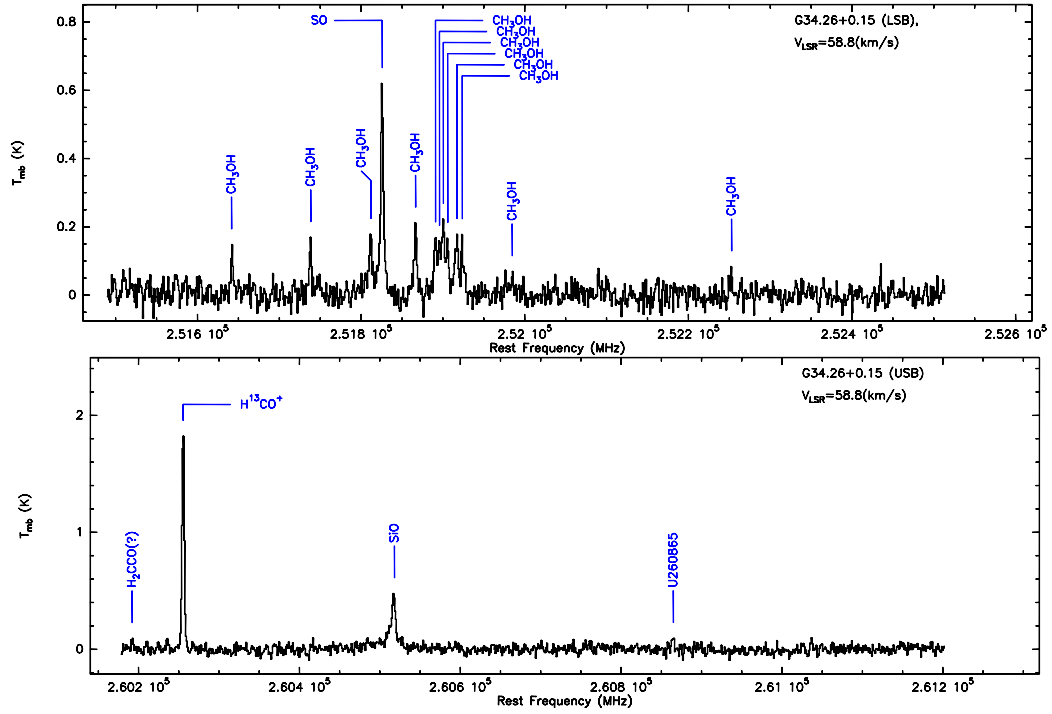


Fig. 10.— (continued) For G34.26+0.15.

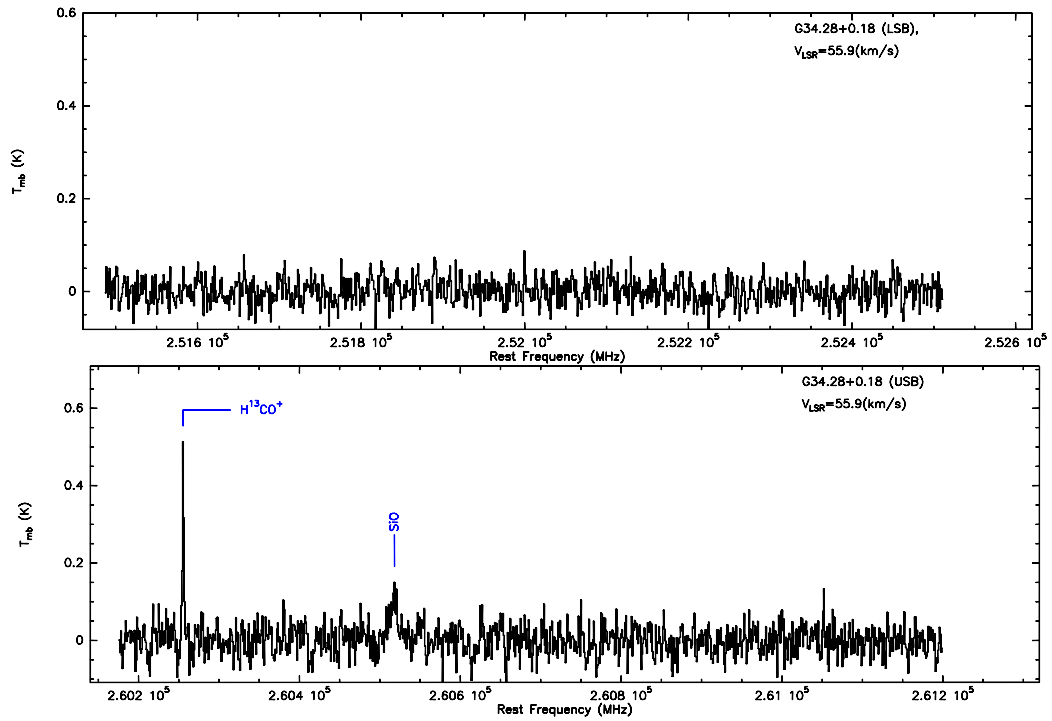


Fig. 10.— (continued) For G34.28+0.18.

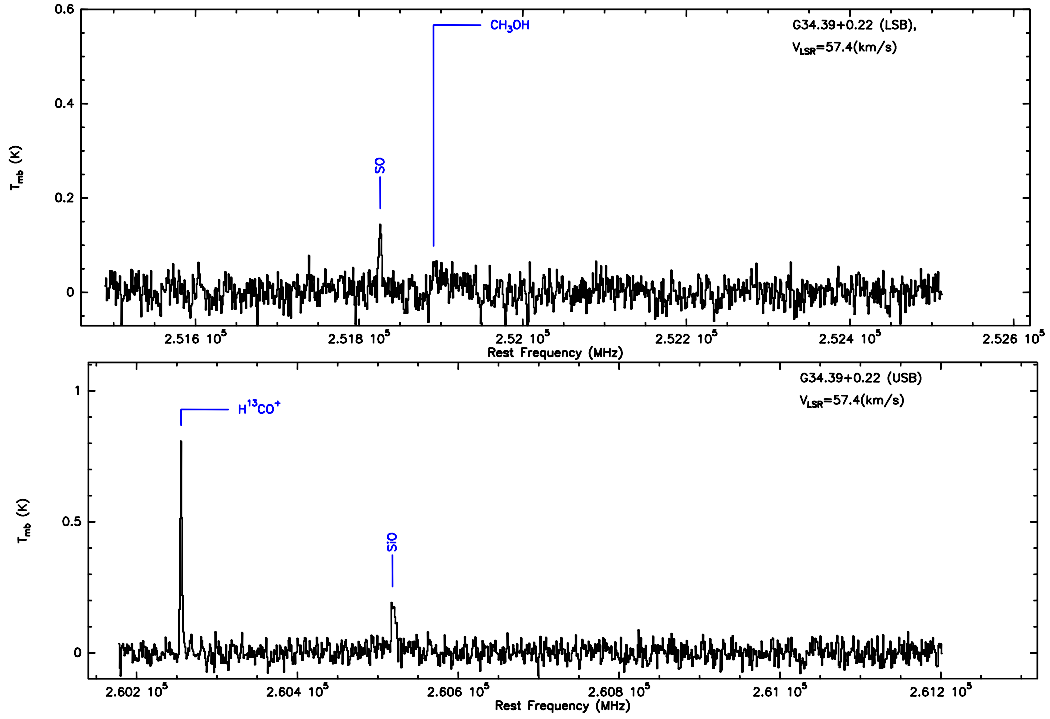


Fig. 10.— (continued) For G34.39+0.22.

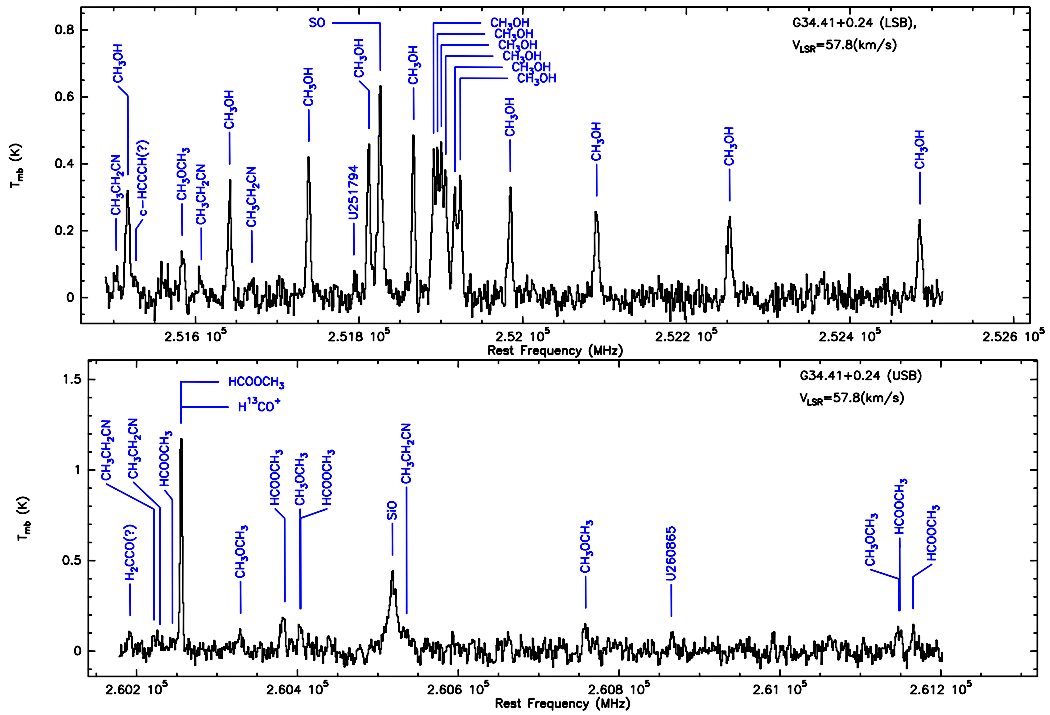


Fig. 10.— (continued) For G34.41+0.24.

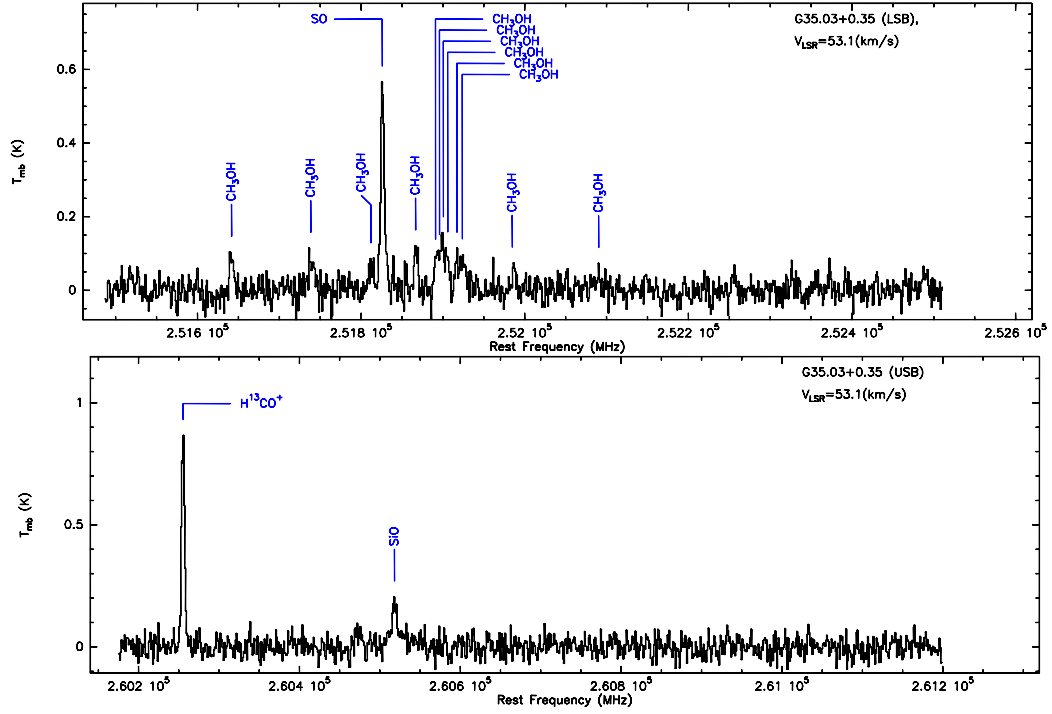


Fig. 10.— (continued) For G35.03+0.35.

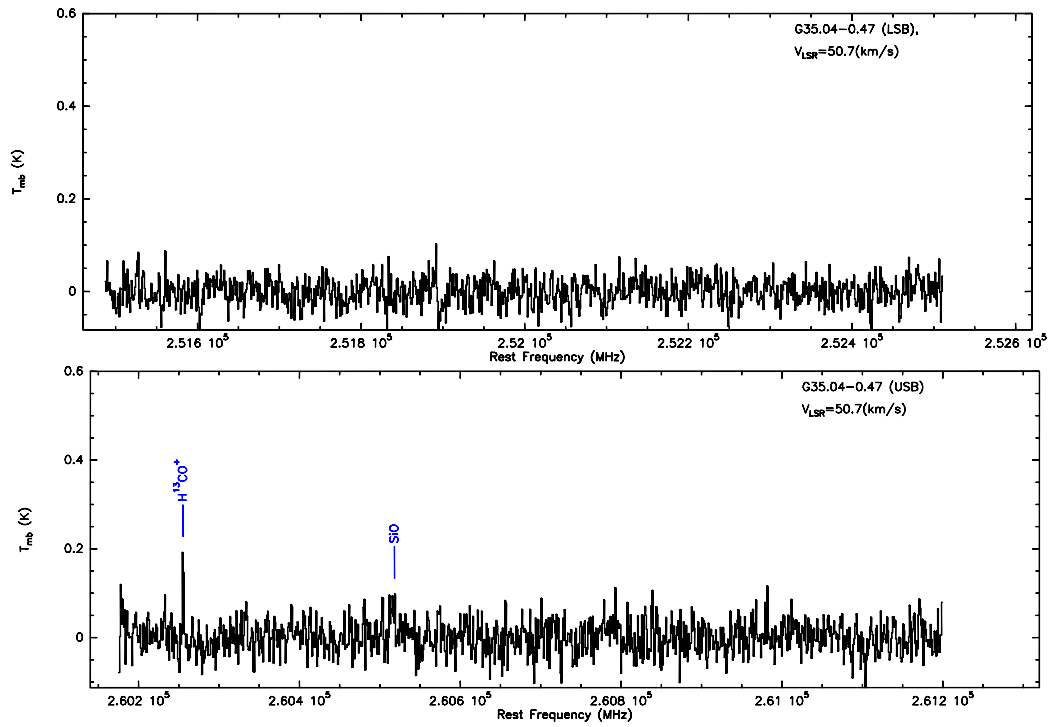


Fig. 10.— (continued) For G35.04-0.47.

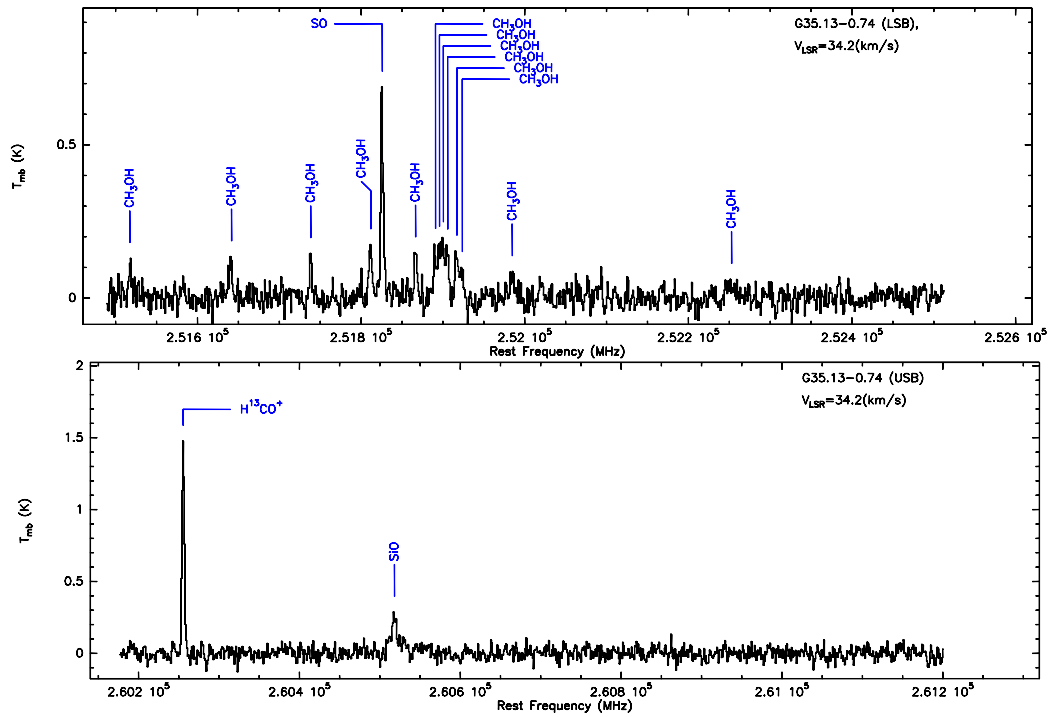


Fig. 10.— (continued) For G35.13-0.74.

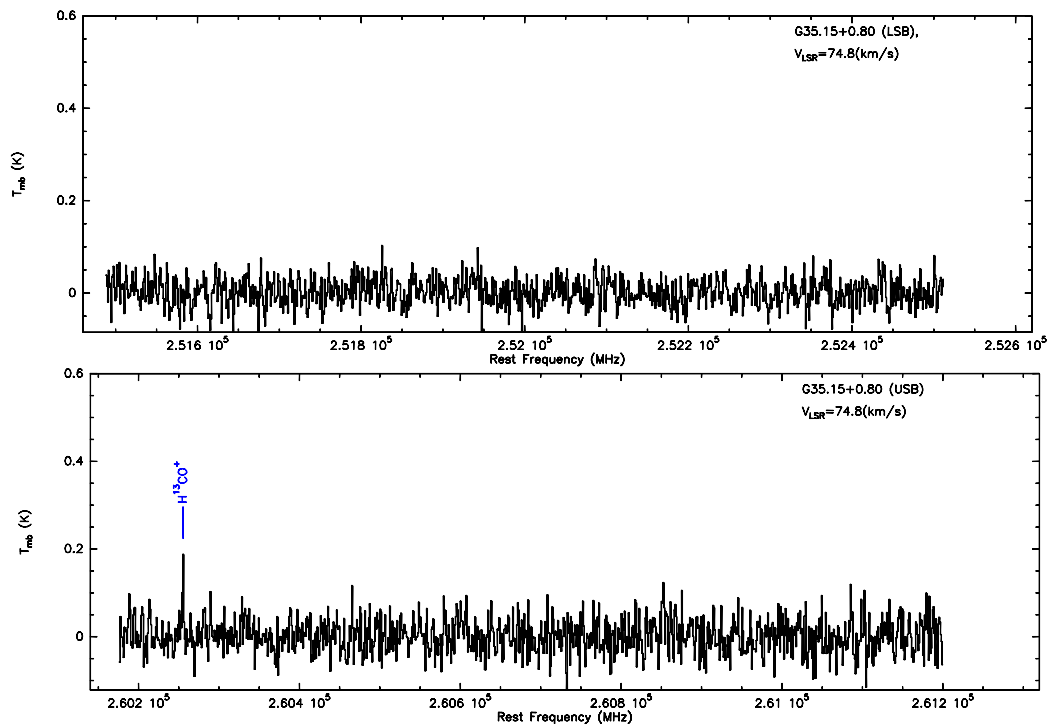


Fig. 10.— (continued) For G35.15+0.80.

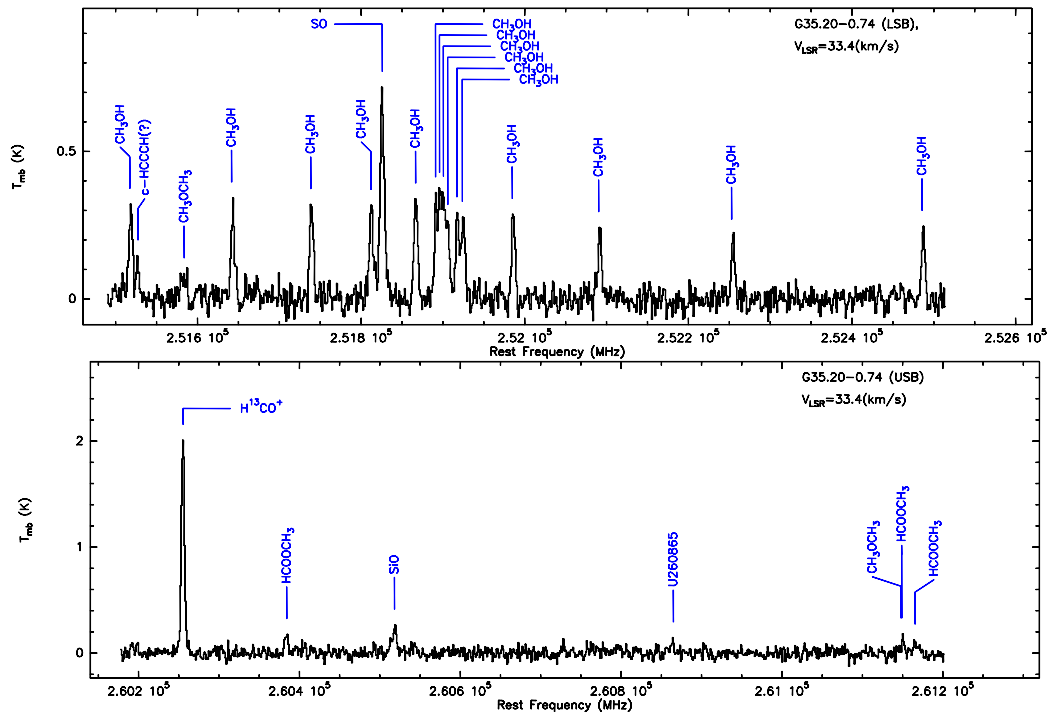


Fig. 10.— (continued) For G35.20-0.74.

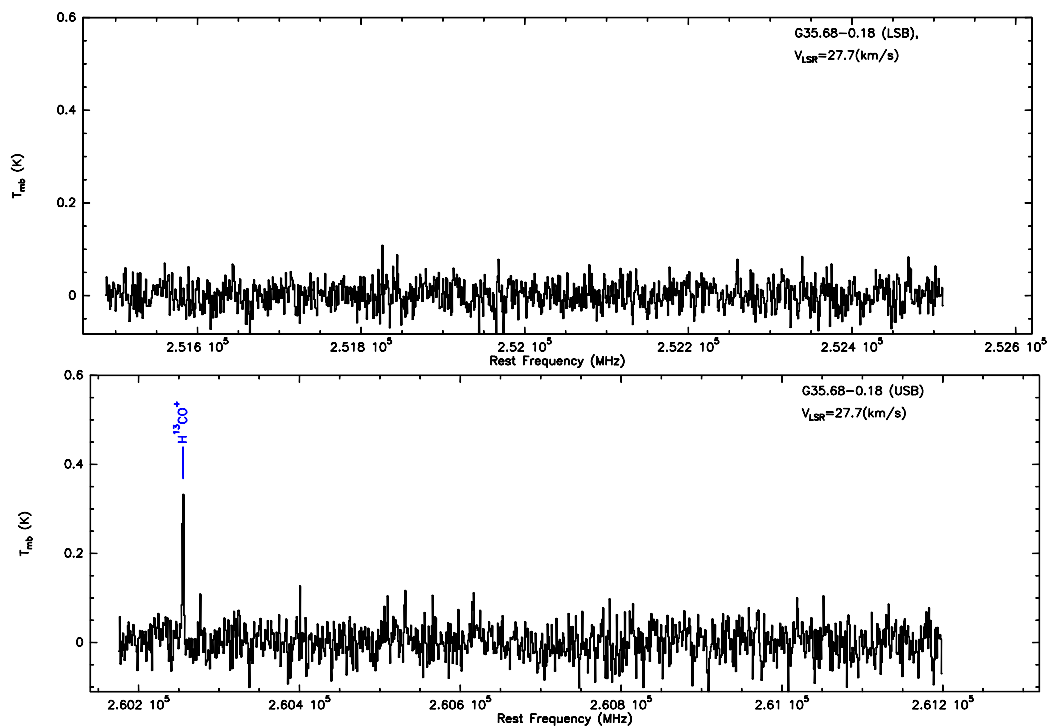


Fig. 10.— (continued) For G35.68-0.18.

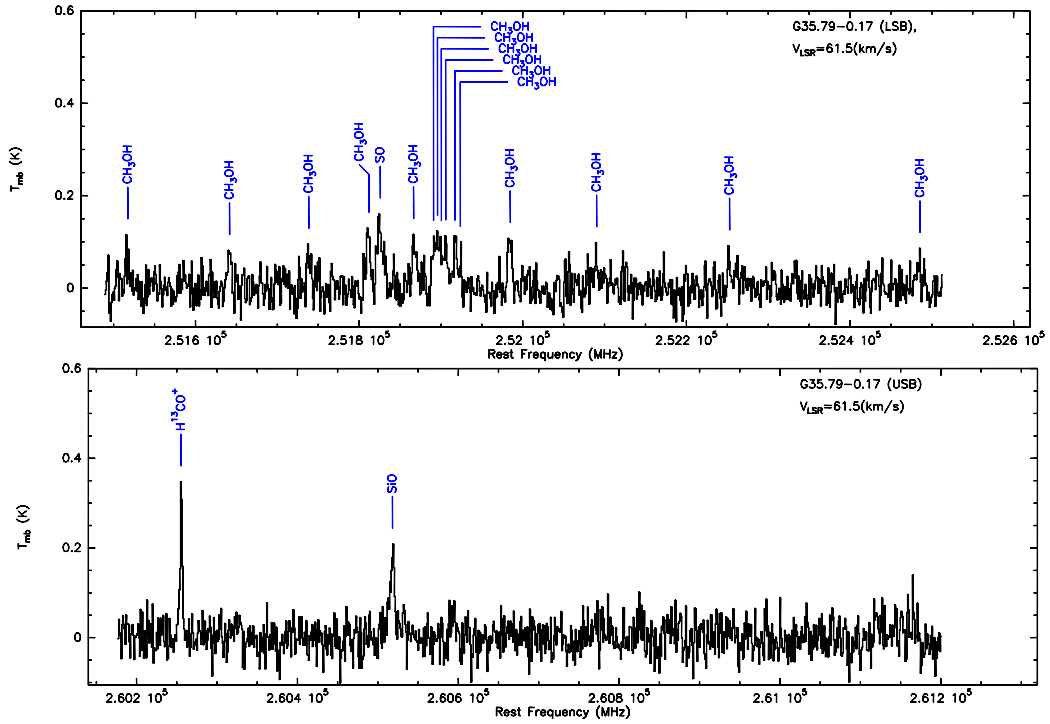


Fig. 10.— (continued) For G35.79-0.17.

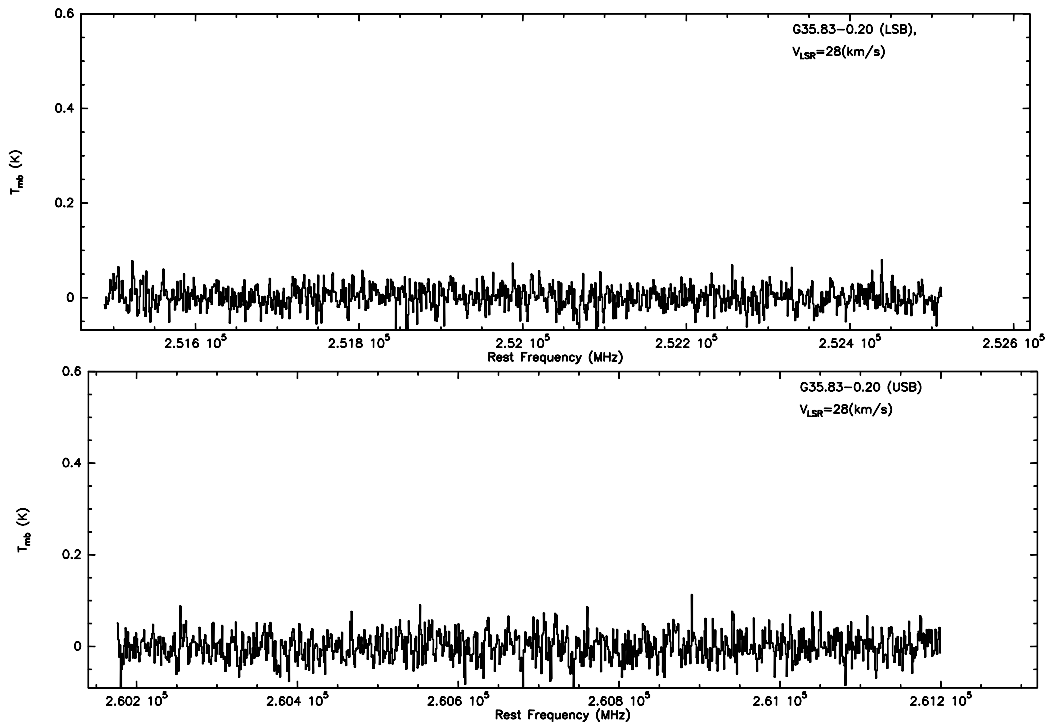


Fig. 10.— (continued) For G35.83-0.20.

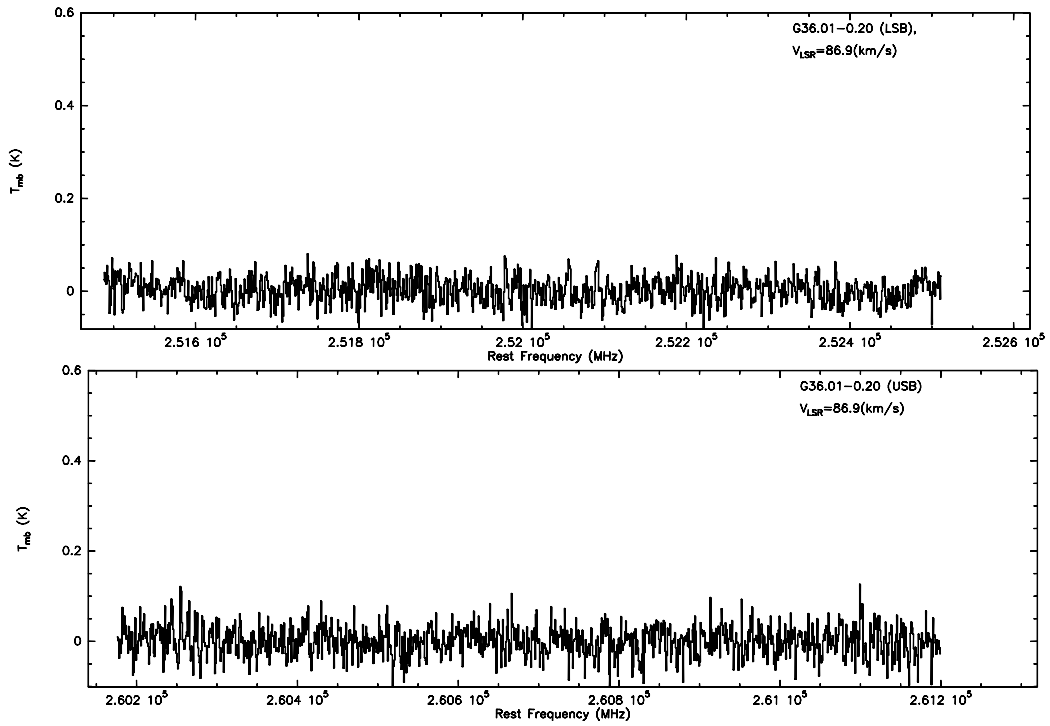


Fig. 10.— (continued) For G36.01-0.20.

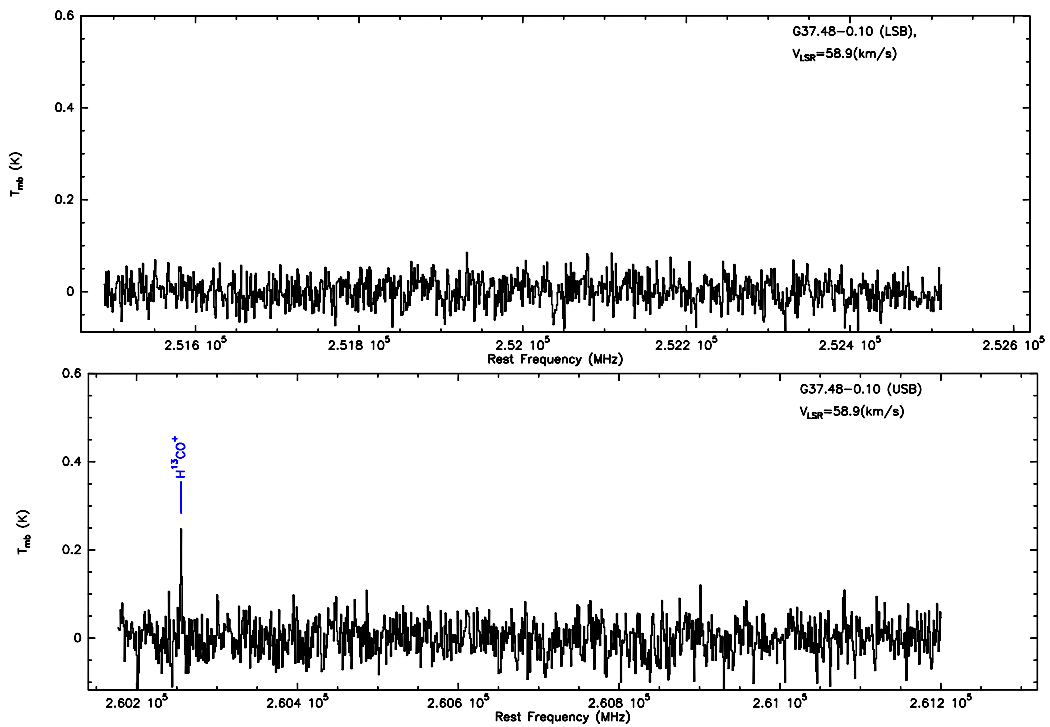


Fig. 10.— (continued) For G37.48-0.10.

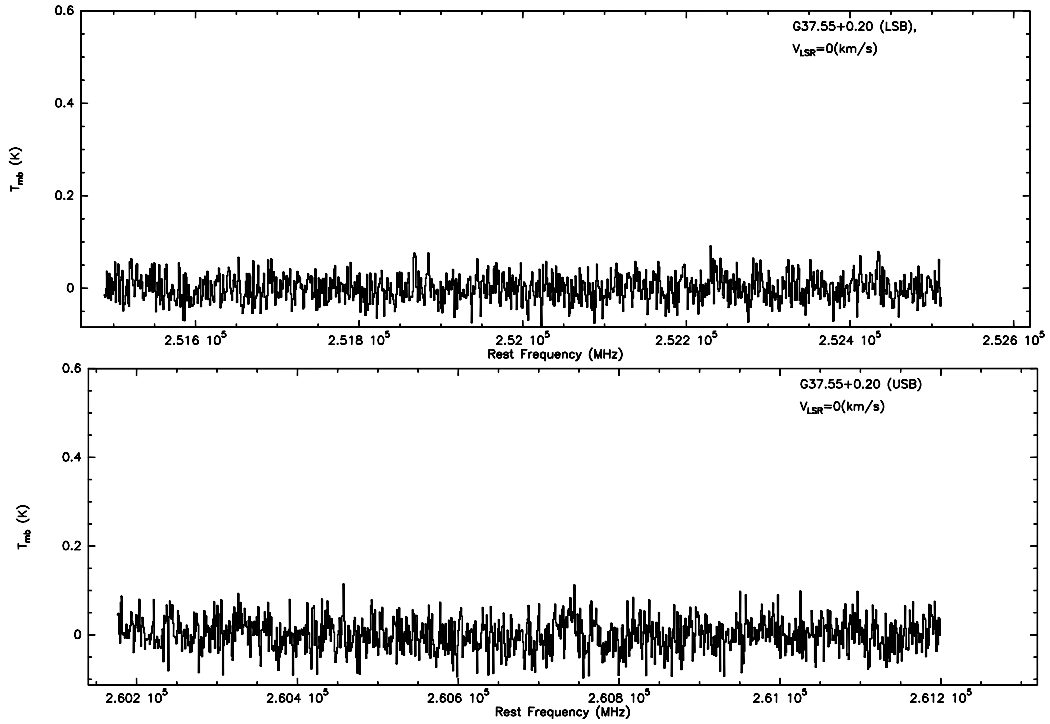


Fig. 10.— (continued) For G37.55+0.20.

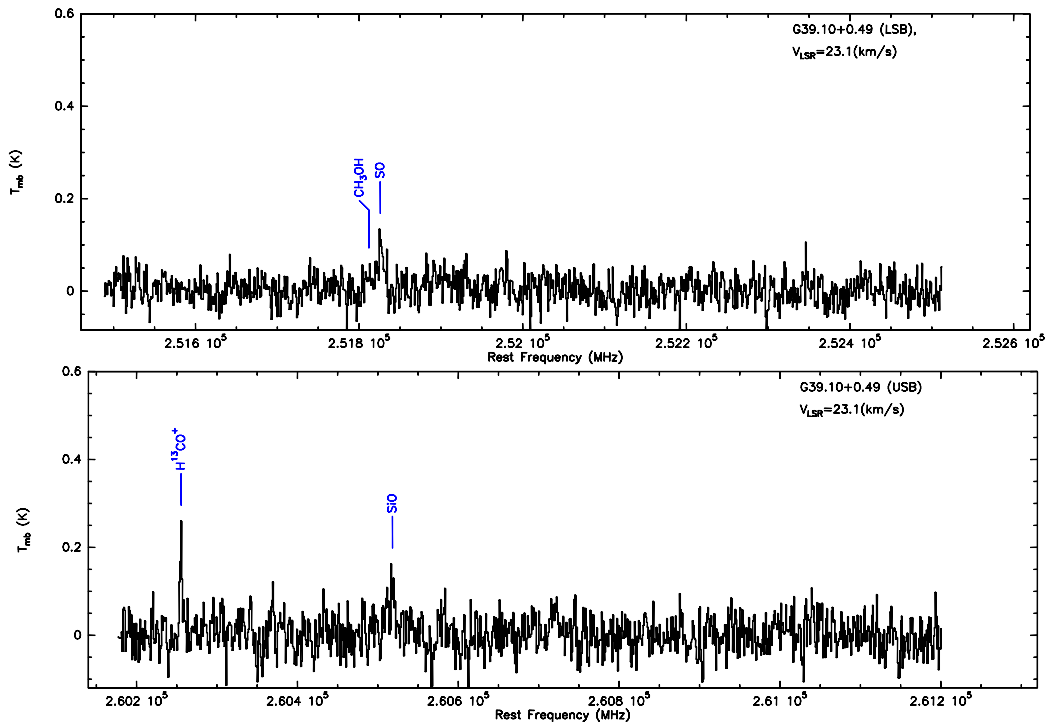


Fig. 10.— (continued) For G39.10+0.49.

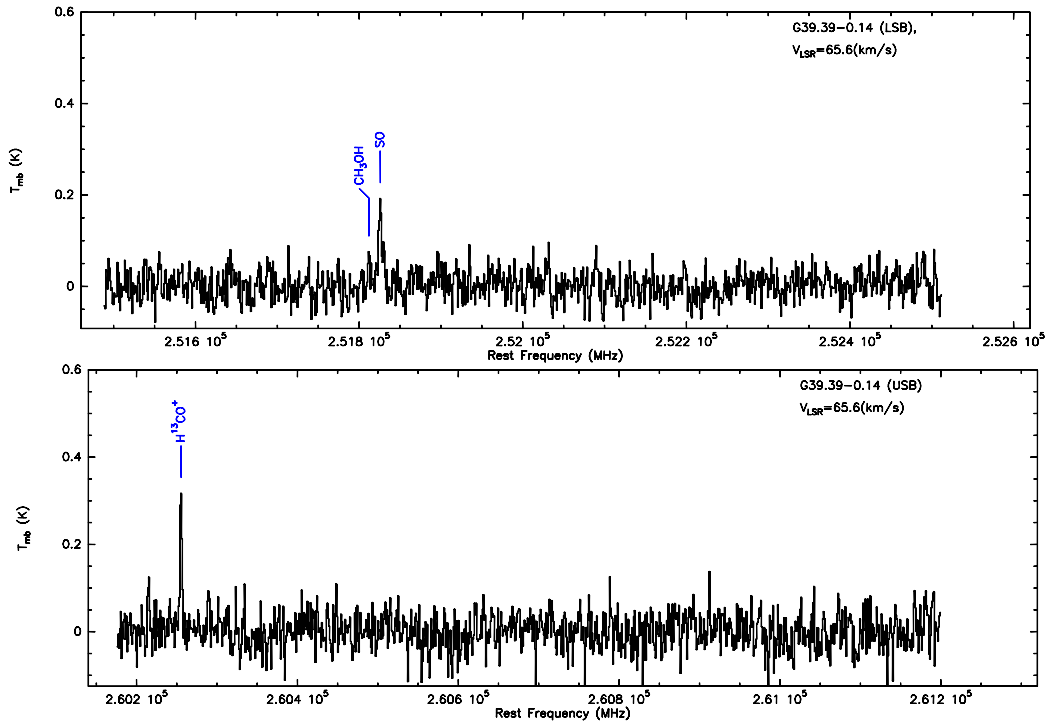


Fig. 10.— (continued) For G39.39-0.14.

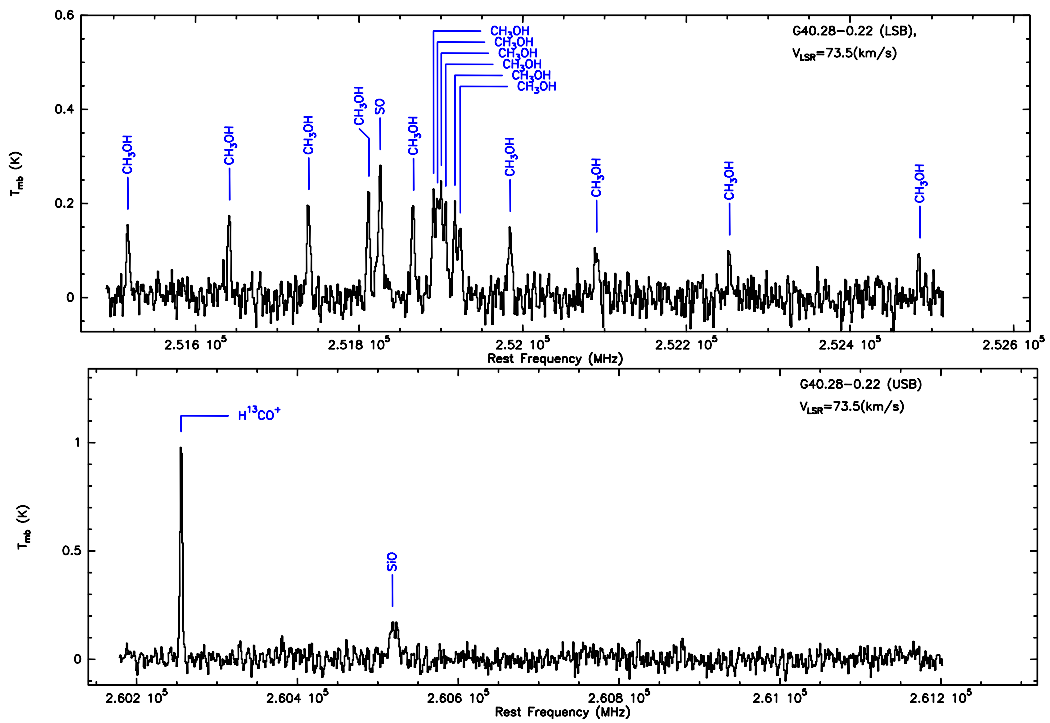


Fig. 10.— (continued) For G40.28-0.22.

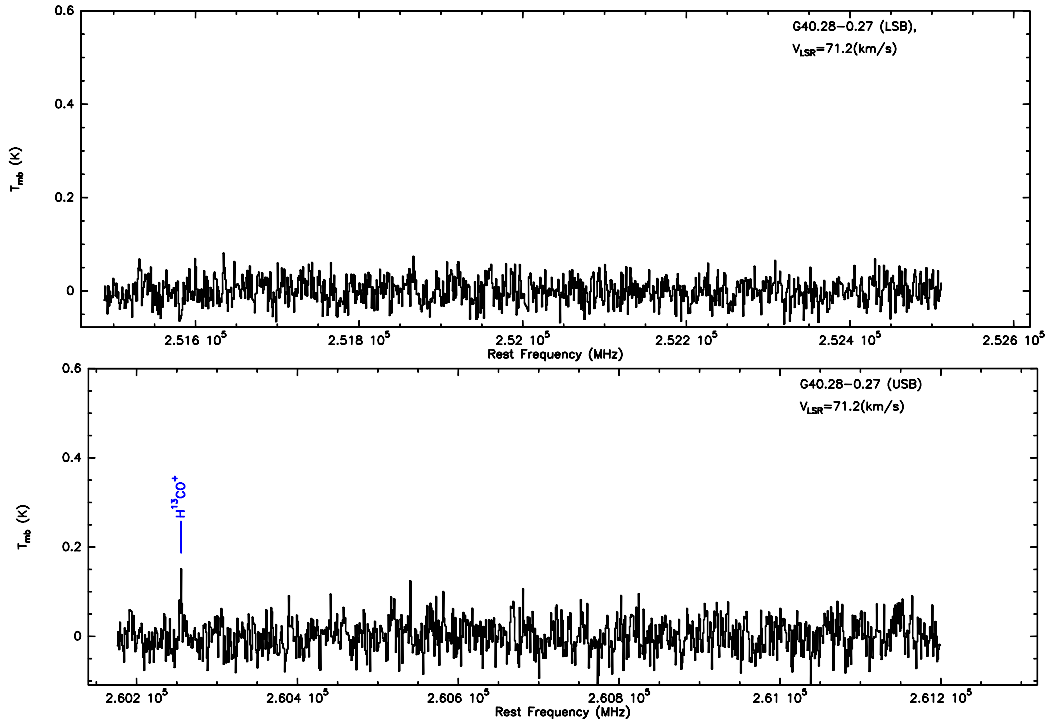


Fig. 10.— (continued) For G40.28-0.27.

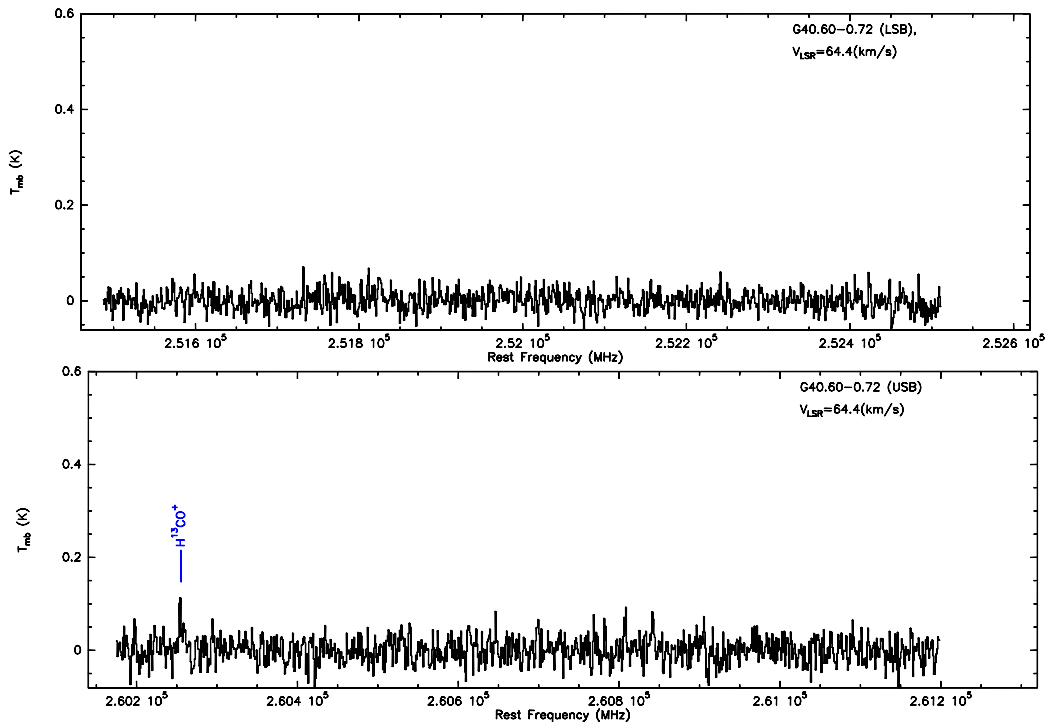


Fig. 10.— (continued) For G40.60-0.72.

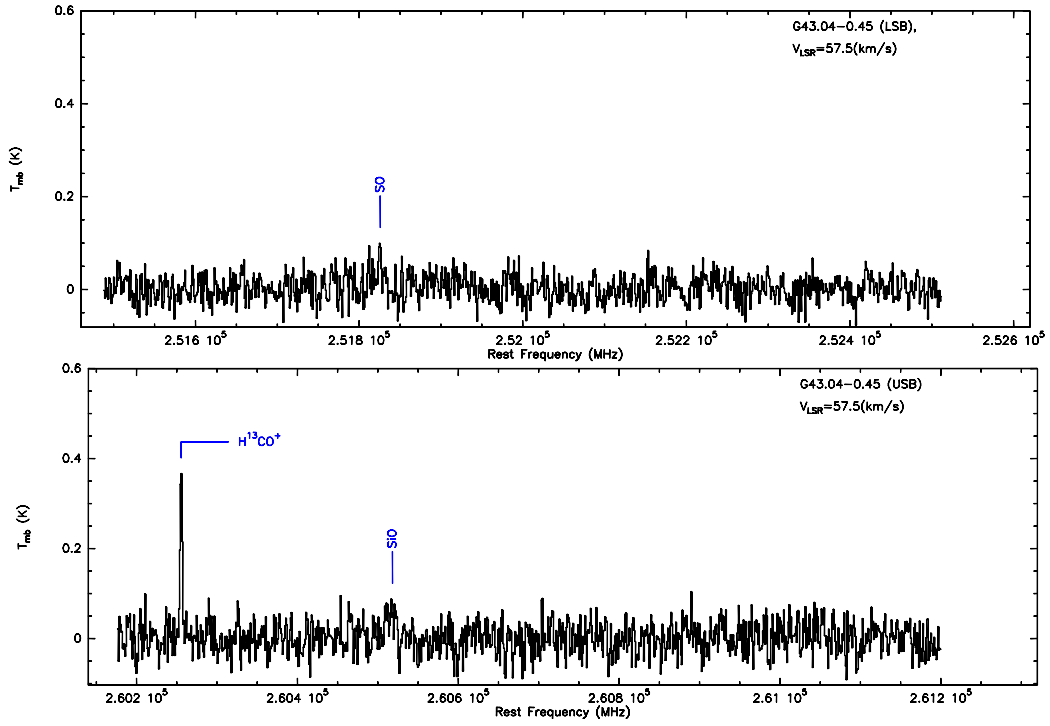


Fig. 10.— (continued) For G43.04-0.45.

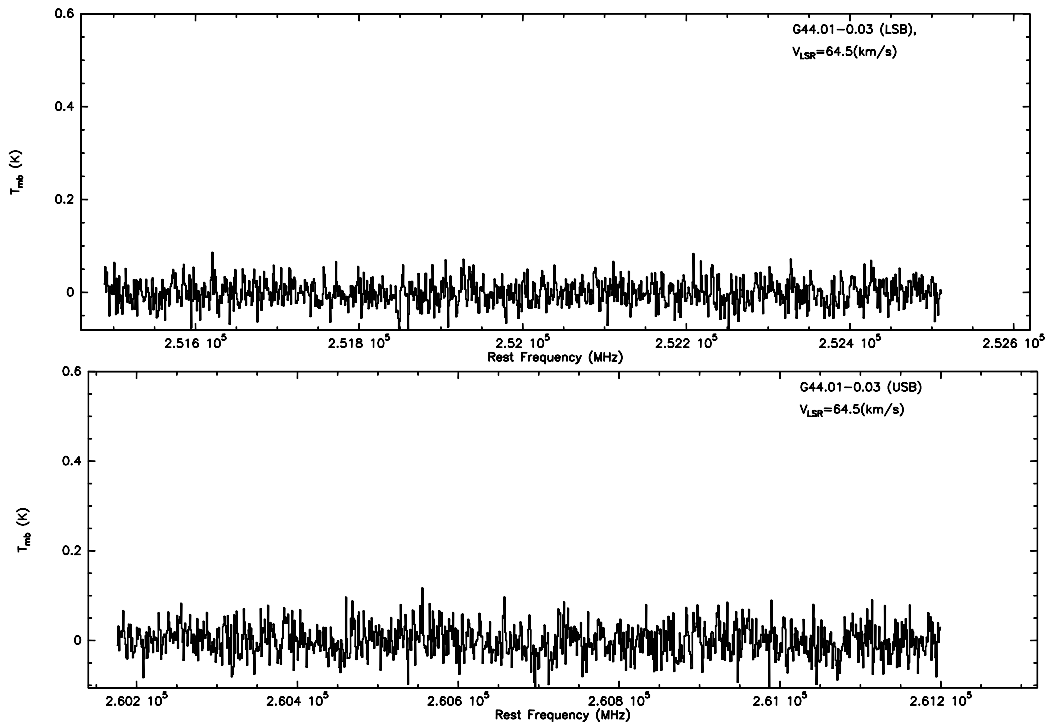


Fig. 10.— (continued) For G44.01-0.03.

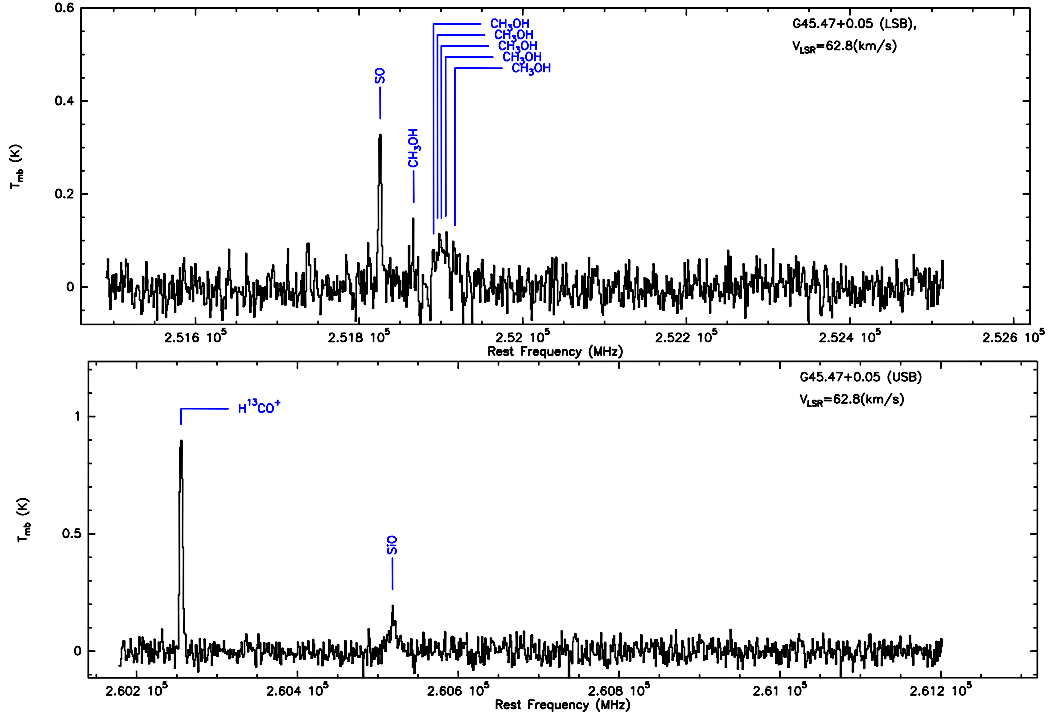


Fig. 10.— (continued) For G45.47+0.05.

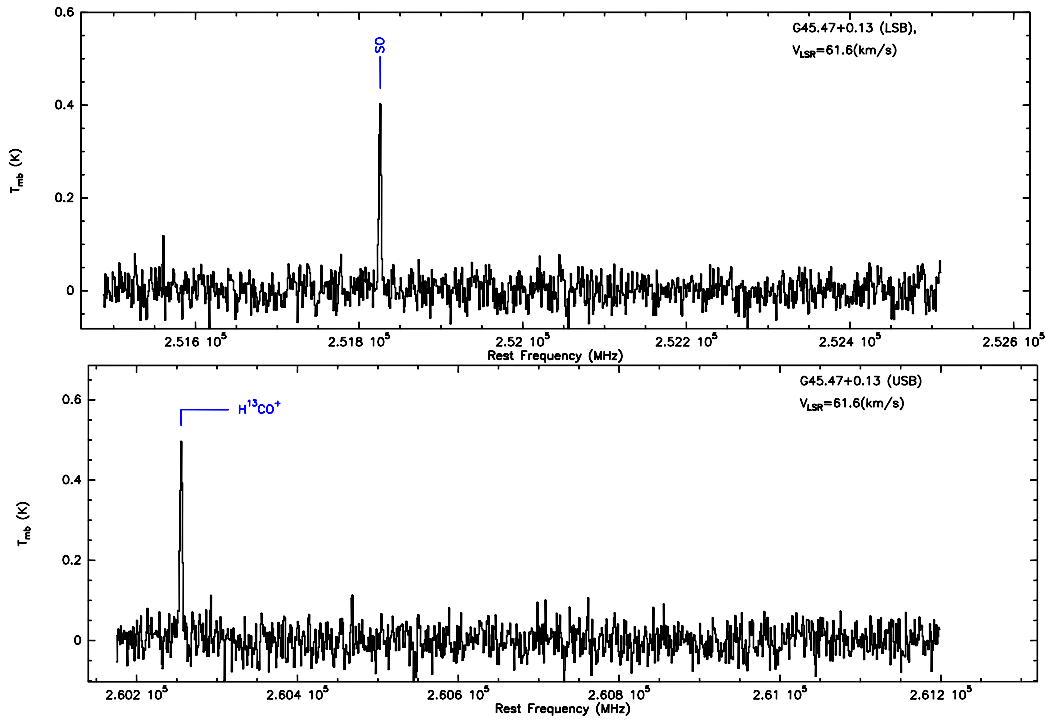


Fig. 10.— (continued) For G45.47+0.13.

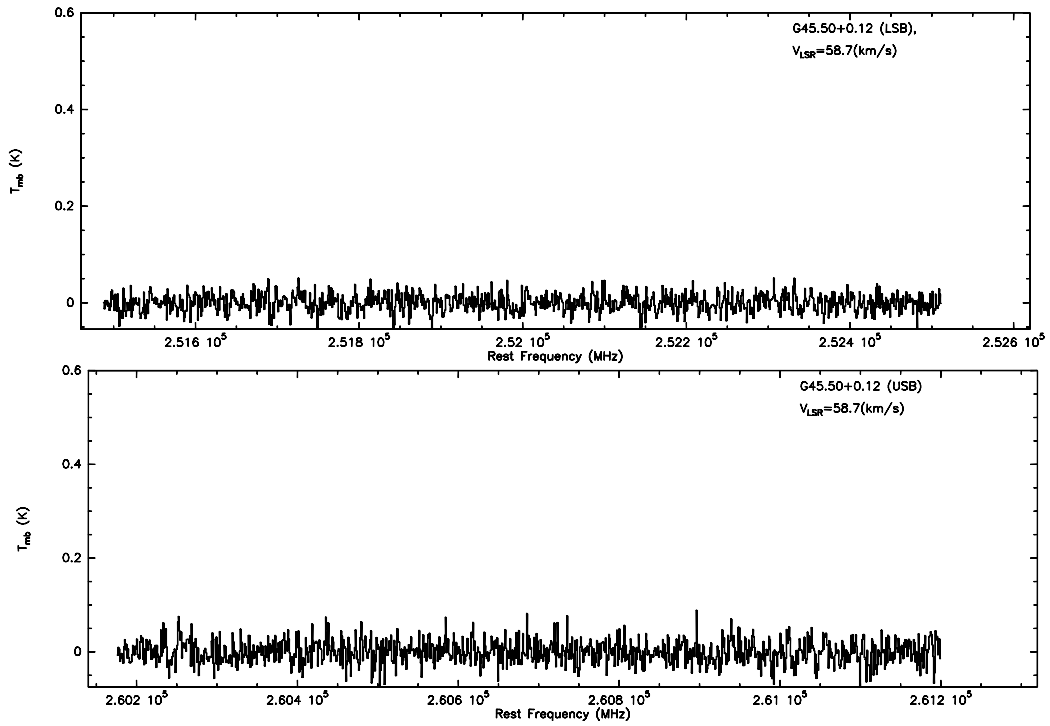


Fig. 10.— (continued) For G45.50+0.12.

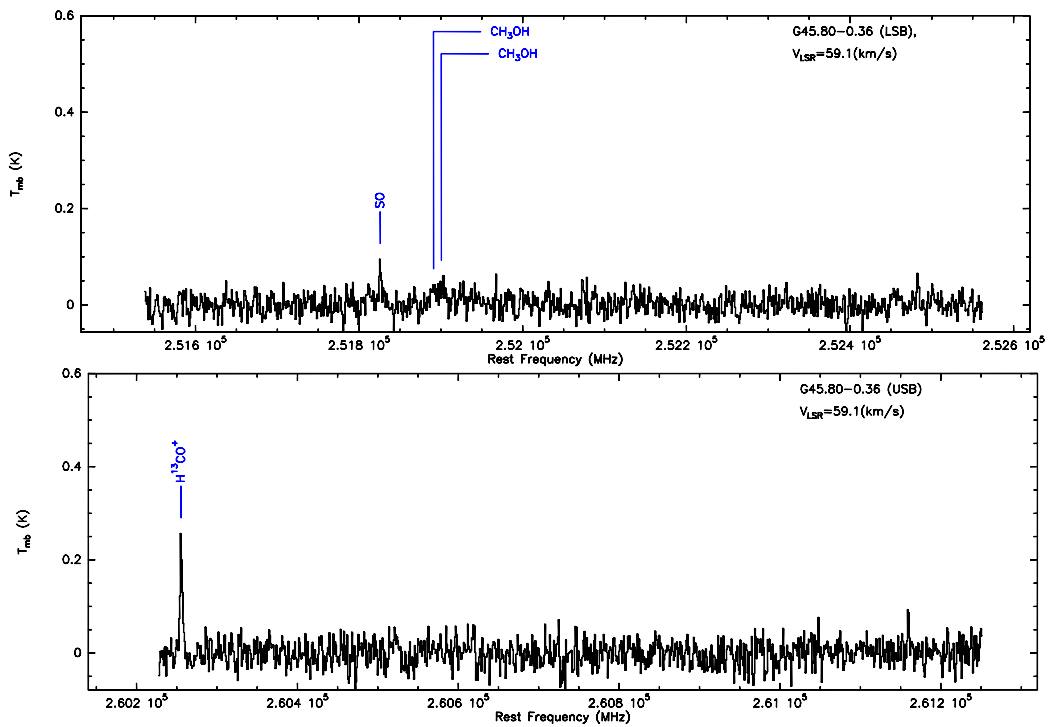


Fig. 10.— (continued) For G45.80-0.36.

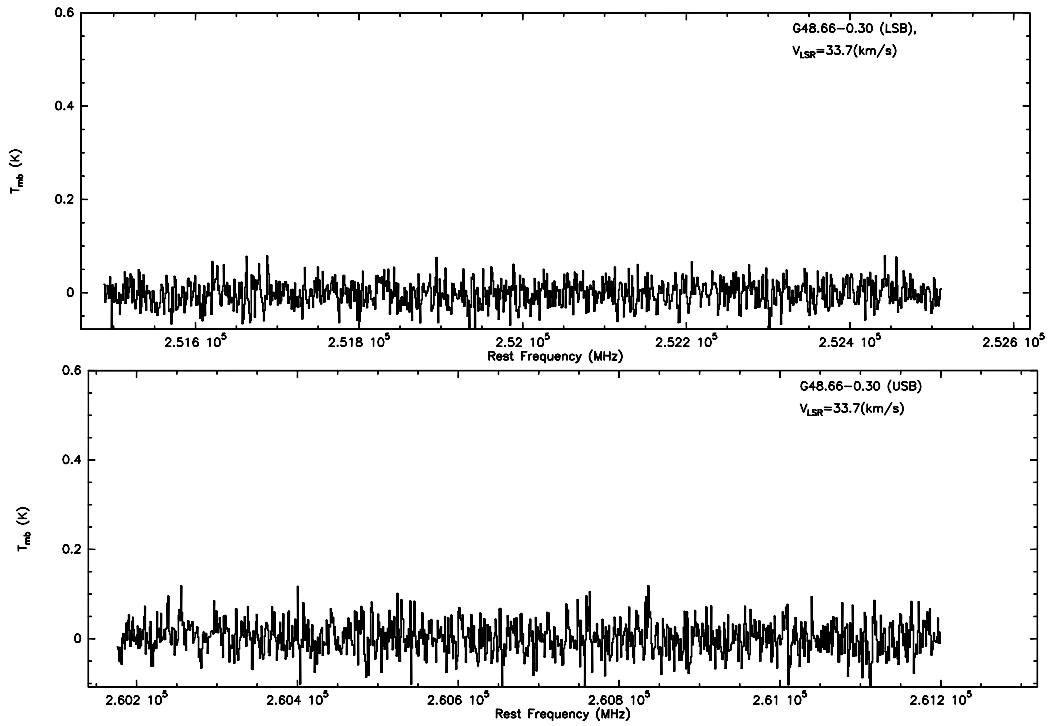


Fig. 10.— (continued) For G48.66-0.30.

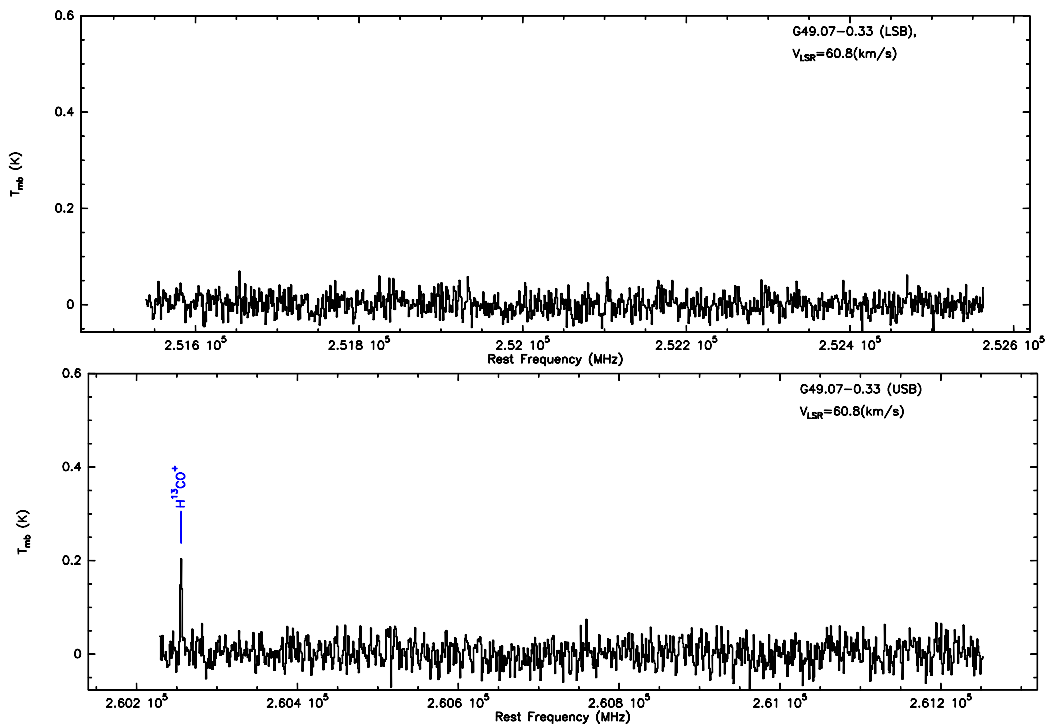


Fig. 10.— (continued) For G49.07-0.33.

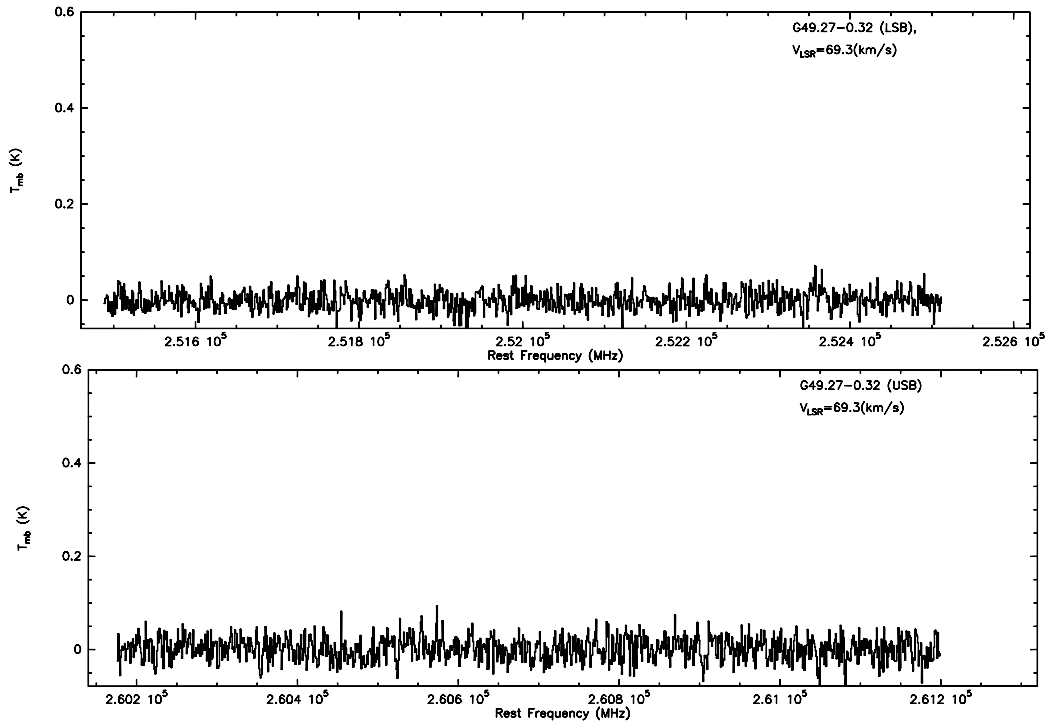


Fig. 10.— (continued) For G49.27-0.32.

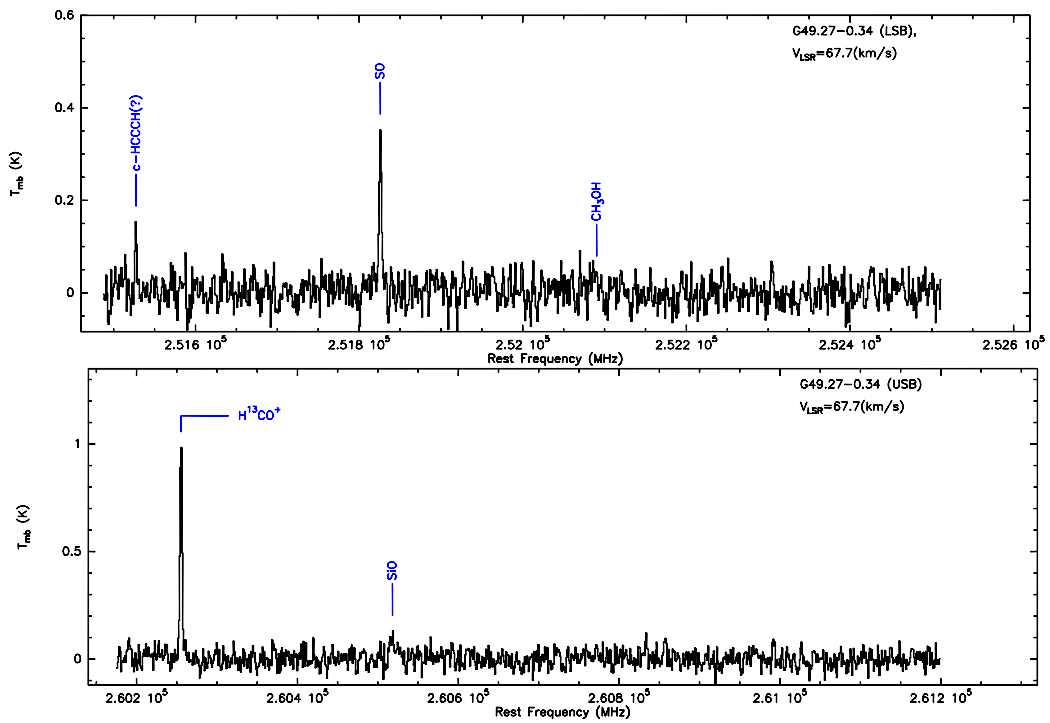


Fig. 10.— (continued) For G49.27-0.34.

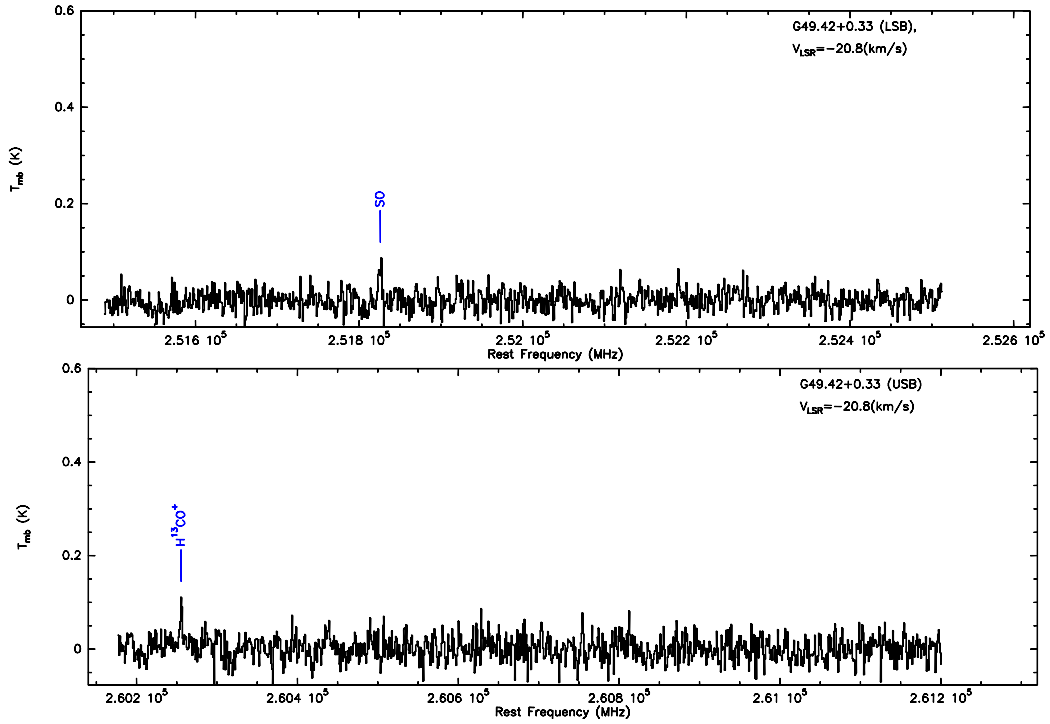


Fig. 10.— (continued) For G49.42+0.33.

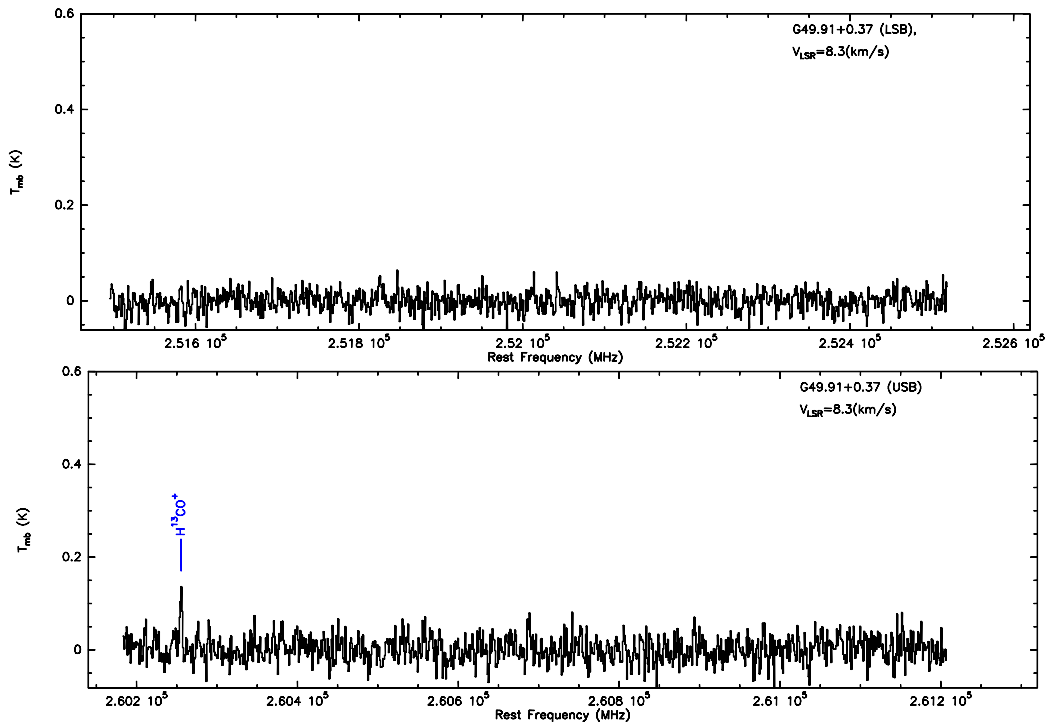


Fig. 10.— (continued) For G49.91+0.37.

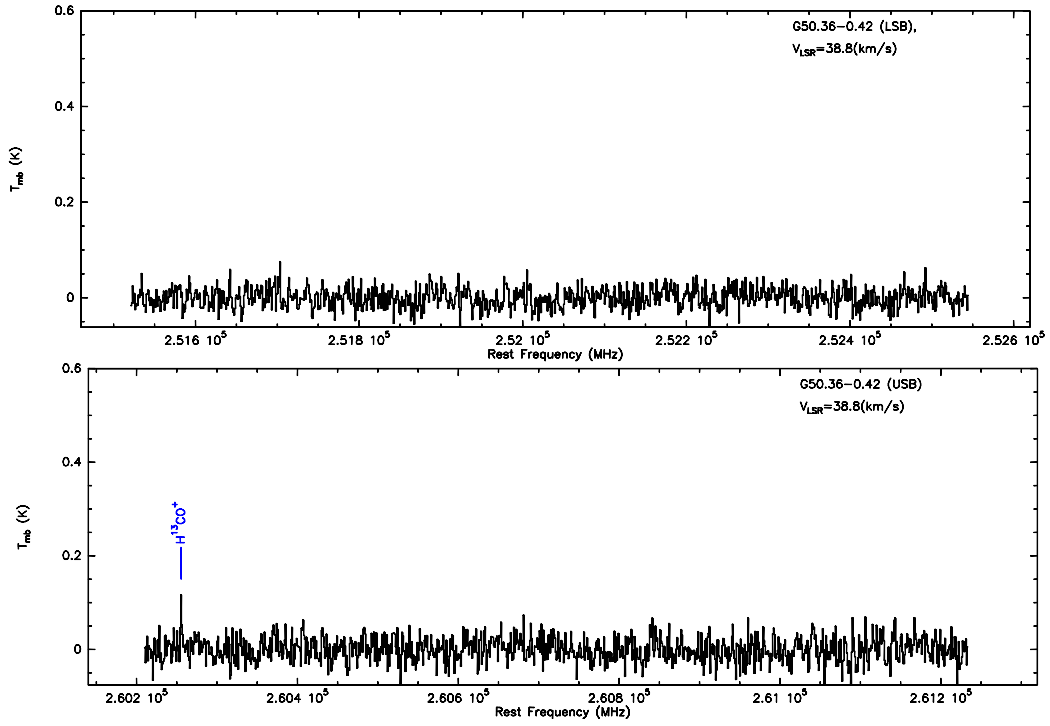


Fig. 10.— (continued) For G50.36-0.42.

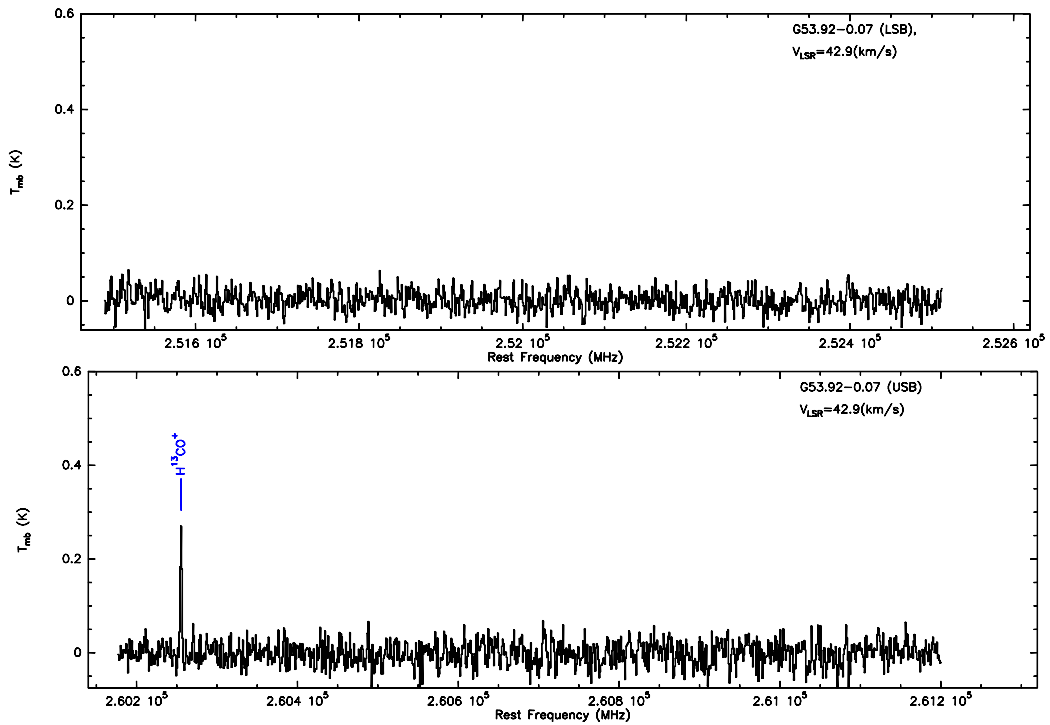


Fig. 10.— (continued) For G53.92-0.07.

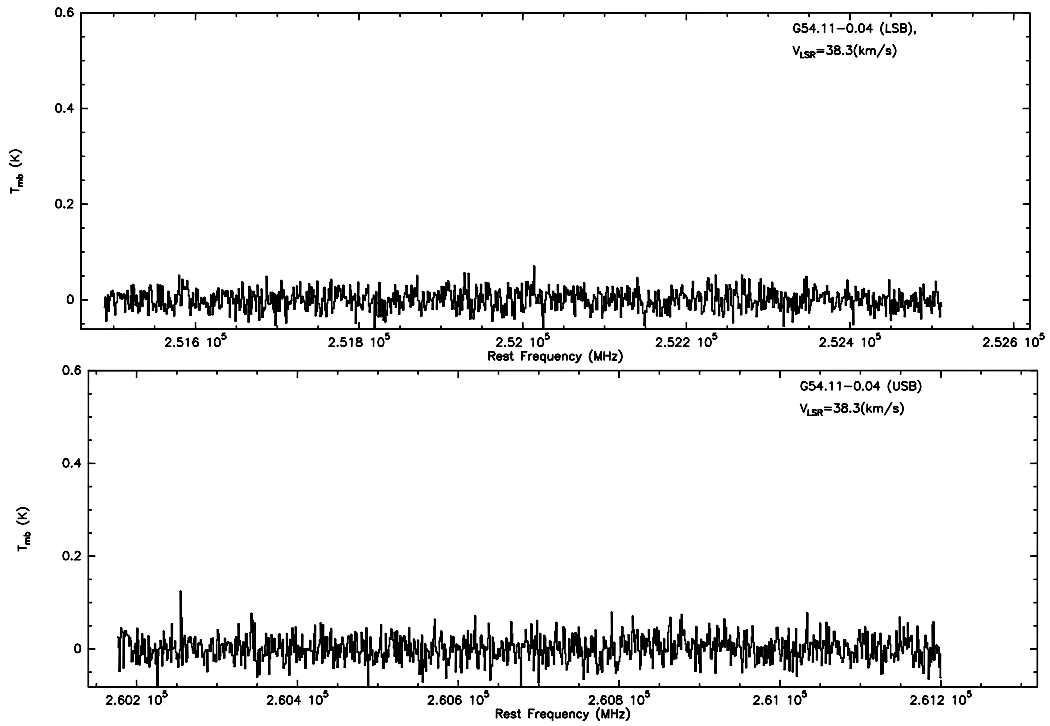


Fig. 10.— (continued) For G54.11-0.04.

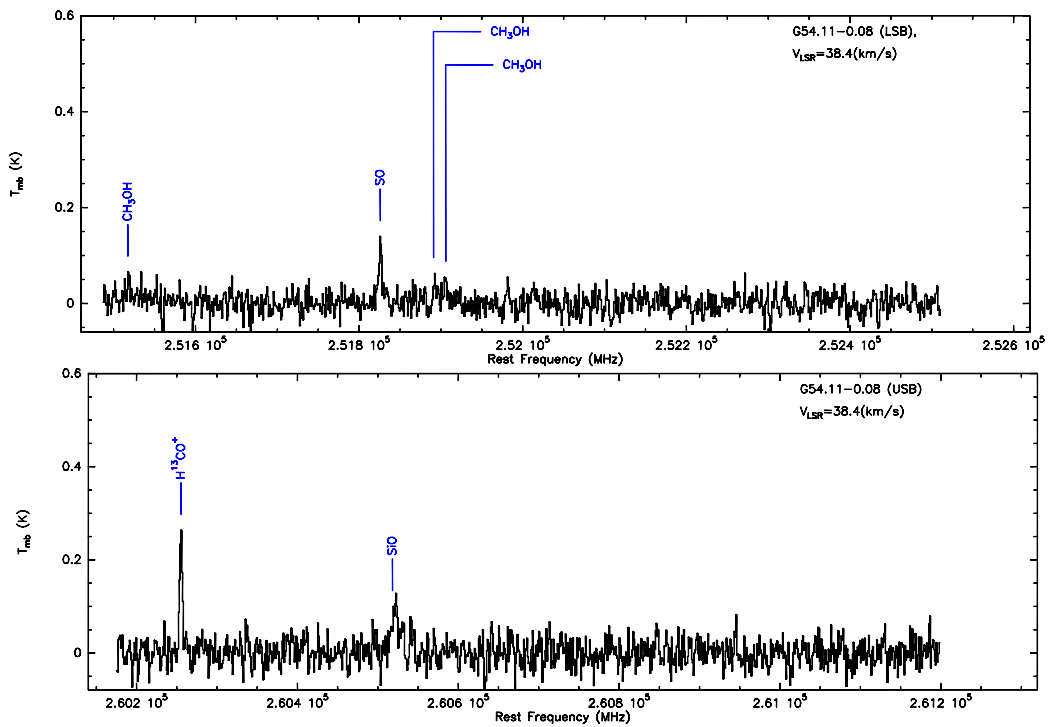


Fig. 10.— (continued) For G54.11-0.08.

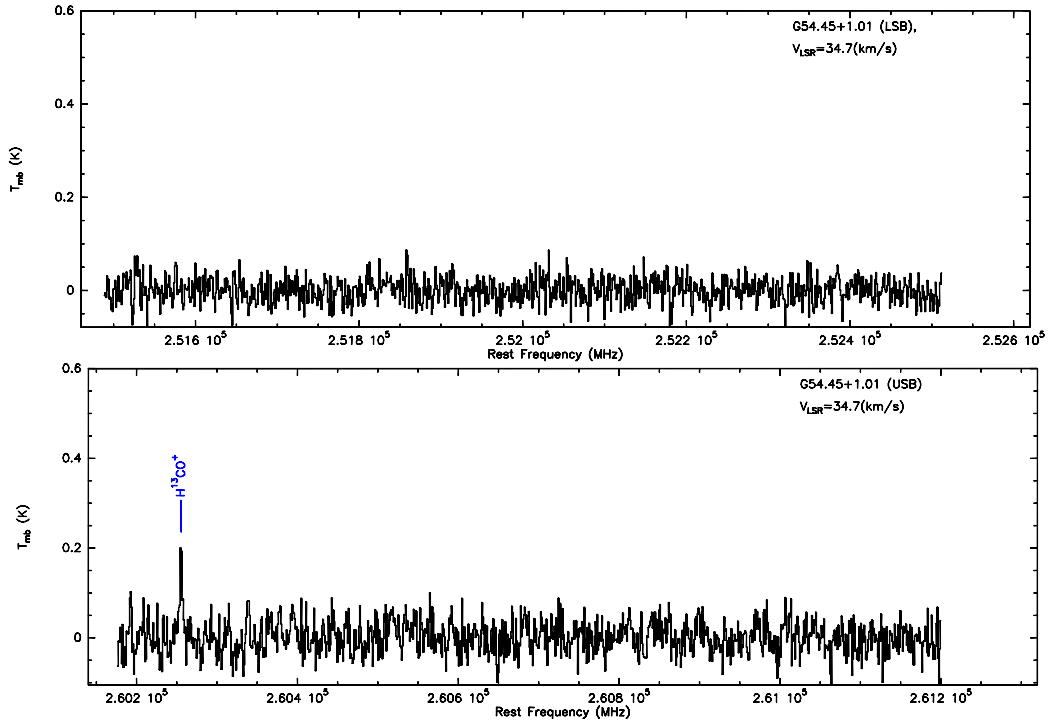


Fig. 10.— (continued) For G54.45+1.01.

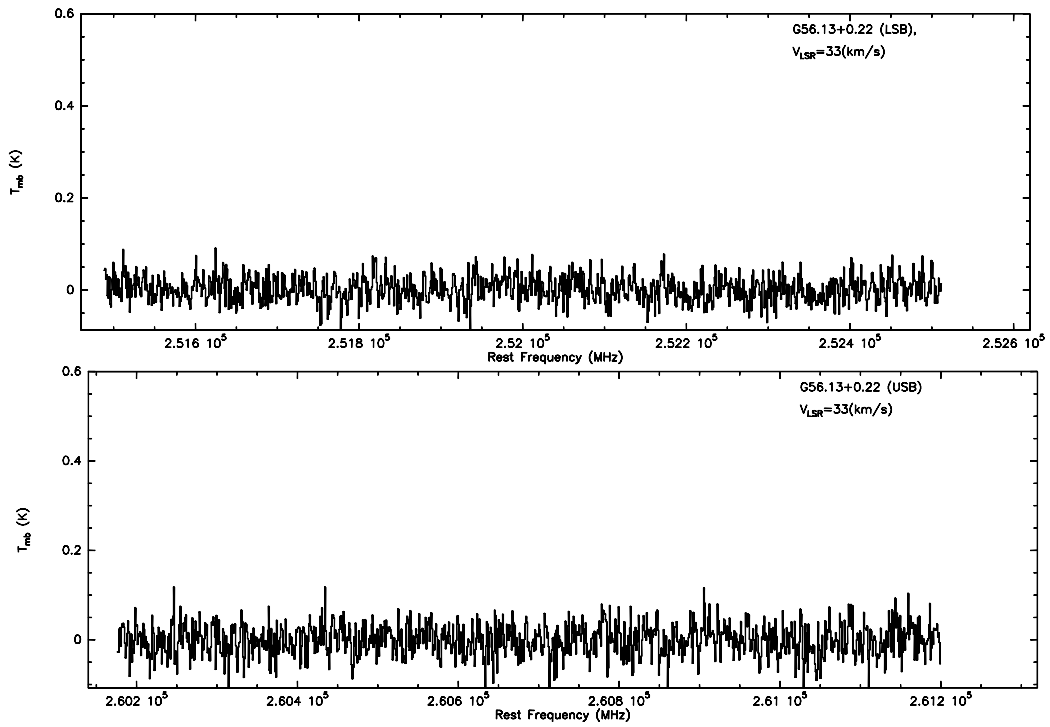


Fig. 10.— (continued) For G56.13+0.22.

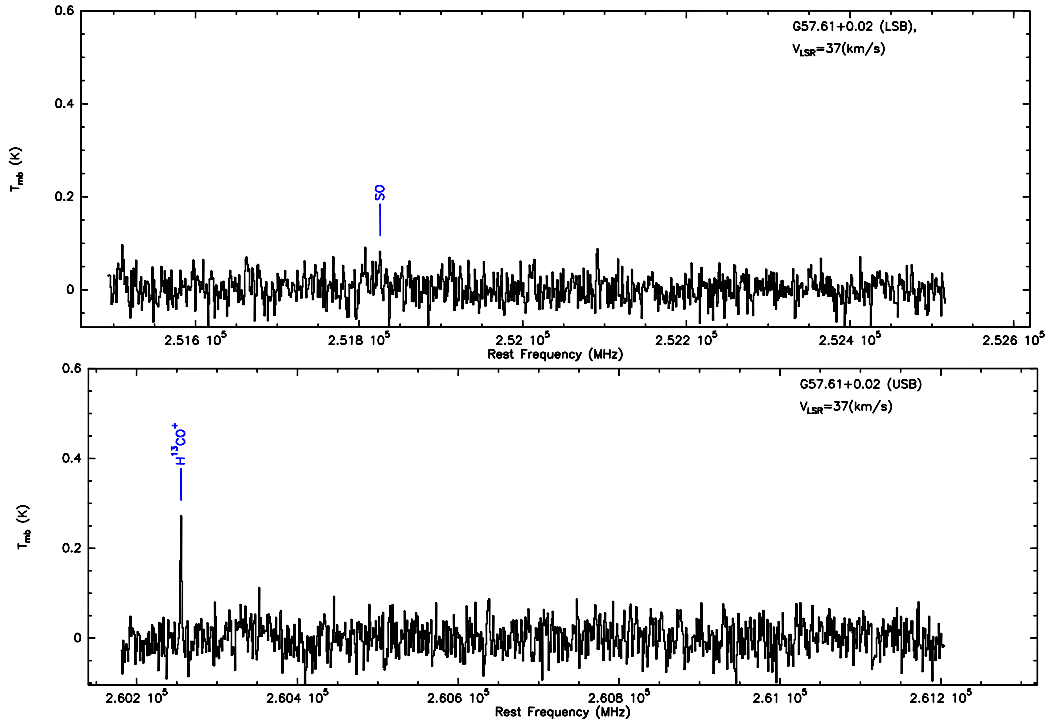


Fig. 10.— (continued) For G57.61+0.02.

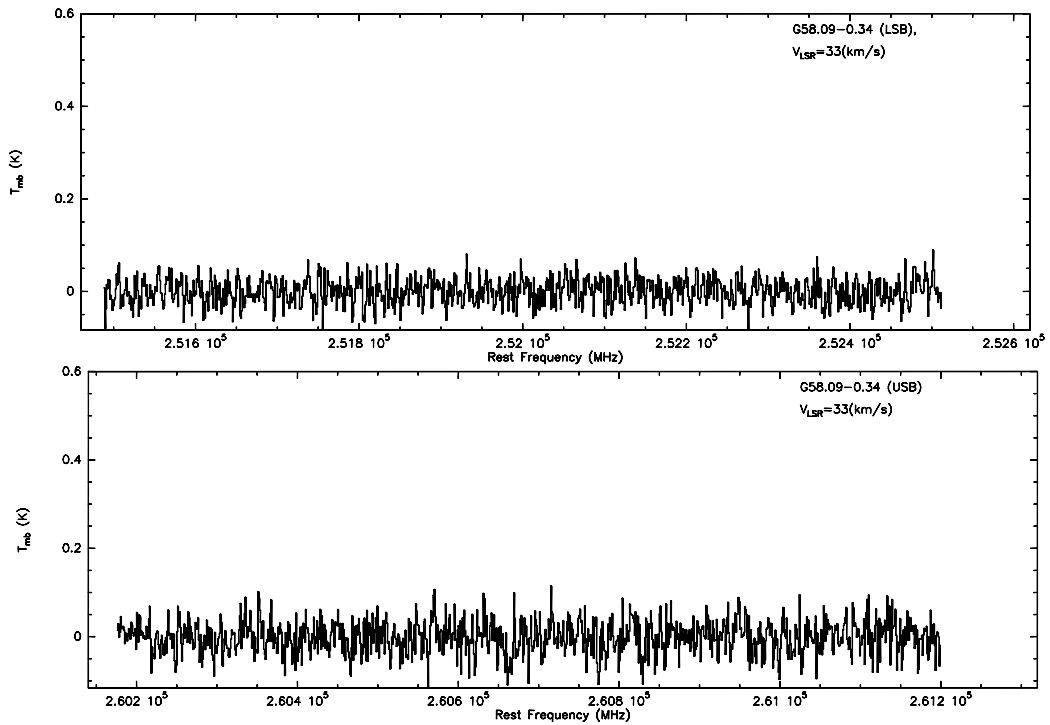


Fig. 10.— (continued) For G58.09-0.34.

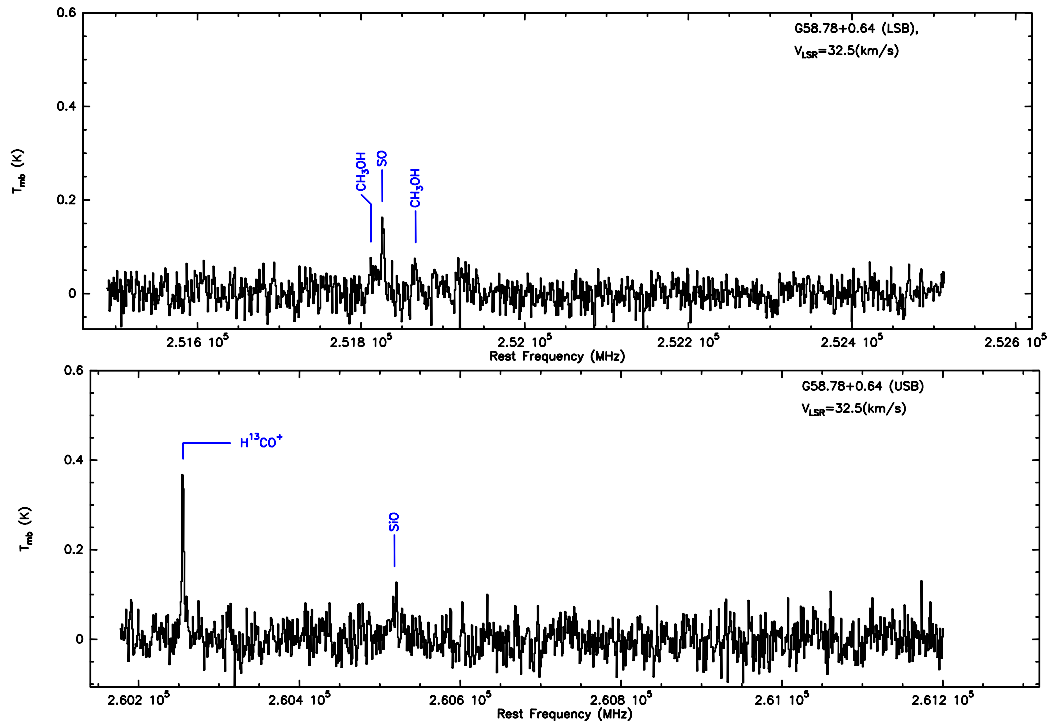


Fig. 10.— (continued) For G58.78+0.64.

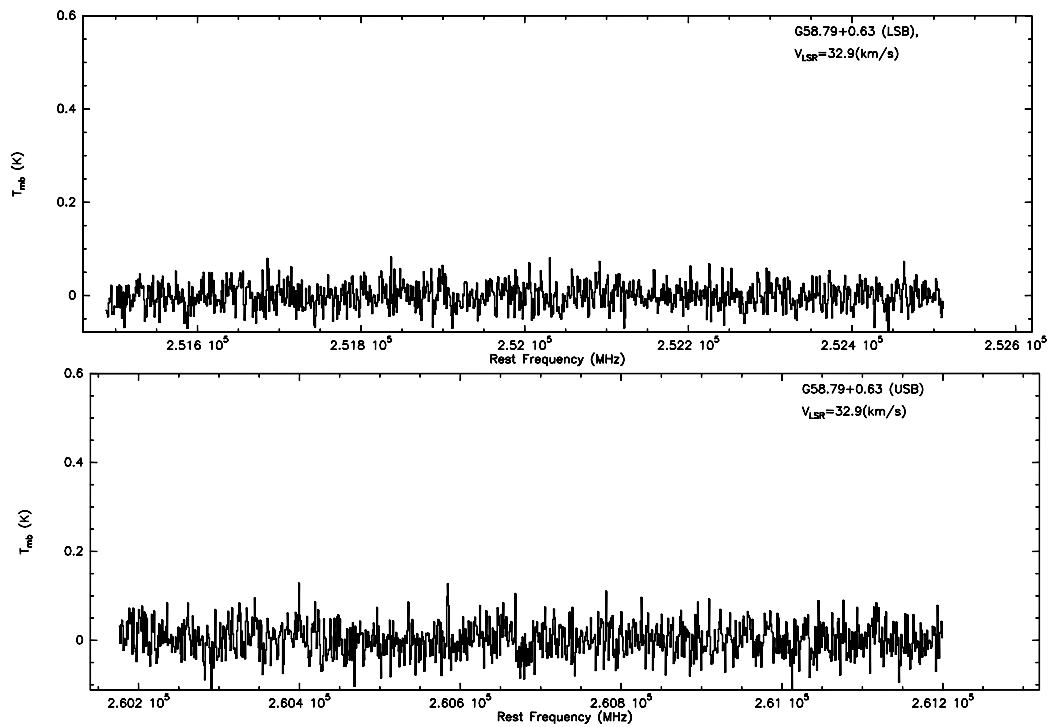


Fig. 10.— (continued) For G58.79+0.63.

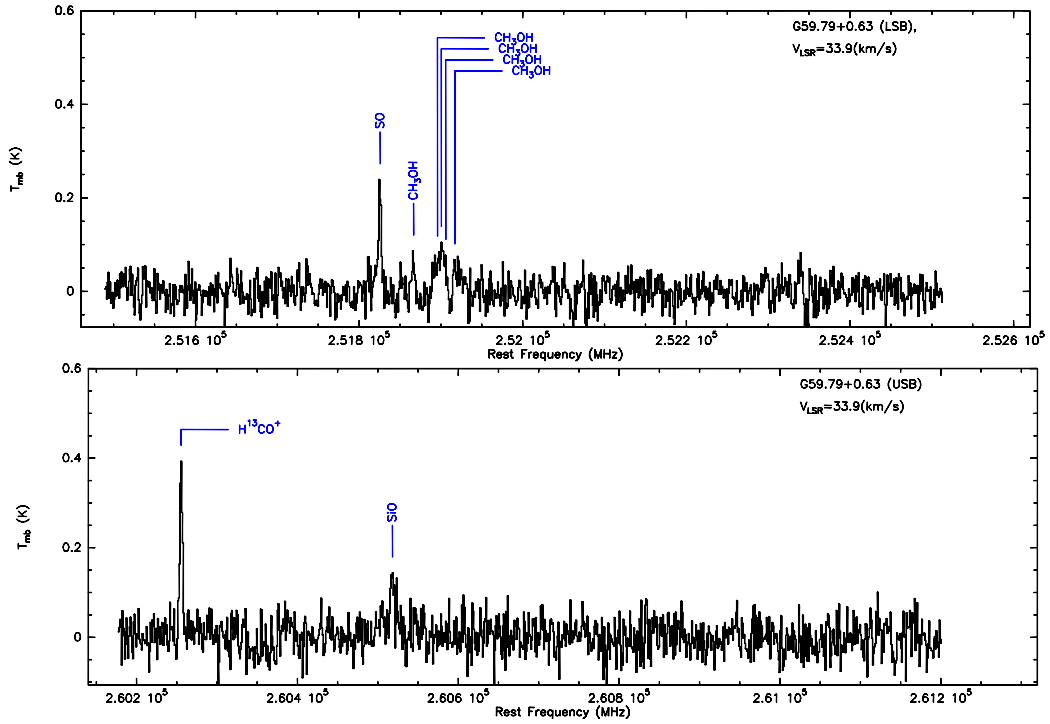


Fig. 10.— (continued) For G59.79+0.63.

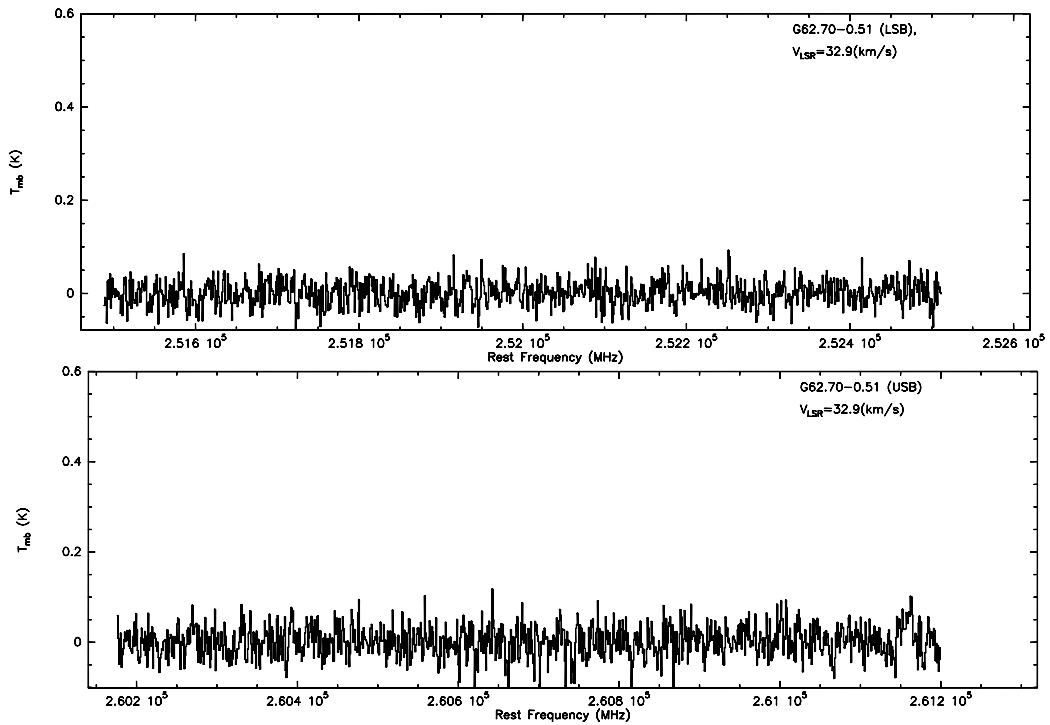


Fig. 10.— (continued) For G62.70-0.51.

REFERENCES

- Charnley, S. B. 1997, *ApJ*, 481, 396
- Chen, X., Ellingsen, S. P., & Shen, Z. 2009, *MNRAS*, 396, 1603
- Chen, X., Ellingsen, S. P., Shen, Z.-Q., Titmarsh, A., & Gan, C.-G. 2011, *ApJS*, 196, 9
- Chen, X., Shen, Z., Li, J., Xu, Y., & He, J. 2010, *ApJ*, 710, 150
- Cragg, D. M., Sobolev, A. M., & Godfrey, P. D. 2005, *MNRAS*, 360, 533
- Cyganowski, C. J., Brogan, C. L., Hunter, T. R., & Churchwell, E. 2009, *ApJ*, 702, 1615
- . 2011a, *ApJ*, 743, 56
- Cyganowski, C. J., Brogan, C. L., Hunter, T. R., Churchwell, E., & Zhang, Q. 2011b, *ApJ*, 729, 124
- Cyganowski, C. J., et al. 2008, *AJ*, 136, 2391
- Dame, T. M., Hartmann, D., & Thaddeus, P. 2001, *ApJ*, 547, 792
- De Buizer, J. M., & Vacca, W. D. 2010, *AJ*, 140, 196
- Ellingsen, S. P. 2006, *ApJ*, 638, 241
- Goodman, A. A., Barranco, J. A., Wilner, D. J., & Heyer, M. H. 1998, *ApJ*, 504, 223
- Gusdorf, A., Cabrit, S., Flower, D. R., & Pineau Des Forêts, G. 2008, *A&A*, 482, 809
- Hartquist, T. W., Dalgarno, A., & Oppenheimer, M. 1980, *ApJ*, 236, 182
- Herbst, E., Millar, T. J., Wlodek, S., & Bohme, D. K. 1989, *A&A*, 222, 205
- Hollenbach, D. 1997, in *IAU Symposium*, Vol. 182, *Herbig-Haro Flows and the Birth of Stars*, ed. B. Reipurth & C. Bertout, 181–198
- Kolpak, M. A., Jackson, J. M., Bania, T. M., Clemens, D. P., & Dickey, J. M. 2003, *ApJ*, 582, 756
- Larson, R. B. 1981, *MNRAS*, 194, 809
- Lee, H.-T., Takami, M., Duan, H.-Y., Karr, J., Su, Y.-N., Liu, S.-Y., Froebrich, D., & Yeh, C. C. 2012, *ArXiv e-prints*
- Mikami, H., Umemoto, T., Yamamoto, S., & Saito, S. 1992, *ApJ*, 392, L87
- Müller, H. S. P., Schlöder, F., Stutzki, J., & Winnewisser, G. 2005, *Journal of Molecular Structure*, 742, 215
- Müller, H. S. P., Thorwirth, S., Roth, D. A., & Winnewisser, G. 2001, *A&A*, 370, L49
- Neufeld, D. A., & Dalgarno, A. 1989a, *ApJ*, 340, 869
- . 1989b, *ApJ*, 344, 251
- Noriega-Crespo, A., et al. 2004, *ApJS*, 154, 352
- Pickett, H. M., Poynter, R. L., Cohen, E. A., Delitsky, M. L., Pearson, J. C., & Müller, H. S. P. 1998, *J. Quant. Spec. Radiat. Transf.*, 60, 883
- Rathborne, J. M., Jackson, J. M., & Simon, R. 2006, *ApJ*, 641, 389
- Rathborne, J. M., Simon, R., & Jackson, J. M. 2007, *ApJ*, 662, 1082
- Reid, M. J., et al. 2009, *ApJ*, 700, 137
- Reiter, M., Shirley, Y. L., Wu, J., Brogan, C., Wootten, A., & Tatematsu, K. 2011, *ApJS*, 195, 1
- Roman-Duval, J., Jackson, J. M., Heyer, M., Johnson, A., Rathborne, J., Shah, R., & Simon, R. 2009, *ApJ*, 699, 1153
- Rosolowsky, E., et al. 2010, *ApJS*, 188, 123
- Sakai, T., Sakai, N., Hirota, T., & Yamamoto, S. 2010, *ApJ*, 714, 1658
- Schilke, P., Walmsley, C. M., Pineau des Forêts, G., & Flower, D. R. 1997, *A&A*, 321, 293
- Schöier, F. L., van der Tak, F. F. S., van Dishoeck, E. F., & Black, J. H. 2005, *A&A*, 432, 369
- Simon, R., Jackson, J. M., Rathborne, J. M., & Chambers, E. T. 2006a, *ApJ*, 639, 227

- Simon, R., Rathborne, J. M., Shah, R. Y., Jackson, J. M., & Chambers, E. T. 2006b, *ApJ*, 653, 1325
- Simpson, J. P., Cotera, A. S., Burton, M. G., Cunningham, M. R., Lo, N., & Bains, I. 2012, *MNRAS*, 419, 211
- Smith, M. D., & Rosen, A. 2005, *MNRAS*, 357, 1370
- Solomon, P. M., Rivolo, A. R., Barrett, J., & Yahil, A. 1987, *ApJ*, 319, 730
- Takahashi, S., Saito, M., Takakuwa, S., & Kawabe, R. 2006, *ApJ*, 651, 933
- van der Tak, F. F. S., Boonman, A. M. S., Braakman, R., & van Dishoeck, E. F. 2003, *A&A*, 412, 133
- Wakelam, V., Castets, A., Ceccarelli, C., Lefloch, B., Caux, E., & Pagani, L. 2004, *A&A*, 413, 609
- Walmsley, C. M., Pineau des Forêts, G., & Flower, D. R. 1999, *A&A*, 342, 542
- Zinnecker, H., & Yorke, H. W. 2007, *ARA&A*, 45, 481
- Ziurys, L. M., Friberg, P., & Irvine, W. M. 1989, *ApJ*, 343, 201